EXPERIMENTAL STUDY OF BOUNDARY LAYER SUCTION IN A TRANSONIC COMPRESSOR

by

Duncan P. Reijnen

Ir. Aerospace
Delft Technical University, 1992

SUBMITTED TO THE DEPARTMENT OF AERONAUTICS AND ASTRONAUTICS
IN PARTIAL FULFILLMENT OF THE REQUIREMENTS FOR THE DEGREE OF

DOCTOR OF PHILOSOPHY
AT THE
MASSACHUSETTS INSTITUTE OF TECHNOLOGY

JANUARY 1997
[FEBRUARY 1997]

Signature of Author: ______________________
Department of Aeronautics and Astronautics
January 15, 1997

Certified by: ______________________
Jack L. Kerrebrock
Maclaurin Professor of Aeronautics and Astronautics
Thesis Supervisor

Certified by: ______________________
Mark Drela
Associate Professor of Aeronautics and Astronautics
Committee Member

Certified by: ______________________
Hugh L. McManus
Class of 1943 assistant Professor of Aeronautics and Astronautics
Committee Member

Certified by: ______________________
Gerald R. Guenette
Principal Research Engineer
Committee Member

Accepted by: ______________________
Jaime Peraire
Professor of Aeronautics and Astronautics
Chairman, Committee for Graduate Students

Study of Boundary Layer Suction in a Transonic Compressor

by

Duncan P. Reijnen

Submitted to the Department of Aeronautics and Astronautics
on January 10, 1997 in Partial Fulfillment of the
Requirements for the Degree of Doctor of Philosophy in
Aeronautics and Astronautics

ABSTRACT

As part of a comprehensive program of research on the enhancement of compressors by removal of the fluid that suffers from viscous interaction, boundary layer suction was applied just prior to the shock impingement on the suction surface of the blades of a transonic rotor, this being a situation where the impact of boundary layer control was expected to be large. The suction by the means of a boundary layer scoop which removed 0.6% of the passage flow, was applied to 5 of the 23 blades providing a direct comparison of the flow behavior with and without suction. Testing the rotor in the MIT Gas Turbine Laboratory Blowdown Compressor Facility revealed a significant change in flow behavior. The blades with suction had enhanced resistance to stall and the flow more closely followed the suction surface near the trailing edge. The differences between the sucked and normal blades were most pronounced when the rotor was close to stall. The third and fourth of the blades in the group with suction appear to be representative of the behavior to be expected of a rotor with suction on all blades. They exhibit improved efficiency and mass flow. The rotor as a whole with suction was more resistant to rotating stall than its counterpart without boundary layer control.

Thesis Supervisor: Jack Kerrebrock
Title: Maclaurin Professor of Aeronautics and Astronautics

Acknowledgments

First, I want to thank my wife Paula and my supervisor Professor Jack Kerrebrock. Their positive attitude and support always encouraged me in sometimes turbulent times.

Paula provided the opportunity and very often the means which made this piece of work possible. The difficulties we faced and lessons we learned during our first year in U.S.A. will never be forgotten. The education we received via her work in Dorchester is not available in Cambridge and changed our views on life for ever.

Professor Kerrebrock taught me that high obstacles should not discourage a person just persevere ones determination. I will always remember the words with which he concluded the conversation in which he hired me for this project: "If it is not very hard, somebody else would already have done it."

I also want to thank my parents, sisters, and brother. They provided an environment which promoted creativity, learning and excellence, and gave me abundant help and advise.

Without the many hours of support of Jerry Guenette, Professor Mark Drela, Professor Mohammed Durali and Professor Hugh McManus this thesis would have been impossible. They guided me when problems concerning detailed experimental setup, computational simulation, and structural integrity and design arouse.

Our staff in the laboratory has been extremely helpful in transforming ideas into physical hardware. Often the help and support I received from Victor Dubrowski, James Letendre, Bill Ames and many others, was far beyond the call of duty. In addition, I want to thank Al Supple for his help with the plastic explosives and the production of the graphite/epoxy blades.

The U.S. Air Force I thank for believing in us and our ideas. They provided the financial means which made this project possible.

Finally, my fellow students. Jed Dennis and I had the time of our lives while working often day and literally night. Larry Smilg and Willy Ziminsky provided great support. Ali Merchant time was extremely appreciated. He helped me solve my specific MISES problems and provided the final modifications to MISES which I needed. Rory, Jinwoo, Yang and Yi provided countless interesting discussions during lunch. John I must thank for being patient.

Table of Contents

List of Figures

Nomenclature

γ	specific heat ratio Cp/Cv	[ ]
δ	deviation	[Deg]
δ	boundary layer thickness	[m]
δ^*	boundary layer displacement thickness	[m]
η	isentropic efficiency	[ ]
θ	tangential (swirl) angle, measured from axial	[Deg]
θ	boundary layer moment thickness	[m]
λ	wave length	[m]
μ	viscosity	[s kg/m]
ν	dynamic viscosity, μ/ρ	[m^2s]
π	pi	[]
ρ	density	[kg/m^3]
σ	solidity, c/s	[ ]
τ	temperature ratio (over rotor)	[ ]
ϕ	radial angle, measured from axial, positive for radial outward flow	[deg]
ω, Ω	rotational speed of rotor	[Hz, rad/s, rev/s]

c	chord	[m, In]
BL	boundary layer	
Cp	specific heat at constant pressure	[J/kg Deg C]
Cv	specific heat at constant volume	[J/kg Deg C]
Cf	friction constant	[]
f	frequency	[Hz]
h	height	[m]
In	inches	[In]
$\dot{m}$	mass flow	[kg/s]
M	Mach number	[]
P	pressure	[Pa]
R	gas constant	[J/kg Deg C]
Re	Reynold number	[]
s	blade spacing, entropy	[m,In,J/K)
St	Stanton number	[]
T	temperature	[Deg K]

Subscripts

0	station at inlet of CFD domain
1,2,3,4,5,6,7	stations in experiment, CFD code, therm. comp. model
dmp	dump tank
inl	inlet
r	reference
s	static
sup	supply tank
t	total
rel	relative frame
v	viscous
w	wall

Chapter 1 Introduction

1.1 Motivation for boundary layer control

Since the pioneering days of Whittle and Von Ohain, gas turbine designers have been on a quest to produce lighter, higher thrust, more fuel efficient engines. The key to doing this is of course to develop engines with higher pressure ratios while keeping the number of stages down to control the weight of the engine. The required higher pressure ratio per stage can be achieved by increasing the speed of the rotor or increasing the aerodynamic loading of the blade row. However, the speed of rotor is usually bounded by stress constraints and in the case of a transonic compressor also by shock losses which scale with $(M-1)^3$ where M is the Mach number of the flow relative to the rotating blade row. Aerodynamic loading is bounded by viscous effects. When the static pressure rise over the blade row is too high, the boundary layer on the suction side of the airfoil separates. In the case of a transonic compressor, it is usually the high pressure gradient across the shock which induces separation of the boundary layer.

1.2 Related Problems and their Solutions

A similar situation occurs in supersonic inlets so research on supersonic inlets can provide valuable insight to what happens when a passage shock induces separation on a compressor blade. Supersonic inlets typically compress the air entering the engine using a oblique and normal shock as is seen in figure 1.1. The normal shock separates the boundary layer on the inlet ramp which causes separated flow to be sucked into the engine deteriorating its performance. This problem is solved by sucking off part of the boundary layer just upstream of the shock. It improves the profile of the boundary layer allowing it to withstand the pressure gradient over the shock. The literature review discusses different methods to achieve this boundary layer suction and discusses the amount of suction required to avoid separation.

1.3 Validity and Benefits of Boundary Layer Suction

The present study applies boundary layer control to a transonic compressor rotor. With the advent of hollow blades for structural and weight reasons, it becomes feasible to consider meeting the desire for higher pressure rises per stage by using the flow area in the blade to remove low momentum fluid from the airfoils, thereby controlling the boundary layer and avoiding boundary layer separation and hence allowing a higher diffusion over a blade row. The removed fluid can be put to good use for cooling hot components or can be completely removed from the flow path and used as customer bleed.

Boundary layer suction can provide several additional benefits besides avoiding separation. As will be explained in the thermodynamics chapter, removal of the high entropy fluid in the boundary layer results in an increase in efficiency in a multistage compressor. The lower the entropy of the fluid entering a stage, the less work is required to compress the fluid through a set pressure ratio. This follows directly from the divergence of the isobars in the T-S diagram. Another benefit finds its roots in the effect of rotation on the boundary layers on the blade.

High speed axial compressors are known to have a much lower efficiency near the tip than expected from profile characteristics. Kerrebrock (reference 1.1) speculated that the low efficiency near the tip might be explained by radial flow. Kotidis and Epstein (reference 1.2) made measurements which showed that span wise transport of several percent of the total mass flow occurred in a high pressure ratio axial compressor. In addition, it was found that the fluid which moved radially along the span had considerable higher entropy than the mean flow. Kotidis and Epstein hypothesized that most of the outward transport is in the separated region within the blade boundary layer. This results in the collecting of high entropy fluid near the tip. Boundary layer control and especially boundary layer suction has the potential of avoiding separation and therefore minimizing radial transport of high entropy fluid in the separated region. It decreases the amount of high entropy fluid generated while removing part of the high entropy viscous fluid from the flow path.

1.4 Context of Investigation

This experiment was conceived as part of a comprehensive program of research on the enhancement of compressors by removal of the fluid that suffers from viscous interaction. As such it had the specific and limited purpose of determining the effects of removal of the fluid in the boundary layer just prior to the shock impingement on the suction surface of the blades of a transonic rotor, this being a situation where the impact of boundary layer control was expected to be large. This particular experiment was not intended to show the full benefits that boundary layer control may have for compressors, since these benefits can be fully realized only if the stage design exploits the higher work enables by boundary layer control. It is hoped that such a feasibility demonstration will be provided by subsequent experiments.

Given the limited objective of the experiment, it was decided that boundary layer control would be applied only to a portion (5/23) of the blades on an existing MIT Blowdown Compressor rotor. The existing rotor was used because it was available and because there was a large inventory of data on its behavior, including three dimensional visualizations of its shock structure. The boundary layer control was applied to only a fraction of the blades for three reasons. First it was thought useful to have a direct comparison of the behavior with and without boundary layer removal, other conditions such as corrected speed and pressure ratio being equal. Second, incorporation of the system for handling the flow removed from the rotor was much easier for a small number of blades than for the full complement. And finally, the modification of the blades themselves by addition of boundary layer scoops and flow passages was time-consuming and expensive, so it was attractive to minimize their numbers.
As will be demonstrated, the experiment has met its limited objectives.

1.5 Outline of Investigation

The experimental setup chapter discusses the design process of the modifications and some of the equipment used during the experiment. The bulk of the equipment is described in several detailed appendices which are specifically written with the needs of future students in mind. The methods which were used to obtain the performance of the rotor, are described in the performance chapter.

During this investigation extensive use has been made of Computational Fluid Dynamics (CFD). In order to do boundary layer control it is essential to have a good understanding of the general flow and especially the development of the boundary layer on the suction surface. For this purpose MISES was used. The capabilities of the code and the results obtained will be discussed in the CFD chapter.

Finally this report concludes with a discussion of experimental results, a comparison to CFD calculations and recommendations.

References:

1.1 Kerrebrock, J.L., "Flow in Axial Compressors", AIAA Paper 80-0124, Dryden Lectureship in research, Pasadena, CA.

1.2 Kotidis, P.A., and Epstein, A.H., "Unsteady Radial Transport in a Transonic Compressor Stage", J. Turbo machinery, Vol. 113, April 1991, pp. 207-218.

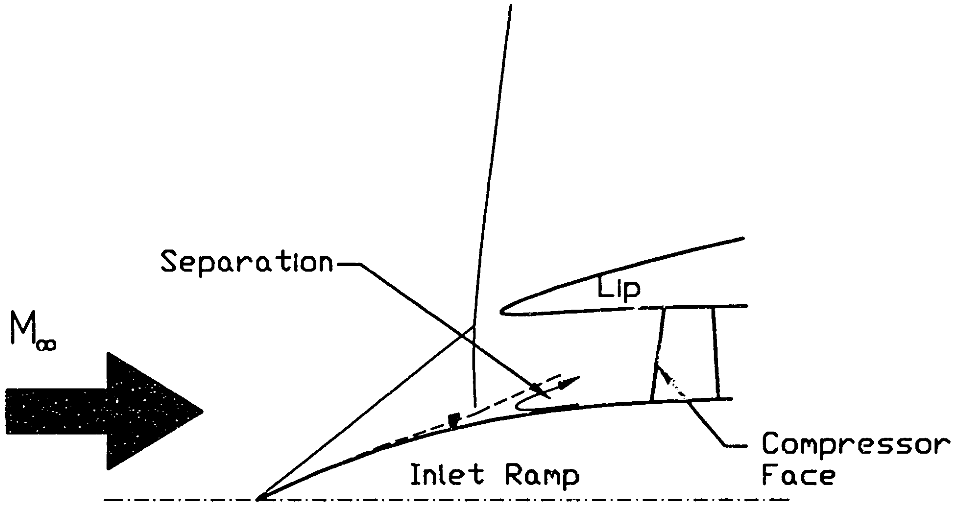

Figure 1.1 Schematic of typical supersonic inlet

Chapter 2 Literature Review

The literature review can be subdivided into two parts. The first, very short, section discusses boundary layer suction on airfoils in turbo machinery applications. The second section discusses in a more general context the details of shock boundary layer interaction control by suction or blowing.

2.1 Boundary Layer Suction on Airfoils in Turbo Machinery Applications

Although the adverse effects of boundary layer separation in compressor blading are well known and numerous compressors operate at least partly separated, very little research has been done to prevent separation by the means of boundary layer control, even though this method has received extensive attention in the aircraft airfoil and especially in the supersonic inlet design context, and several patents were found dating back as far as 1943 which propose the application of boundary layer suction to axial compressors. One reason for this is the geometrical complexity and the harsh operating environment of turbo machinery blades. The blades are often very small, rotating, or very close to high speed rotating objects which makes extensive instrumentation difficult.

Stalker proposed boundary layer control using blowing and bleeding slots as early as June 1943 and was awarded 4 patents (ref. 2.1, 2.2 and 2.3). While the details of the patents differ the concept is the same for all four. Using slots on the suction surface of a rotor or stator blade at a stage aft in an axial compressor, boundary layer fluid is removed from the blade surface and is re-injected with the objective of re-energizing the boundary layer at some earlier stage in the compressor. In the later versions of the patent casing boundary layer fluid aft of the last stage of the compressor is also used for blowing at earlier stages. In the first patent (ref. 2.1) Stalker concentrated the suction on the back of the suction surface enabling him to design a blade which had its maximum thickness more aft of the leading edge. The result is an airfoil with a lower acceleration on the front part of the suction surface and hopefully no supersonic flow on the suction surface eliminating shocks or postponing them to higher rotational speeds.

Later patents (ref. 2.2 and 2.3) eliminated blowing on the back of the suction surface and replaced it by blowing just aft of the area of strong curvature due to the leading edge radius and on the blades with bleed additional suction was added on a similar position as the blowing blades, just aft of the leading edge radius. The main idea here was to design blades with larger leading edge radii in order to allow larger changes in the angle of attack of the blades at which the multi stage compressor would be able to operate successfully.

Erwin (ref. 2.4) proposed in contrast to Stalkers discrete slots to apply continuous boundary layer control either on the casing, rotor or stator blade using porous or laminated materials. He also proposed the idea of taking the fluid inward in the rotor after which the boundary layer fluid is removed from the rotating disk and the hub area of the engine via an hollow (maybe also bleeding) stator to the casing after which he proposed to use this fluid for cooling or customer bleed air or simply dump to the atmosphere. The main objective here was to avoid separation, increase the operating range of the compressor and decrease the losses in the compressor.

Conrad et al. (ref. 2.5) at Daimler-Benz proposed to apply boundary layer suction by the means of a slot or a set of holes to a stator blade with the intention to keep the boundary layer laminar, or avoid separation by an adverse pressure gradient such as for example a shock.

Meauze et al. (ref. 2.6) at ONERA proposed a supersonic axial compressor with a convergent casing in order to reduce the blade relative Mach number and to apply boundary layer suction by the means of relatively wide slot at the shock impingement location of shock on the rotor suction surface and the casing with the goal of reducing the shock strengths and losses, and avoiding separation of the boundary layer at the shock impingement location.

The only experimental study of relevance to this work known to the author was done by Loughery et al. in 1971 at Allison Engines . Loughery (reference 2.7), tested different stator configurations behind a high subsonic rotor. Stator inlet Mach numbers ranged from 0.6 at the tip to 0.75 at the hub. Both blowing and suction were tested as means to prevent separation on the suction side of the stator. The 6 different configurations are shown in figure 2.1. In the case of blowing the air was ingested on the pressure side near the leading edge of the blade and ejected on the aft part of the suction surface. This proved to cause problems at negative incidence and the overall performance of the stator with blowing was inferior to that of the baseline.

The stators with suction showed significant increases in performance. Removal of a third of the boundary layer was set as the goal. This required removal of 1.5% of the flow through the stator for the 3 slot bleed stator and 1.8% for the single slot bleed stator. Both suction stators exhibited superior performance compared to blowing and in the case of the 3 slot bleed stator also to the baseline. Because the single slot stator had a different diffusion factor no baseline was available for comparison. Direct comparison of the 3 slot stator and the base line showed that the stator with bleed had a 3 times lower minimum loss coefficient, a 3 degrees lower deviation and 10% higher diffusion factor and a larger operating range than the baseline stator. In addition to the stator bleed it was found that bleed on the casing at the hub led to a 2% increase in performance of the complete stage while bleed on the tip casing had no noticeable effect.

2.2 The Details of Boundary Layer Shock Interaction and Separation Control

The field of boundary layer shock interaction is dominated by supersonic inlet designers. In a typical supersonic inlet the flow is decelerated to a subsonic Mach number by the combination of an oblique and a normal shock. The latter is sometimes referred to as the terminal shock. The Mach number just upstream of this normal shock is usually in the 1.4 to 2.0 range. This is more than sufficient to separate the boundary layer. The separation distorts the flow into the engine and is therefore high undesirable. A common solution to this problem is bleeding the wall boundary layer near the location of the normal shock and a considerable amount of research has been done to determine the optimum bleed configuration which avoids boundary layer separation.

Syber and Koncsek (reference 2.8) provide an excellent overview of the possible configurations. Basically the choice consists of a scoop, flush slot or bleed holes. An idea how these choice could be applied to compressor blade is illustrated in figure 2.2. Scoops provide excellent pressure recovery and therefore increase the efficiency of the system. Flush slots are known to improve the boundary layer due to their 2 dimensional removal of fluid and if angle to the surface will also partially recover the dynamic head. However in inlets, bleed holes are usually the design of choice due to their versatility and ease of fabrication. Holes are easily drilled and plugged which makes them ideal for testing and allows easy modification of the experimental setup. As a result the bulk of literature in this field concerns experiments using bleed holes.

In addition to the experimental studies several analytical and numerical studies of interest were found. They provide supplemental insight to the interaction of shocks and boundary layers in the event of suction.

Hamed and Shang (reference 2.9) provide a fairly recent survey of shockwave boundary layer interaction experiments including experiments with suction and blowing. Although none of the experiments combines suction with a normal shock, much can be learned of the numerous studies of an oblique shock boundary layer interaction. When suction is applied through bleed holes in the surface it is usually found that less suction is required to control separation when the suction is applied upstream of the shock. In addition two studies (reference 2.10 and 2.11) reported fuller velocity profiles at the interaction, a shorter interaction length and an increased pressure gradient in the interaction zone. Blowing out of normal holes proved ineffective and was found to have similar effects as increased surface roughness: Squire (reference 2.12) reported an increase in the interaction length while the interaction moved forward and the shock strength for incipient separation was found to be insensitive to blowing.
Wong (reference 2.13) tried tangential blowing on an inlet of the type used on F5 aircraft. The blowing was applied just upstream of the terminal normal shock wave. Wong reported successful suppression of induced separation by normal shock waves of up to Mach 2. He required a momentum flux of approximately twice the momentum deficit of the boundary layer ($C\mu = \dot{m}_{jet}(U_j-U_e)/(\rho_e U_e^2 \theta s) = 1.5\text{-}2.0$). The blowing holes were incorporated in a small step in the surface ($h=3\delta^*$) and were positioned parallel to the flow direction $2\delta^*$ (=s) apart. The disadvantage of this method of boundary layer separation suppression is the very high total pressure in the jets needed to be effective. In the most severe case (M=2.0) a total pressure of 16 times the mean flow total pressure was required in the jets to obtain the momentum flux mentioned above.
The investigation with the highest relevance was done by Morris et al. (reference 2.14). They explored the consequences of imposing mass removal in a 2D channel flow with a typical boundary layer ($d^*=1.4\%$ of channel height) and inlet Mach number ($M_{inlet}=1.48$) for a supersonic inlet. The boundary layers on the sides and the bottom of the channel were removed using scoops removing approximately 20% of the total flow in the channel. The normal shock in the channel was positioned by a scoop on the bottom surface and impinged on the top flat surface which contained a section with a bleed hole pattern. The holes were 0.05 mm in diameter and 0.20 mm apart. Morris et al. found that if the shock was positioned in the middle of the suction region when no suction was applied, applying suction pulled the top part of the shock backwards to the trailing edge of the suction zone while the bottom part of the shock stayed attached to the scoop creating a oblique shock. Positioning the suction region just aft of the no suction shock position led to large amplitude shock oscillation of the order of 65% of the length of the bleed zone. Best results were obtained when the suction region was completely upstream of the no suction shock position. In this configuration separation was avoided when roughly δ^* was removed and the boundary layer thickness downstream was cut in half. The lambda foot of the normal shock disappeared and instead some expansion waves appeared at the leading edge of the bleed zone to turn the flow to the bleeding wall.
An additional experimental investigation of boundary layer separation induced by a normal shock was conducted by Wong, W.J., (reference 2.15). Using bleed holes upstream and over the shock boundary layer interaction region he was able to suppress the separation induced by a normal shock with a strength up to $M_{upstream}=1.9$ while removing 3% of the flow captured by the inlet. He concludes that continuous bleed was required upstream and through the shock boundary layer

interaction region. In addition, separated bleed cells were necessary to avoid local recirculation through the bleed system. The size of the bleed holes often proves to be critical. During this study Wong successfully used holes normal to the wall, of the size of the local undisturbed δ^*. This indicates that very small holes are not necessary.
Wong also compared his data to a model by Hall (reference 2.16). Basically the model states that fluid who's total pressure upstream of the shock minus the losses over shock does not exceed the static pressure behind the shock has to be removed in order to avoid separation. The critical Mach number is illustrated in figure 2.3. So to find the critical Mach number for say a normal shock with M=1.82, one looks up the static pressure ratio over the shock: $p_2 / p_1 = 3.698$. Then one finds the Mach number who's total over static pressure equals 3.7. In this case $M_c = 1.57$ provides $p_{t2}/p_1 = 3.69$. When Wong compared the upstream mass flow required to avoid separation to the model very good agreement was found. To allow for difference of the boundary layer characteristics he advised to remove 1.5 times the amount predicted by the model in order to avoid separation. For example in the case of the M=1.82 normal shock wave he required bleeding of approximately half of the boundary layer upstream as is predicted by the model of Hall but also more than twice that amount over the interaction region.

Recent numerical studies by Rimlinger (reference 2.17) and Hamed (reference 2.18) found slightly different conclusions than most experiments. Hamed finds a bleed slot just over the interaction length of the shock to be the most effective, while suction downstream of the interaction length provides the most favorable velocity profiles and skin friction recovery downstream of the interaction region. Therefore Hamed advises a combination of bleed slots over the interaction and downstream of the interaction. Rimlinger found that best results were obtained by placing the bleed holes just upstream of the shock because this eliminates propagation of the adverse pressure gradient upstream by the means of a barrier shock.

2.3 Conclusion

From these investigations one can conclude that although not supported by all numerical studies, upstream suction and suction over the shock wave boundary layer interaction region provides the best results in avoiding boundary layer separation. The mass flow removed has to exceed the flow defined by the critical Mach number in the Hall model thus the resulting flow must have a local Mach number which results in a higher total pressure behind its normal shock than the static pressure behind the normal shock in the inviscid flow.

References:

2.1 Stalker, E.A., “Axial Blower”, U.S. Patent 23,108, May 3, 1949.

2.2 Stalker, E.A., “Compressors”, US Patent 2,749,025./2.749,027 June 5 ,1956.

2.3 Stalker, E.A., “Compressors”, US Patent 2,830,754. April 15, 1958.

2.4 Erwin, J.R., “Continuous Boundary Layer Control in Compressor”, US Patent 2,720,356, Oct. 11 1955.

2.5 Conrad, O., et al., “Guide Blades of Axial Compressors”, Daimler-Benz, US Patent 3,694,102, Sept 26 1972.

2.6 Meauze, G.D., et al., “Supersonic Compressor”, ONERA, US Patent 3,993,414, Nov. 23 1976.

2.7 Loughery, R.J., Horn, R.A. and Tramm, P.C., "Single Stage Experimental Evaluation of Boundary Layer Blowing and Bleed Techniques for High Lift Stator Blades", NASA CR-54573, March 1971.

2.8 Syber, J. and Koncsek, J.L., "Bleed System Design Technology for Supersonic Inlets", AIAA Paper 72-1138, Nov. 1972.

2.9 Hamed, A. and Shang, J.S., "Survey of Validation Data Base for Shockwave Boundary Layer Interaction in Supersonic Inlets", J. Propulsion, Vol. 7, No.4, July-Aug. 1991, pp. 617-25.

2.10 Strike, W.T. and Rippy, J., "Influence of Suction on the Interaction of an Oblique Shock with a Turbulent Boundary Layer at Mach 3", Arnold Engineering Development Center TN-61-129, Oct. 1961.

2.11 Hingst, W.R. and Tanji, F.T., "Experimental Investigation of Two-Dimensional Shock Boundary Layer Interaction with Bleed", AIAA Paper 83-0135 also NASA TM-83057, 1983

2.12 Squire, L.C. and Smith, M.G., "Interaction of a Shock Wave with a Turbulent Boundary Layer Disturbed by Injection", Royal Aeronautical Society, May 1980, pp. 85-110.

2.13 Wong, W.J., "Application of Boundary Layer Blowing to Suppress Strong Shock Induced Separation in Supersonic Inlets", AIAA Paper 77-147, Jan. 1977

2.14 Morris, M.J., Sajben, M. and Kroutil, J.C., "Experimental Investigation of Normal-Shock/Turbulent Boundary Layer Interactions with and without Mass Removal", AIAA Journal, Vol. 30, No. 2, Feb. 1992.

2.15 Wong, W.J., "The Application of Boundary Layer Suction to Suppress Strong Shock Induced Separation in Supersonic Inlets", AIAA Paper 74-1063, Oct. 1974.

2.16 Hall, G.R., "A Criterion for Prediction of Airframe Integration Effects on Inlet Stability with Application to Advanced Fighter Aircraft", Technical paper presented at Agard Symposium on Airframe/Propulsion interaction, Rome, Italy 3-6 Sept. 1974, AGARD CP 150.

2.17 Rimlinger, M.J., Shih, T.P., and Chyu, W.J., "Three Dimensional Shock Wave Boundary Layer Interactions with Bleed through a Circular Hole", AIAA Paper 92-3084.

2.18 Hamed, A. and Lehnig, T.," The Effect of Bleed configuration on Shock Boundary Layer Interactions", AIAA Paper 91-2014.

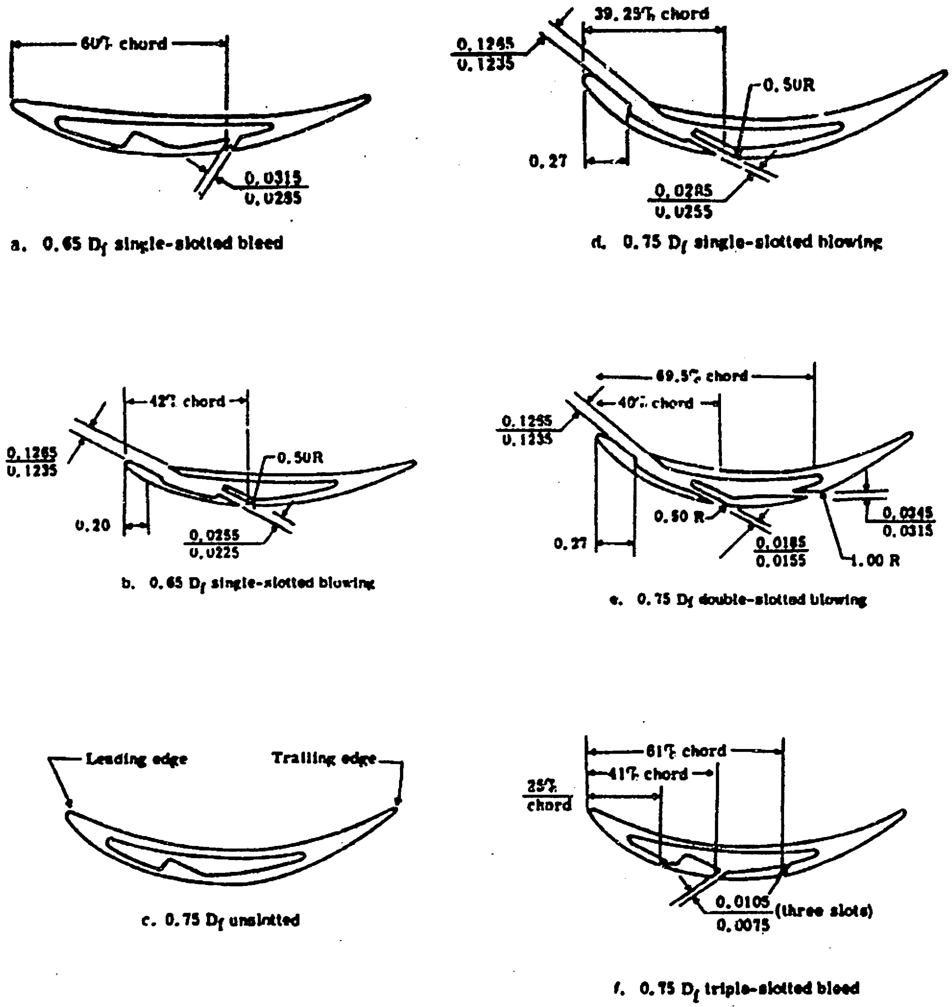

a. 0.65 D_f single-slotted bleed

d. 0.75 D_f single-slotted blowing

b. 0.65 D_f single-slotted blowing

e. 0.75 D_f double-slotted blowing

c. 0.75 D_f unslotted

f. 0.75 D_f triple-slotted bleed

Figure 2.1 Stator configurations tested by Loughery et al..(From Ref. 2.7)

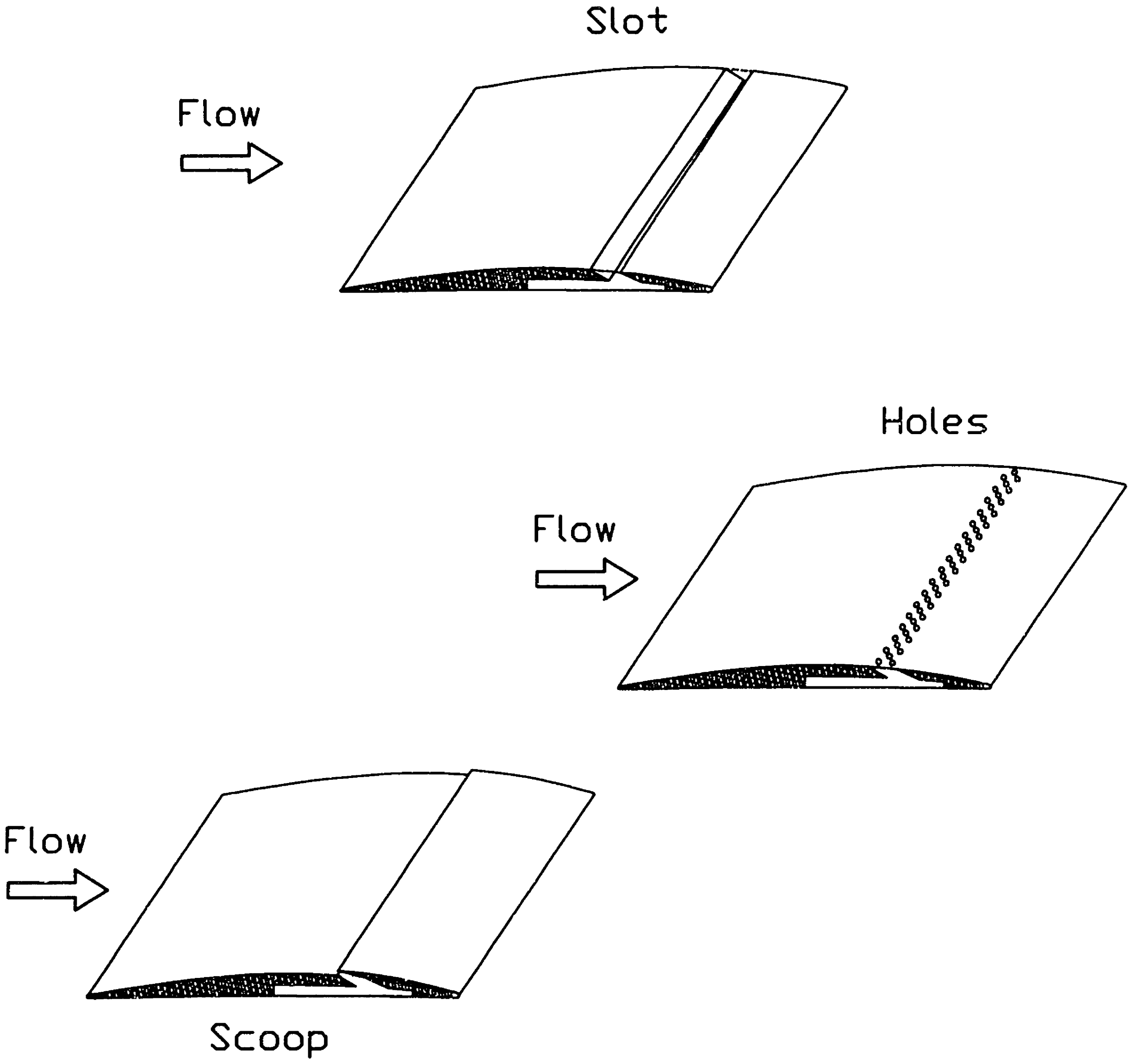

Figure 2.2 Example of application of slot, hole and scoop to compressor blade

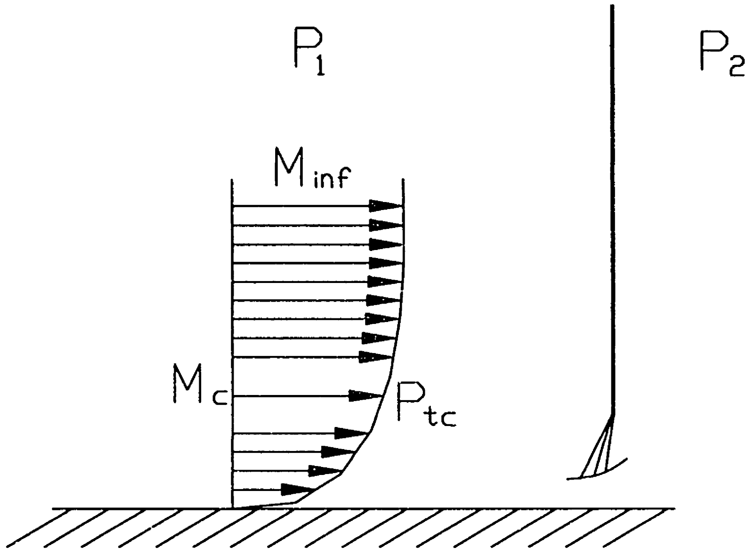

Figure 2.3 Hall criterion schematic

Chapter 3 Thermodynamic Benefits of Suction

3.1 Introduction

Removal of high entropy fluid can lead to an increase of efficiency. It will be shown that for a given amount of fluid compressed to a given pressure ratio in a multi stage machine, it requires less work to start with slightly more fluid and remove the high entropy fluid which is generated in the first couple of stages. The reason for this is that the lower the initial entropy of the fluid, the lower the amount of work it takes to compress a certain amount of fluid. This follows directly from the diverging constant pressure lines in the T-S diagram. Because of this it is more beneficial to control boundary layer separation by removing the high entropy /low momentum fluid rather than by re-energizing the boundary layer by some form of blowing which leaves the high entropy fluid in the flow path and increases the initial entropy at the entrance of each subsequent stage relative to suction. So basically the effect of not removing the high entropy fluid is to make every subsequent compression more costly.
This principle was recognized by Professor Kerrebrock and the following is the explanation of Professor Kerrebrock's model which accompanied the proposal for this investigation.

3.2 Model Definition

Consider a compressor as is shown in figure 3.1 which compresses fluid from pressure P_1 to P_3. At any particular blade row (station 2) a small amount of fluid $\delta \dot{m}$ that has suffered an entropy rise due to viscous effects, is extracted from the flow path. The remainder of the flow ($\dot{m}$-$\delta\dot{m}$) continues through the compressor. The T-S schematic for this compressor is shown in figure 3.2. The conventional compressor is denoted by the solid line and compresses a mass flow $\dot{m}$ from inlet conditions at station 1 via an intermediate station 2 to discharge conditions at station 3. When high entropy fluid removal is applied the compression is identical up to station 2. At station 2, the mass flow is separated in two parts. A small part of the fluid that has undergone high viscous interaction hence has high entropy as is indicated by condition 6, is removed from the flow field and is (conceptually) expanded back to compressor entrance pressure while the remainder of the fluid ($\dot{m}$-$\delta\dot{m}$) is compressed to the discharge pressure. This is shown in figure 3.2 by the dashed line from condition 4 to condition 5. In an actual application the removed fluid might be used for cooling hot parts in the engine or be provided to the airframe as customer bleed air thereby recovering work invested in it. Rather than complicating the analysis with the details of these systems, the most optimal approach from the point of view of efficiency is chosen by assuming that the high entropy fluid is ideally expanded back to compressor entrance pressure. So basically one can think of the compressor with suction as a combination of two virtual compressors operating in parallel denoted by the dashed lines in the lower part of the T-S diagram. One compresses core fluid ($\dot{m}$-$\delta\dot{m}$) from condition 1 to condition 4 and incurs a low entropy rise (Δs_c) while the second compresses a remaining small amount of fluid ($\delta\dot{m}$) from condition 1 to 7 and incurs in addition to the normal entropy rise (Δs_c) an extra entropy rise due to high viscous interaction (Δs_v). The remaining fluid in the flow path ($\dot{m}$-$\delta\dot{m}$) is compressed from P_2 to P_3 using less work due to the lower initial entropy at condition 4 which results in a lower efficiency for the complete compression system. Obviously this high entropy extraction can be repeatedly applied in each stage but for the sake of simplicity high entropy extraction at just one location is analyzed in the following.

3.3 Compressor Work

In order to asses the effect of high entropy removal on a multi stage compressor quantitatively, a comparison will be made between a compressor with suction and one without suction which both deliver a unit mass per second at the same pressure at the exit plane of the compressor. The polytropic efficiency will be assumed to be identical before and after the mass removal.

3.3.1 Compressor work without suction

The required work to compress fluid from P_1 to P_3 without application of bleed is expressed by:

$$W_{nb} = \dot{m} C_p (T_3 - T_1) \qquad [3.1]$$

Therefore per unit mass delivered the work is:

$$\frac{W_{nb}}{\dot{m} C_p T_1} = \frac{T_2}{T_1}\left(\frac{T_3}{T_2} - 1\right) + \left(\frac{T_2}{T_1} - 1\right) \qquad [3.2]$$

This can be rewritten using the constant polytropic efficiency.

$$\frac{T_2}{T_1} = \left(\frac{P_2}{P_1}\right)^{\frac{\gamma-1}{\gamma\eta_p}} \qquad \frac{T_3}{T_2} = \left(\frac{P_3}{P_2}\right)^{\frac{\gamma-1}{\gamma\eta_p}} \qquad [3.3]$$

$$\frac{W_{nb}}{\dot{m} C_p T_1} = \left[\left(\frac{P_3}{P_1}\right)^{\frac{\gamma-1}{\gamma\eta_p}} - 1\right] \qquad [3.4]$$

Or written in a more complicated way which facilitates future comparisons:

$$\frac{W_{nb}}{\dot{m} C_p T_1} = \left(\frac{P_2}{P_1}\right)^{\frac{\gamma-1}{\gamma\eta_p}}\left[\left(\frac{P_3}{P_2}\right)^{\frac{\gamma-1}{\gamma\eta_p}} - 1\right] + \left(\left(\frac{P_2}{P_1}\right)^{\frac{\gamma-1}{\gamma\eta_p}} - 1\right) \qquad [3.5]$$

3.4.2 Compressor Work with Suction Applied

The work needed to compress a unit mass fluid from P_1 to P_3 while removing high entropy fluid at station 2 is the sum of the work necessary to compress mass $\dot{m}$ from station 1 to station 2 and the work needed to compress the remaining ($\dot{m}$-$\delta\dot{m}$) from station 4 to station 5 minus the work released by expanding the bleed air back to ambient:

$$\dot{W}_{tot\ b} = \dot{m}C_p(T_2-T_1) + (\dot{m}-\delta\dot{m})C_p(T_5-T_4) - \delta\dot{m}C_p(T_6 - T_7) \qquad [3.6]$$

Or reorganized:

$$\frac{\dot{W}_{tot\ b}}{C_p(\dot{m}-\delta\dot{m})} = \frac{\dot{m}}{\dot{m}-\delta\dot{m}}T_1(\frac{T_2}{T_1}-1) + T_4(\frac{T_5}{T_4} - 1) + \frac{\delta\dot{m}}{\dot{m}-\delta\dot{m}}T_6(\frac{T_7}{T_6} - 1) \qquad [3.7]$$

The temperature ratios can be replaced for pressure ratios using the following expressions:

$$\frac{T_2}{T_1} = \left(\frac{P_2}{P_1}\right)^{\frac{\gamma-1}{\gamma\eta_p}} \qquad \frac{T_5}{T_4} = \left(\frac{P_3}{P_2}\right)^{\frac{\gamma-1}{\gamma\eta_p}} \qquad \frac{T_7}{T_6} = \left(\frac{P_1}{P_2}\right)^{\frac{\gamma-1}{\gamma}} \qquad [3.8]$$

$$\frac{\dot{W}_{tot\ b}}{C_p(\dot{m}-\delta\dot{m})} = \frac{\dot{m}}{\dot{m}-\delta\dot{m}}T_1[(\frac{P_2}{P_1})^{\frac{\gamma-1}{\gamma\eta_p}} - 1] + T_4[(\frac{P_3}{P_2})^{\frac{\gamma-1}{\gamma\eta_p}} - 1] + \frac{\delta\dot{m}}{\dot{m}-\delta\dot{m}}T_6[(\frac{P_1}{P_2})^{\frac{\gamma-1}{\gamma}} - 1] \qquad [3.9]$$

At the pressure P_2 the flow is assumed to be dividable into a small portion $\delta\dot{m}$ that has suffered an entropy rise due to viscous effects, and the larger fraction ($\dot{m}$-$\delta\dot{m}$) that we consider the core flow. We further assume that the separation is done in such a fashion that the pressure of the higher entropy fluid and the core flow are equal. Then the entropy of the extracted flow relative to that of the remaining flow at point 4 can be written as:

$$\Delta s_v = C_p \ln(\frac{T_6}{T_4}) \qquad [3.10]$$

The energy in the flow at station 2 is the mass averaged sum of the extracted high entropy fluid and the core flow:

$$\dot{m}T_2 = (\dot{m}-\delta\dot{m})T_4 + \delta\dot{m}T_6 \qquad [3.11]$$

Using equation 3.10 and 3.11 we can solve for T_4 and T_6. Assuming $\delta\dot{m}/\dot{m} \ll 1$ T_4 and T_6 reduce to:

$$\frac{T_4}{T_2} = 1 - \left(e^{\frac{\Delta s_v}{C_p}} - 1\right)\frac{\delta\dot{m}}{\dot{m}} \qquad [3.12]$$

$$\frac{T_6}{T_2} = e^{\frac{\Delta s_v}{C_p}}\left[1 - \left(e^{\frac{\Delta s_v}{C_p}} - 1\right)\frac{\delta\dot{m}}{\dot{m}}\right] \qquad [3.13]$$

Substituting 3.12 and 3.13 into equation 3.9 and subtracting the result from equation 3.5 we obtain after rearranging terms:

$$\frac{W_{nb}}{\dot{m}C_pT_1} - \frac{W_b}{(\dot{m}-\delta\dot{m})C_pT_1} = \frac{\delta\dot{m}}{\dot{m}}\left[1 + \left(\frac{P_3}{P_1}\right)^{\frac{\gamma-1}{\gamma\eta_p}}\left(e^{\frac{\Delta s_v}{C_p}} - 1\right) - e^{\frac{\Delta s_v}{C_p}}\left(\frac{P_2}{P_1}\right)^{\frac{\gamma-1}{\gamma}\left(\frac{1}{\eta_p}-1\right)}\right] \qquad [3.14]$$

Equation 3.14 represents the reduction in work which can be achieved by extracting a certain fraction of the fluid ($\delta\dot{m}/\dot{m}$) that incurred an additional entropy rise relative to the core flow (Δs_v) at an intermediate pressure P_2. From the above expression one can conclude that the benefit increases when the pressure ratio of the complete machine or the amount of fluid extracted is increased or the extraction takes place at a lower intermediate pressure.

Equation 3.14 can be written as the percent wise change in work by dividing it by equation 3.5:

$$\frac{\frac{W_{nb}}{\dot{m}} - \frac{W_b}{(\dot{m}-\delta\dot{m})}}{\frac{W_{nb}}{\dot{m}}} = \frac{\delta\dot{m}}{\dot{m}}\left(e^{\frac{\Delta s_v}{C_p}}\left[1 - \frac{\left(\frac{P_2}{P_1}\right)^{\frac{\gamma-1}{\gamma}\left(\frac{1}{\eta_p}-1\right)} - 1}{\left(\frac{P_3}{P_1}\right)^{\frac{\gamma-1}{\gamma\eta_p}} - 1}\right] - 1\right) \qquad [3.15]$$

From this equation one can draw two important conclusions. First the gain increases when the mass flow extracted is increased. Second, the gain increases with an increase in excess entropy but there is a certain entropy excess below which no gain is obtained. This will be explored in the following paragraph.

3.5 Magnitude of $\Delta s_v/C_p$

In order to assess the likely magnitude of $\Delta s/C_p$, consider a boundary layer like flow over a compressor blade surface. When it is assumed that the static pressure remains constant over the boundary layer and it is assumed that the blade surface is adiabatic, it follows that the temperature at the surface is close to the stagnation temperature and the entropy excess of the boundary layer fluid approaches

$$\frac{\Delta s_v}{C_p} = \ln\left(1+\frac{\gamma-1}{2}M^2\right) \qquad [3.16]$$

or

$$e^{\frac{\Delta s_v}{C_p}} = \left(1+\frac{\gamma-1}{2}M^2\right) \qquad [3.17]$$

Where M is the Mach number relative to the blade.
Substituting this estimate in equation 3.15 we find

$$\frac{\dfrac{W_{nb}}{\dot{m}} - \dfrac{W_b}{(\dot{m}-\delta\dot{m})}}{\dfrac{W_{nb}}{\dot{m}}} = \frac{\delta\dot{m}}{\dot{m}}\left(\frac{\gamma-1}{2}M^2 - \left(1+\frac{\gamma-1}{2}M^2\right)\left[\frac{\left(\frac{P_2}{P_1}\right)^{\frac{\gamma-1}{\gamma}\left(\frac{1}{\eta_p}-1\right)} - 1}{\left(\frac{P_3}{P_1}\right)^{\frac{\gamma-1}{\gamma\eta_p}} - 1}\right]\right) \qquad [3.18]$$

From this one can see that whether high entropy fluid extraction is beneficial depends on the Mach number of the flow. Below a certain Mach number the loss which is incurred by compressing fluid from condition 1 to condition 6 and expanding it back to station 6 is higher than the gain which is achieved in the compression from condition 4 to condition 5. This break even Mach number is expressed by

$$\frac{\gamma-1}{2}M^2 = \frac{\left(\frac{P_2}{P_1}\right)^{\frac{\gamma-1}{\gamma}\left(\frac{1}{\eta_p}-1\right)} - 1}{\left(\frac{P_3}{P_1}\right)^{\frac{\gamma-1}{\gamma\eta_p}} - \left(\frac{P_2}{P_1}\right)^{\frac{\gamma-1}{\gamma}\left(\frac{1}{\eta_p}-1\right)}} \qquad [3.19]$$

As is illustrated in figure 3.3 the minimum Mach number for gain lies between 0.3 and 0.5 for the bleed and compressor pressure ratios of interest. The inlet stages of most modern compressors satisfy this criterion. When there is referral to bleed pressure ratio, the ratio of the pressure at which the bleed is performed over the discharge pressure of the compressor is meant: P_2/P_3.

Using an estimate for the Mach number of the flow relative to the blades we can now quantify the fractional decrease in work due to suction. Furthermore because the ideal work stays constant for a given pressure rise and the changes are of the order of a percent, the fractional decrease in work equals the increase in efficiency.

Assuming a Mach number of 1 the percent wise fractional reduction in work per percent bleed is plotted in figure 3.4. Surprisingly the benefit is quite insensitive to compressor pressure ratio and bleed pressure ratio and amounts to an approximate 0.17% increase in efficiency per percent bleed. The possible amount of bleed is of course limited by the amount of high entropy fluid which can be separated.

For high speed blades the benefit quickly rises as can been seen in figure 3.5. When a relative Mach number of 1.5 is assumed the gain already more than doubles to a 0.4% increase in efficiency per percent bleed.

3.6 Conclusion

Removal of high entropy fluid leads to an increase in efficiency for blades with relative Mach numbers in excess of approximately 0.5. Surprisingly, the benefit is quite insensitive to the pressure ratio of the compressor and the pressure at which the bleed is performed. The relative Mach number however does influence the gain strongly. An increase from M=1 to M=1.5 more than doubles the obtainable efficiency increase per percent bleed from 0.17% to over 0.4%.

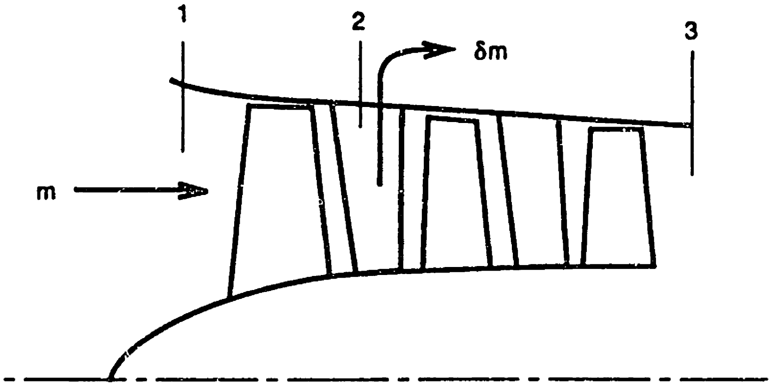

Figure 3.1 Definition of compressor stations

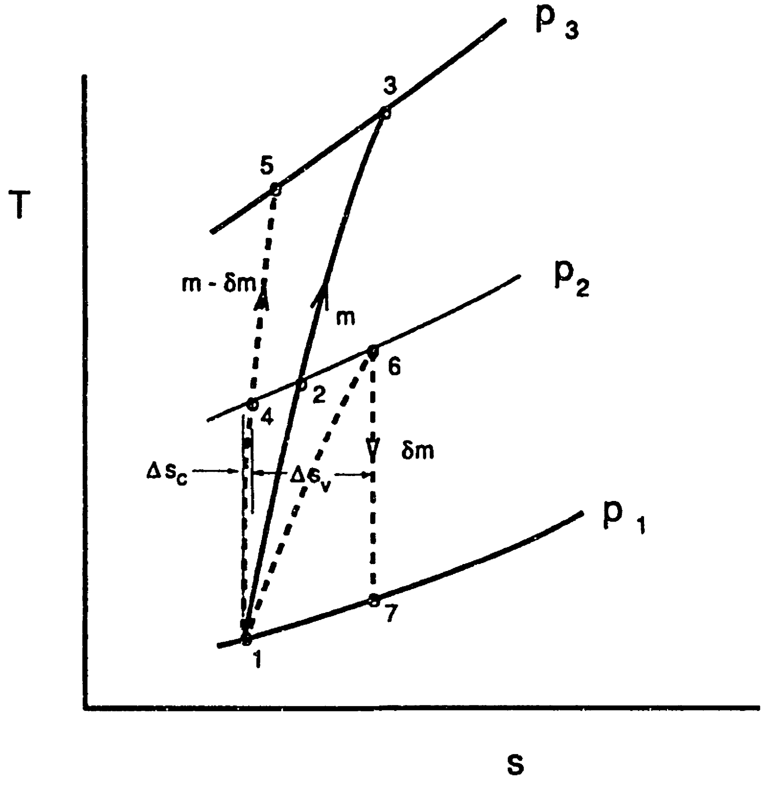

Figure 3.2 T-S diagram of compressor model

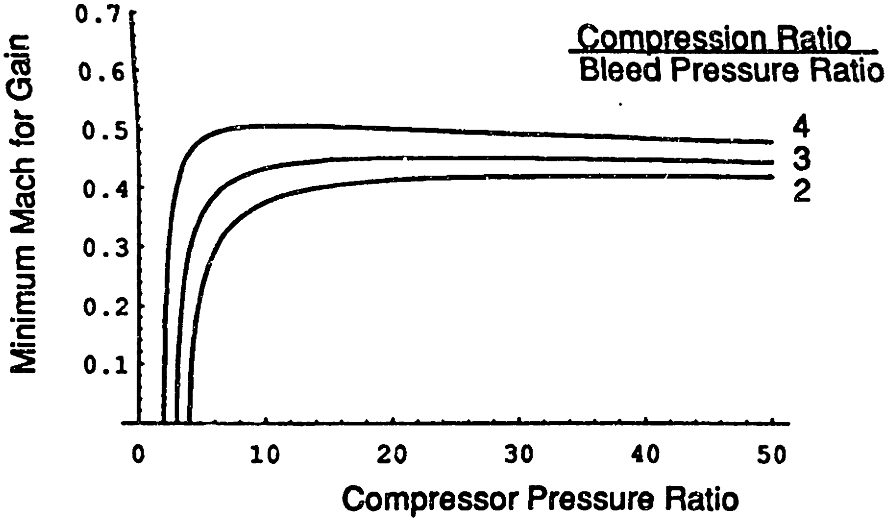

Figure 3.3 Minimum Mach number for which bleed is beneficial vs comp. and bleed press. ratio

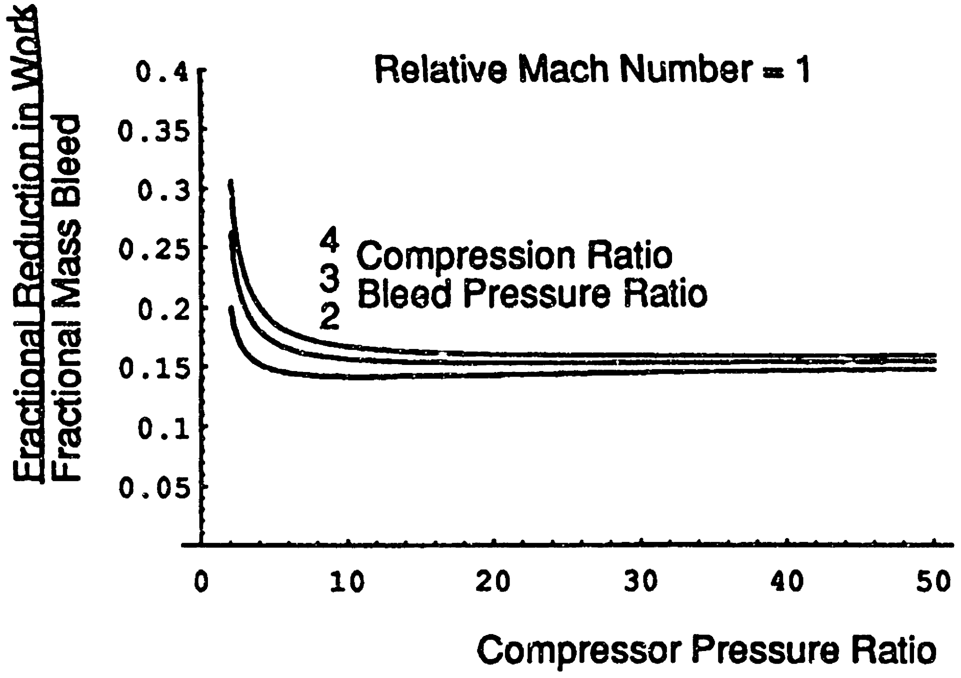

Figure 3.4 Percent wise work decrease per percent bleed for M=1

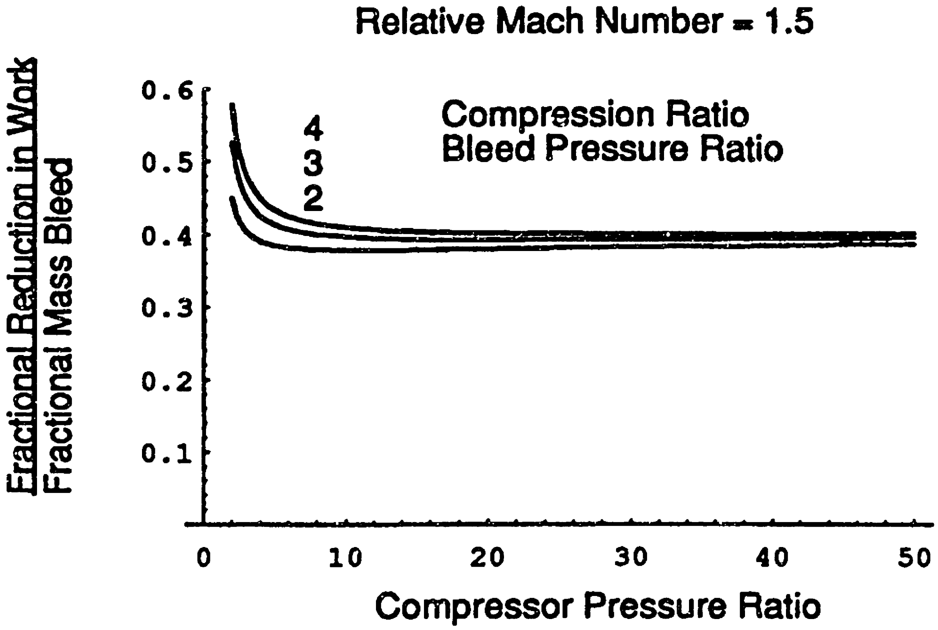

Figure 3.5 Percent wise work decrease per percent bleed for M=1.5

Chapter 4 Experimental Setup

4.1 Introduction

This chapter will describe the physical set up of the experiment. First, the basic operation of the facility will be described. Next, the modifications done to the facility and the rotor will be discussed. Finally the instrumentation will be discussed in detail.

4.2 Blowdown Compressor Facility

4.3.1 Basic Operation of Facility

The experiments were conducted using the Blowdown Compressor Facility at the M.I.T. Gas Turbine Laboratory. The facility is able to test a single compressor/fan stage with a diameter of up to 23.125 Inches (0.587 meter) at rotational speeds in excess of 10,000 RPM at steady state for 70 - 100 milli seconds. The facility is described in detail in reference 4.1 so only a summary will be given here.

The Blowdown Compressor was conceived by Prof. J.L. Kerrebrock in the late sixties and finds its roots at the fact that most aerodynamic phenomena in a gas turbine rotor have time scales of at the most a rotor revolution. For example, the flow time through the rotor is approximately 1/20 of the rotor revolution time. So, relevant aerodynamic data can be acquired when the flow is steady for several rotor revolutions. This enables a very cost effective experiment. Basically the facility consists of a supply tank (125 ft^3) , a dump tank($\approx$ 300 ft^3) and a 61 inch long 2 ft diameter tube connecting both tanks as can been seen in figure 4.1. The supply tank and the tube are separated by a valve. The supply tank is filled with a CO_2/Argon or formerly a Freon12/Argon mixture. The experiment is conducted by evacuating the dump tank and the tube and bringing the rotor (figure 4.2) which is positioned in the tube upstream of a choke plate up to speed using a 9 kWatt electrical motor. When the proper speed is exceeded the electrical motor is turned off and the rotor while freewheeling decelerates slowly. When the required speed is reached, the valve separating the tube and supply tank is opened very quickly and the experiment has started. The gas flows from the supply tank through the tube and the rotor to the dump tank. The rotor does work on the flow and therefore decelerates. The deceleration is determined by the rotor inertia and the amount of work the rotor does. During the experiment the gas in the supply tank expands isentropically (the time scale is very short, of the order of a quarter second) and therefore the temperature of the gas decreases isentropically. As was mentioned above, the rotational speed of the rotor decreases at the same time. By choosing the initial pressure in the supply tank for a given rotor inertia and rotor operating point correctly, the ratio of rotational speed squared over total inlet temperature can virtually be made constant over period of 70 to 100 milliseconds due to the similar form of both functions. So the tip and axial Mach number are constant over this period. Typical pressure traces for the supply and the dump tank, the supply tank temperature, rotational speed and Reynolds number based on tip streamline chord and mean velocity over blade are shown in figure 4.4. The Reynolds number is not constant during the test time but its change is minor and acceptable. The test time is terminated by the unchoking of the choke plate: the axial Mach number decreases while the tip Mach number does not change significantly which results in the operating point moving up the constant corrected speed line until finally the compressor enters a rotating stall. Because no stator was installed during these experiments, the flow contains swirl at the choke plate. This causes the choke plate to unchoke considerably earlier than would be expected from the supply tank and dump tank pressure ratio. The length of the test time can be easily deduced from the pressure ratio over the compressor. Most experiments yielded an usable test time of approximately 80 msec.

In order to obtain clean flow at the inlet of the compressor, upstream of the compressor, a boundary layer bleed is incorporated in the compressor casing allowing approximately 10% of the flow to bypass the compressor.

4.4.2 Modification of Basic Facility

Suction Fluid Removal System

For this specific experiment, the basic facility as described above was modified by Joseph Dennis and the author in the following manner, also described in reference 4.2: To facilitate fluid removal from the blade surfaces, a hollow stationary "spider" was installed in front of the rotor which enabled fluid removal from the rotating disk assembly, via a triple knife-edge rotating seal and hollow struts, to the exterior of the facility. As can be seen in figure 4.6, the "spider" is the long blunt nosed cylinder with the legs. At the exterior the removed fluid was piped to a small 11.4 ft^3 suction dump tank.

Fast Acting Valve

During the course of this research project the explosive diaphragms formerly used to initiate the flow were replaced by a fasting acting valve. For completeness the explosive diaphragms are discussed in the experimental setup appendix. A detailed discussion of the new fast acting pneumatic valve can be found in reference 4.3. It contains detailed drawings and operating instructions.

Test Gas Recycle System

Because of the rising prices of Freon12 and environmental concern a test gas recycle system was added to the facility in conjunction with the valve. It enables the same test gas to be used for multiple experiments. Details are discussed in the experimental setup appendix.

4.5 Blowdown Compressor Rotor

4.5.1 Basic Description

The Blowdown Compressor rotor was designed together with the facility. Its prime use was to be to test the facility. It was fabricated using the Gas Turbine Laboratory Blade Cutter. Two full rotors of this design exist: the regular Blowdown Compressor rotor and the aero elastic Blowdown Compressor rotor. The roots and disks of the two rotors are slightly different. The first has solid steel pins holding the blades in the disk, the second has spring pins. The rotors have a diameter of 23.125 Inches and a constant streamline chord of 3.165 Inches. The shape of the blade is defined by 6 streamline surfaces which are faired into a blade as can be seen in figure 4.7. The aerodynamic properties of the 6 stream surfaces are listed in table 4.1 which is taken from reference 4.1. As can be seen the rotor has an inlet hub to tip ratio of 0.5, 23 blades and a solidity of 1 at the tip. Its design pressure ratio is 1.6 at an efficiency of approximately 88%. As is described in reference 4.1, double circular arc sections were used for the inner (subsonic) portion of the blade and multiple circular arcs were used for the supersonic portion. The supersonic portion has a flat suction surface faired into a circular arc so as to put the point of maximum thickness at 66% chord. Even more details can be found in reference 4.1.

4.5.2 Modification

Boundary Layer & Shock Position Assessment of Base Line Blade

Using MISES which is described in detail in chapter CFD, the boundary layer on the blade was assessed. Typically the boundary layer separates at the impingement of the shock on the suction surface. The boundary layer displacement thickness going into the shock boundary layer interaction was computed to be typically less than 0.3% chord. Because of the extensive separation in this rotor at design point the quasi 3D MISES could not accurately predict the position of the shock in the passage, pictures were used instead. These pictures were made by Epstein (reference 4.4) and show density distributions for several cross sections and thus the position of shock. From the available photos it was established that the passage shock was positioned at 66.7% chord at 88% span, 63.6% at 83% span and 62.2% span at 80% span. These points form approximately a straight line defined by $x/c=0.173 + 0.561\ R/R_t$. The streamline separating the supersonic from the subsonic region enters the rotor at 72% span and leaves the rotor at 79% span. This established the inner end of the shock at approximately 60% chord at 76% span.

Suction system

Traditionally there are three different approaches to doing suction on an airfoil: slot, porous surface or a boundary layer scoop. For this experiment the scoop was chosen. The scoop combines partial recovery of the dynamic head, positioning of the shock and restarting the boundary layer at the shock. Recovery of the dynamic head increases the pressure necessary at the root of the blades in order to suck the fluid down against the centrifugal force. The scoop also acts as a shock trap. It sets and stabilizes the position of the shock. When the scoop is positioned just upstream of the shock, the high pressure behind shock increases the suction mass flow moving the shock backward. When the shock position is just aft of the scoop entrance the opposite occurs.

In order to assess the effect of boundary layer suction in the existing Blowdown Compressor rotor the scoop was positioned at the shock positions as indicated by the pictures taken by Epstein. Because of financial and maximum mass flow constraints, only 5 blades out of 23 were modified to have the scoop and boundary layer suction was only applied in the supersonic region of the blade. Mechanical constraints confined the passages which bring the suction fluid to the root of the blade, to the pressure side of the blade which is rather flat. It would have been more difficult to mill the passages in the suction side and restore the suction side to its original shape. Therefore the suction fluid had to pass from the suction side of the blade to pressure side of blade effectively cutting the original blade in two. In order to retain the structural integrity of the blade the scoop was therefore not extended to the tip. When boundary layer suction is applied to a new design this problem can be circumvented by simply making the blade in two parts which are bonded together.

Based on all these constraints, the resulting scoop extends from 76% to 95% span. The scoop height was set to 1 mm corresponding roughly to a third to a half of the boundary layer thickness. Whether the Hall criterion is satisfied can be roughly checked by assuming a 1/7 power profile considering that the boundary layer typically has a shape factor of around 1.2 to 1.5 upstream of the shock. For a Mach number of 1.4-1.6 entering the shock the critical Mach number is 1.1-1.3. For a 1/7 power profile (figure 4.8) this critical Mach number occurs approximately at 20% of the boundary layer thickness therefore the criterion is satisfied.

The scoop was given a sharp leading edge parallel to the airfoil wall which gradually faired back to the original blade surface at the trailing edge. In addition an internal diffuser was placed directly behind the inlet of scoop to slow down the fluid which just entered the scoop to minimize the mixing losses in the internal channels. The detailed geometry and the process of fabrication of the scoop is described in the blade fabrication appendix.

4.6 Instrumentation

The Blowdown Compressor facility is equipped with two principal groups of sensors: low frequency response sensors and very high frequency sensors.

4.6.1 Low Frequency Response Instrumentation

The low frequency response instrumentation provides information about the state of the facility prior to or after a run. It includes Bourdon gauges to measure the pressure in both tanks, a McLeod vacuum gauge to measure very low pressure, and thermocouples in the supply tank and the suction dump tank. The former enables calculation of the (total) temperature in the supply tank during the experiment using isentropic relations. Recently a device was added to the facility to measure the speed of sound of the mixture in the supply tank prior to the experiment. Details are described in Experimental Setup Appendix.

4.6.2 High Frequency Response Instrumentation

Pressure Transducers

This group consists exclusively of high speed Kulite transducers mounted at various positions in the facility.

To assess the pressure variations on the blowdown time scale, transducers are mounted in the supply tank and the dump tank, at the inlet of the dump tank, and between the rotor and the downstream choke plate. The supply tank pressure probe provides the total pressure and temperature at the rotor face.

For this specific experiment 3 wall static probes were mounted upstream of the rotor. The first was positioned 0.16 Chord (0.5 Inch) upstream. The other 2 were mounted at 0.95 chord and 1.73 chord upstream (3 and 5.5 Inches) as can be seen in figure 4.9. A total pressure probe was mounted in the first port at 2.53 chord upstream (8 inches).

In addition 2 wall statics were mounted at 0.91 chord and 1.83 chord downstream. The final

series of experiments also had wall statics at the opposite side of the casing at 0.11 chord upstream (@180 deg [•]) and 0.95 chord downstream (@228.7 deg [•]). Figure 4.10 illustrates their positions on the back side of the test section.
The wall statics and the total pressure probe are of the type Kulite XCQ-062-25D. This is an ultra miniature transducer which comes in a 0.062 mils diameter and 375 mils long cylinder. It has a natural frequency in excess of 500 kHz and is thus fast enough to register the shockwave in front of the rotor.

[•] angles are measured in the direction of rotor rotation (anti clockwise when looking at the face of the Blowdown Compressor rotor).
[+] Rotor chord at tip is 3.140 Inches.

To be able to measure the mass flow of the removed boundary layer fluid the spider plenum contains a transducer which measures static pressure and a total pressure probe is located in the exit of one of the choked spider legs. The performance chapter will elaborate on the details of the determination of the mass flow.

The most important pressure data is obtained from the 4Way probe which is described in the following section

4Way probe
The 4Way probe was designed to resolve the unsteady flow in the wakes behind turbo machinery blades. The probe features 4 silicon diaphragm type transducers mounted on a elliptical shaped cylinder cut off at a 45 degrees angles. A photograph of the probe is shown in figure 4.11. The 4 small transducers which set the diameter of the probe to 130 mils, are mounted directly in the flow in order to achieve a frequency response of the order of 25 kHz to 50 kHz depending on the quantity desired. The four transducers measure four pressures which can be converted using a suitable calibration into a total pressure (P_t), static pressure (P_s), tangential (θ) and radial angle (ϕ). (This can easily be seen when considering that the P_1 & P_4 provide radial angle information, P_1 & P_2/P_3 provide static and total pressure information and P_2 & P_3 provide the tangential angle.) Using P_t, P_s, θ and ϕ, the flow Mach number and its components can be determined. For a detailed discussion of this probe's geometry, transducers, calibration scheme and error analysis see appendix C.

Position Indicators
To be able to measure the rotational position of the rotor and its rotational speed the shaft is equipped with magnetic and optical encoders. All translating probes are equipped with position indicators allowing determination of the exact position of the probes during the experiment. The fast acting valve is also equipped with a position indicator. Details on the use of these indicators can be found in the Experimental Setup appendix.

4.7 Data Acquisition System

During December 1992 the old data acquisition system of the Blowdown Compressor was replaced by the current: A Dell 450DE 80486 32MB RAM EISA computer and initially two but later three ADTEK 12 Bit data acquisition cards. This enables simultaneous recording of 3*8=24 independent data channels at 333 kHz for more than a second. This data is automatically stored on the hard disk of the computer and can be easily loaded in mathematical programs such as Matlab for further handling. More details about these cards and their software can be found in the Experimental Setup appendix.

4.8 Filtering and Amplification

No signal expected to contain high frequencies of interest was filtered. The relative total pressure transducer on one of the rotor blades, the absolute total pressure probe in port 1, the transducer in the spider and the linear position of the valve were filtered using a 50 kHz low pass filter. The positional indicator of the 4Way probe and the P_t were filtered using 1 kHz and 10 kHz low pass filters, respectively.
All signals expected to be of great importance were amplified using Pacific Instruments 10 channel amplifiers: P_{4w1-4}, dP_{21}, dP_{22}, P_{trel}, P_{t1}, P_{s4}, P_{s3}. All other pressure signals were amplified by either the system pressure built in amplifier (Epstein amplifier) or older Burr Brown amplifiers. When the amplifier did not contain a balancing circuit one of the balancing boxes was used. They contain a balancing circuit and a rechargeable battery to supply power to the transducer.

References:

4.1 Kerrebrock, J. L., The MIT Blowdown Compressor Facility, MIT Gas Turbine Report 108, Sept 1975.

4.2 Dennis, J., An experimental study of blade tip clearance suction applied to a high speed compressor, Master's thesis, Department of Aeronautics and Astronautics, Massachusetts Institute of Technology, 1993.

4.3 Ziminsky, W.S., Design of a high pressure ratio transonic compressor stage with active boundary layer control. Master's thesis, Department of Aeronautics and Astronautics, Massachusetts Institute of Technology, 1996.

4.4 Epstein, A.H., Quantitative density visualization in a transonic compressor rotor. MIT-GTL report No 124, September 1975.

4.5 Epstein, A.H., "Quantitative Density Visualization in a Transonic Compressor Rotor", Journal of Eng. for Power, Vol. 99, July 1977, pp. 460-475.

r_1/r_T	0.50	0.60	0.70	0.80	0.90	1.0
r_2/r_T	0.64	0.71	0.78	0.85	0.93	1.0
M_T	0.60	0.72	0.84	0.96	1.08	1.2
M_T'	0.78	0.88	0.98	1.07	1.19	1.3
β_1'	50.2	55.2	59.2	62.5	65.2	67.4
β_2'	23.8	35.7	44.2	50.6	55.6	59.3
σ_r	2.00	1.67	1.43	1.25	1.11	1.00
D_r	0.50	0.49	.45	0.43	0.40	0.38
i_c	11.5	10.4	9.9	7.7	4.5	1.3
ϕ	22.0	14.7	9.0	7.5	6.7	8.1
α_1	38.7	44.8	49.3	55.0	61.2	66.1
α_2	16.7	30.1	40.3	47.5	54.1	58.0
γ	28.9	38.1	45.0	51.1	56.3	61.7
t/c	0.10	0.086	0.072	0.058	0.044	0.030
M_3	0.68	0.65	0.62	0.60	0.58	0.57
β_3	47.5	44.6	42.0	39.4	37.0	35.0
r_4/r_T	0.68	0.74	0.80	0.86	0.93	1.00
σ_s	1.57	1.41	1.28	1.18	1.08	1.00
D_s	0.55	0.53	0.52	0.50	0.48	0.47

Table 4.1 Aerodynamic properties of Blowdown Compressor Rotor

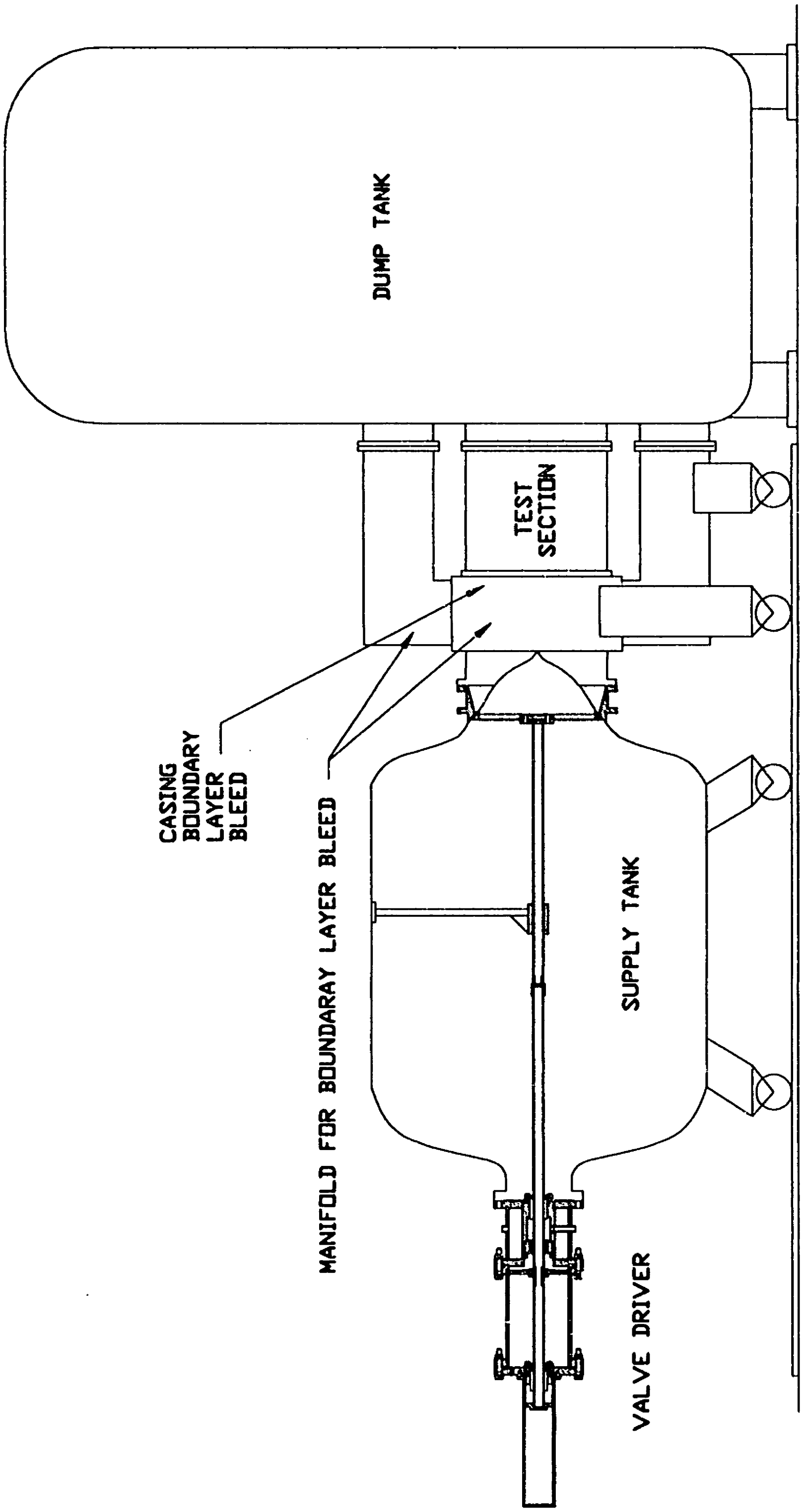

Figure 4.1 Blowdown Compressor Test Facility

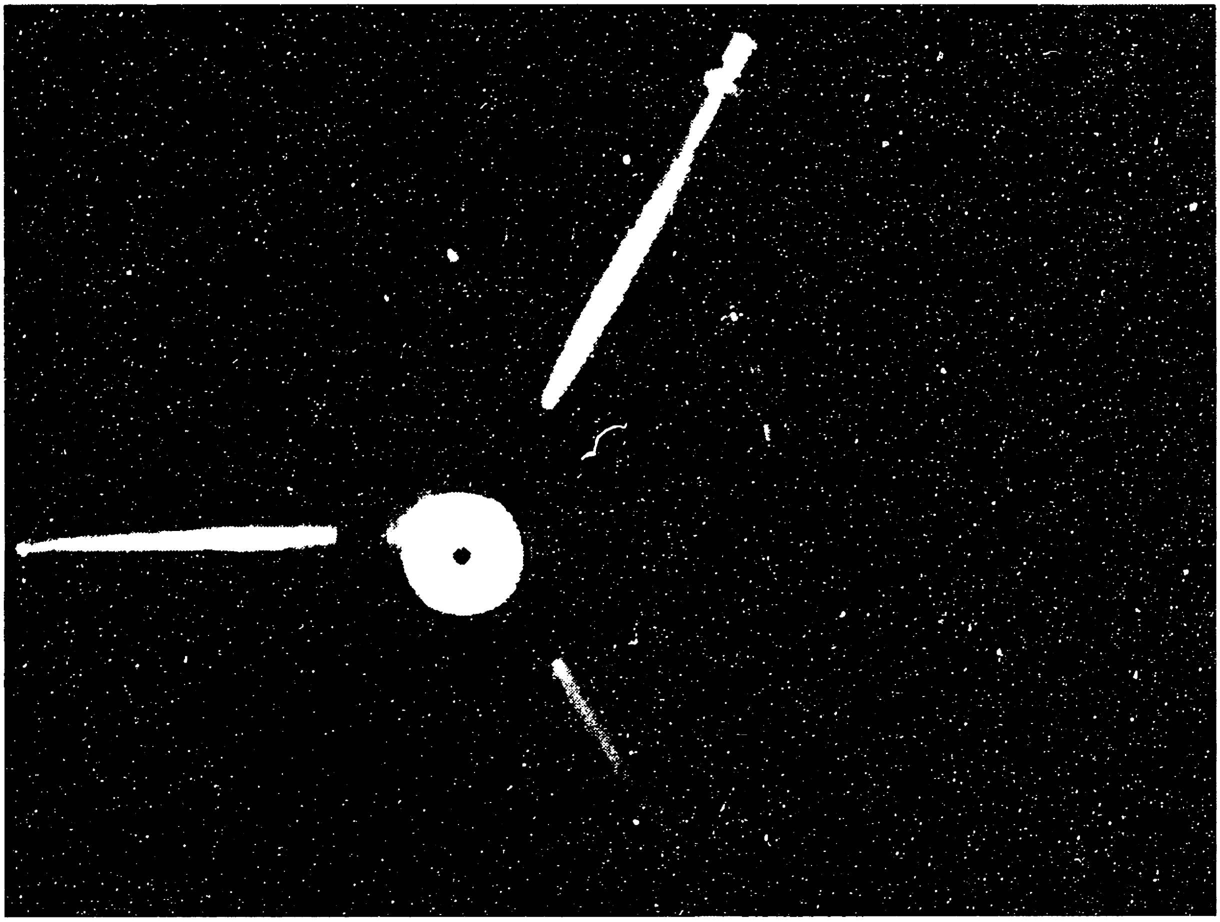

Figure 4.2 View of Rotor Installation.

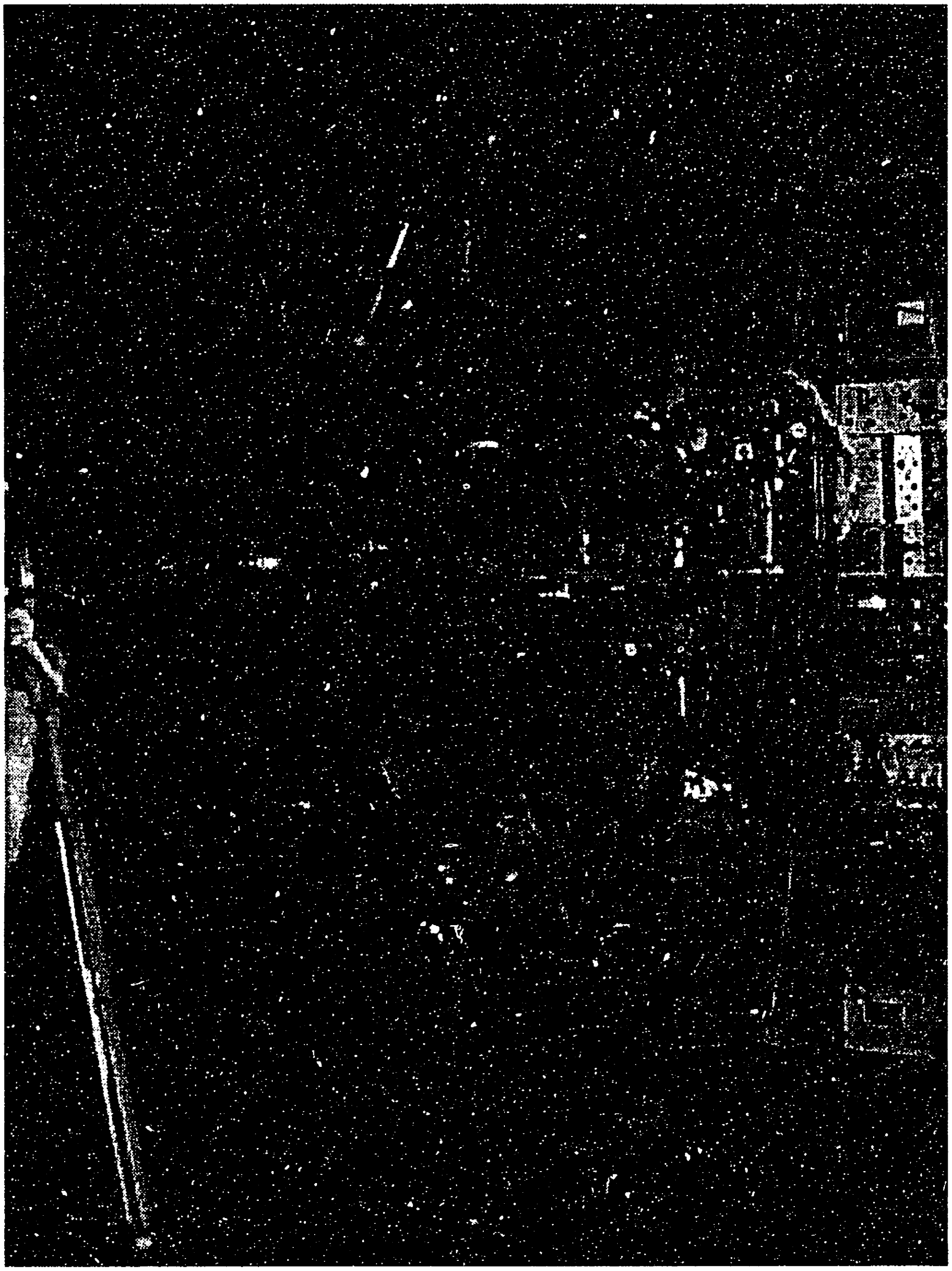

Figure 4.3 Test section of Blowdown Compressor

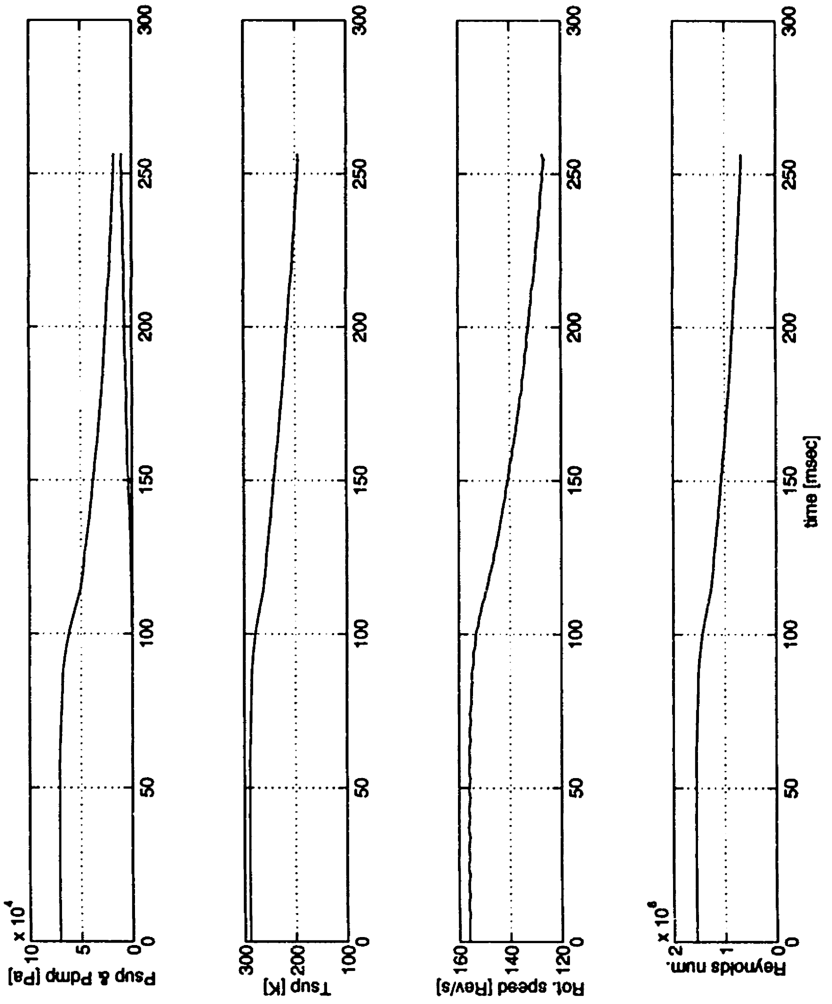

Figure 4.4 Typical pressure, temperature, rotational speed and Reynolds versus time

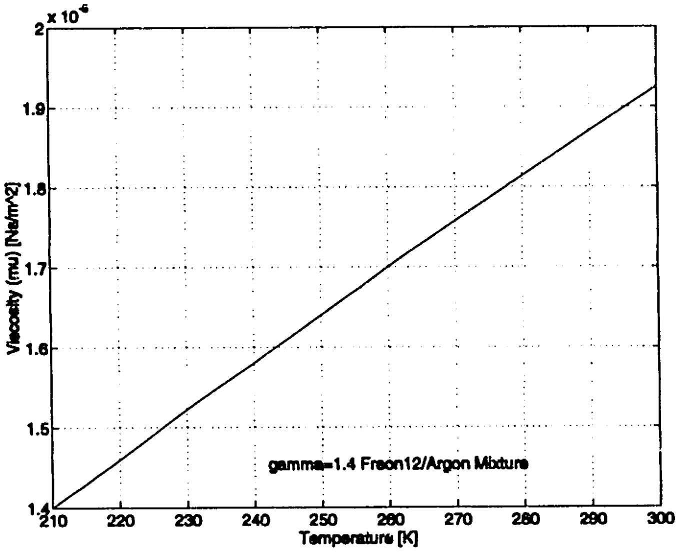

Figure 4.5 Viscosity of Freon12/Argon mixture as function of temperature

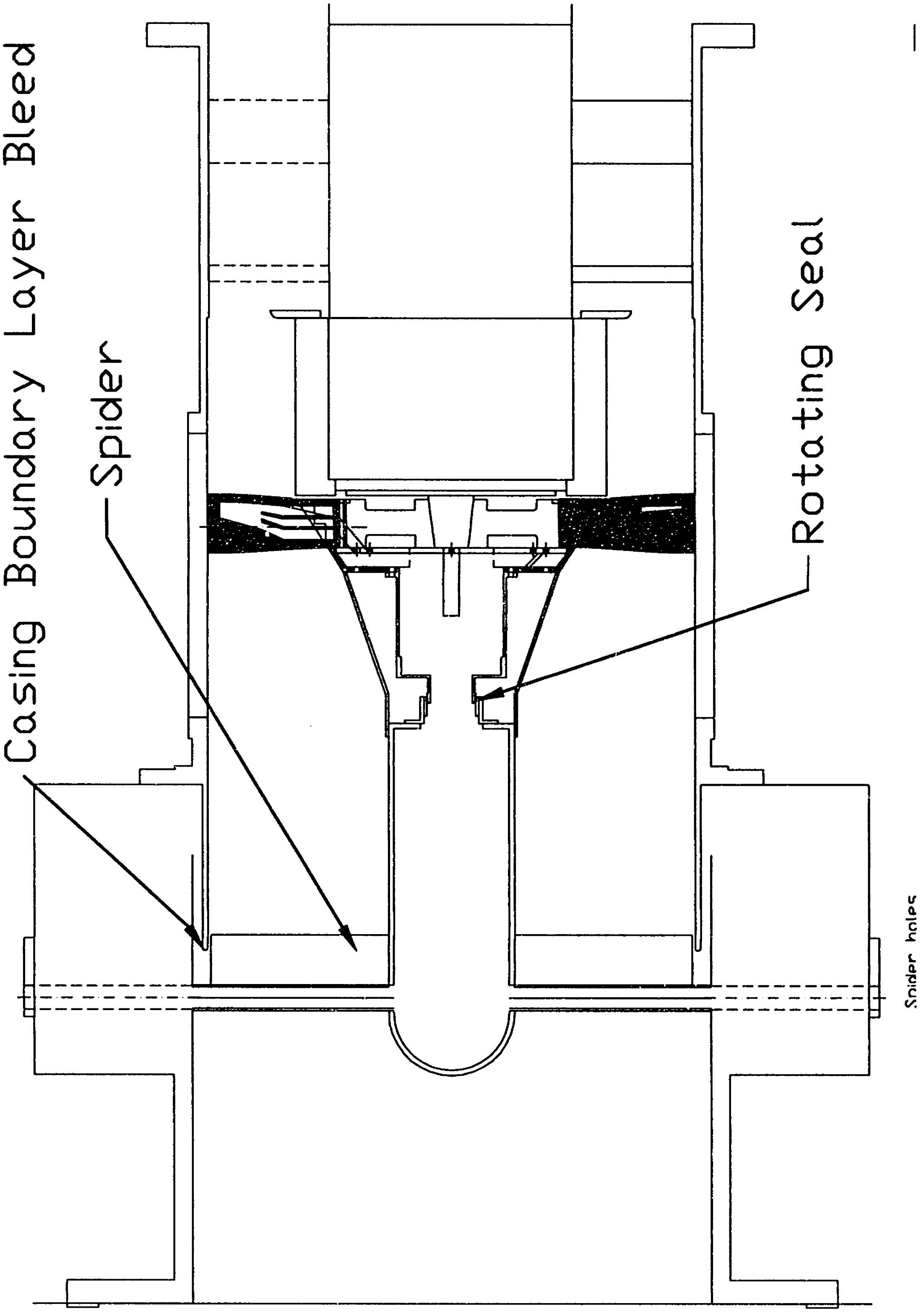

Figure 4.6 Cross section of test section with boundary layer fluid system installed

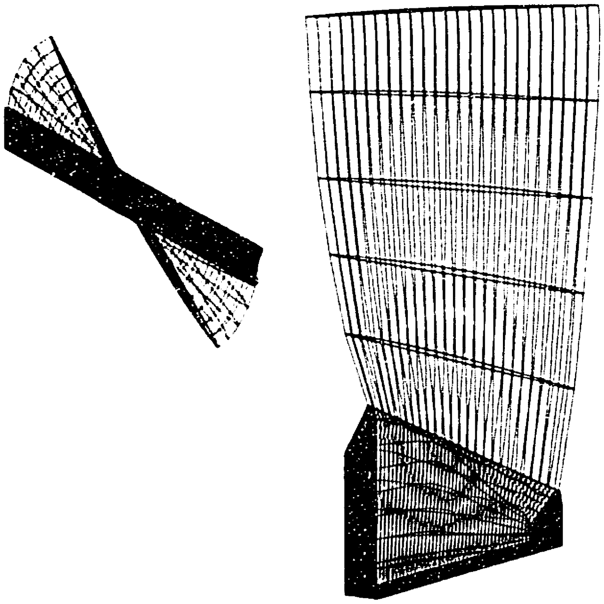

Figure 4.7 Streamline surfaces of Blowdown Compressor Rotor

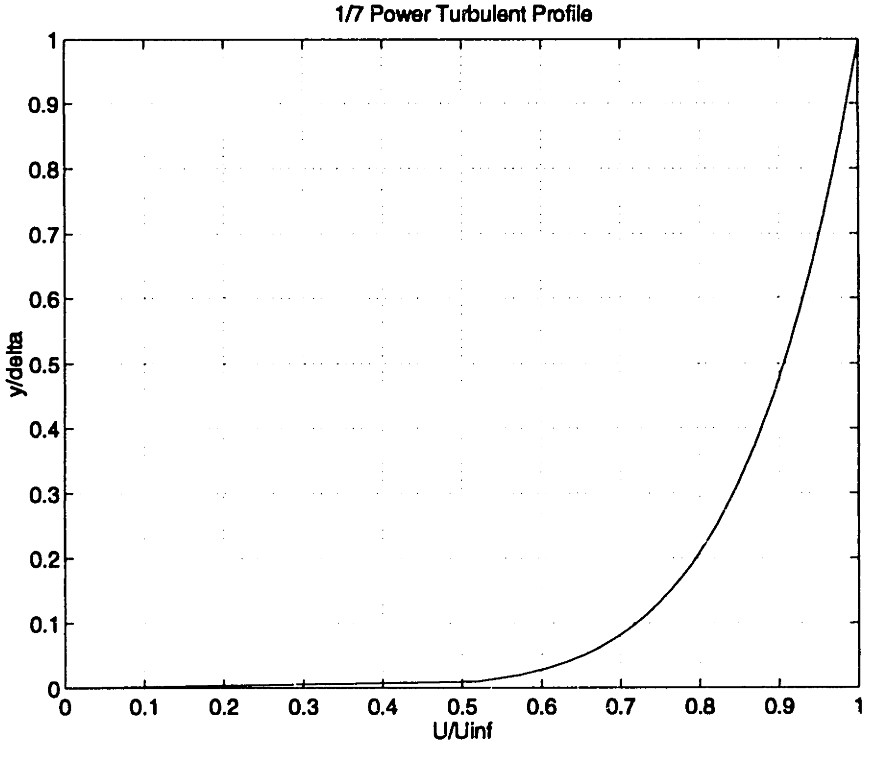

Figure 4.8 Nondimensionalized 1/7 power boundary layer profile

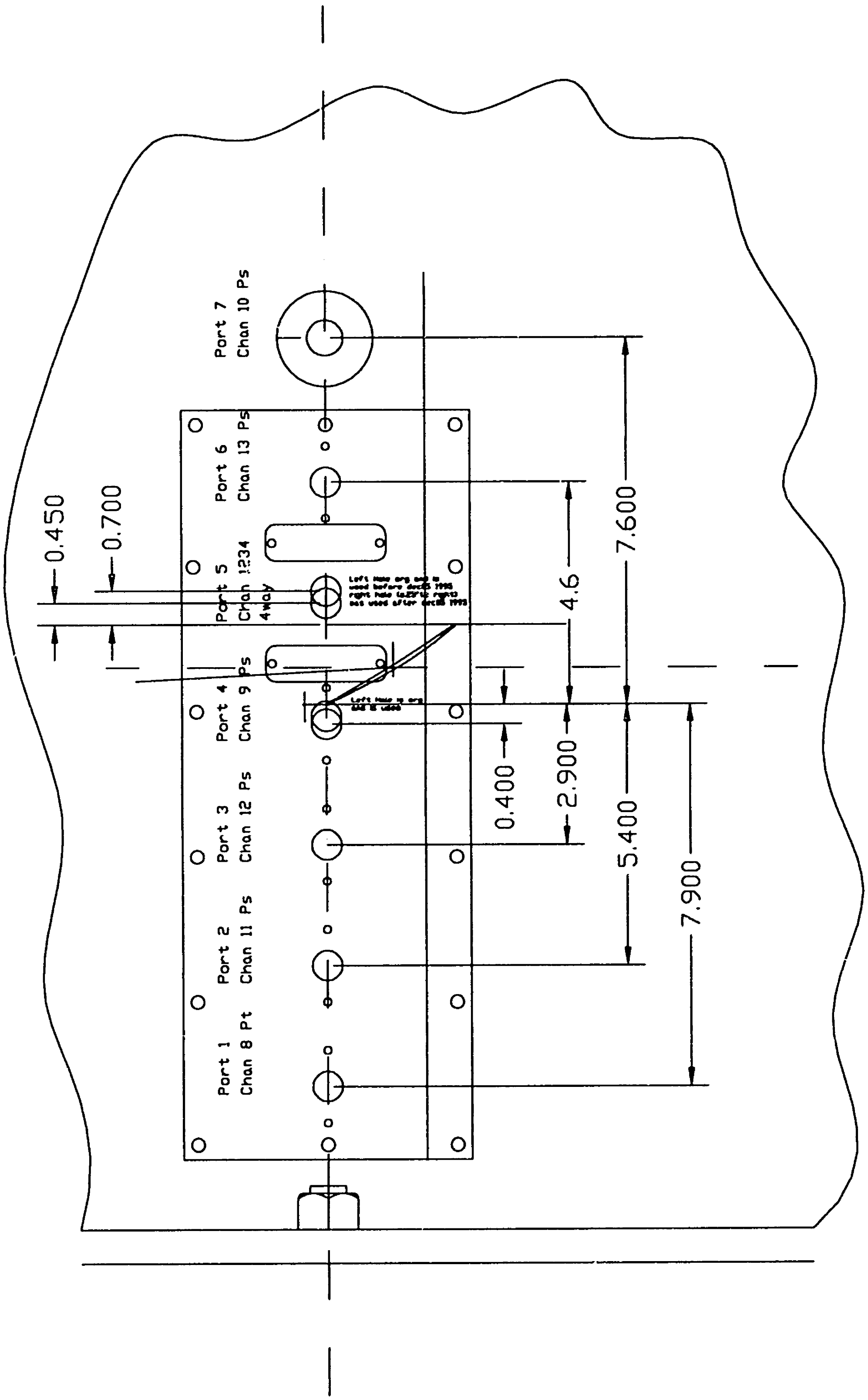

Figure 4.9 Position of wall static probes relative to rotor

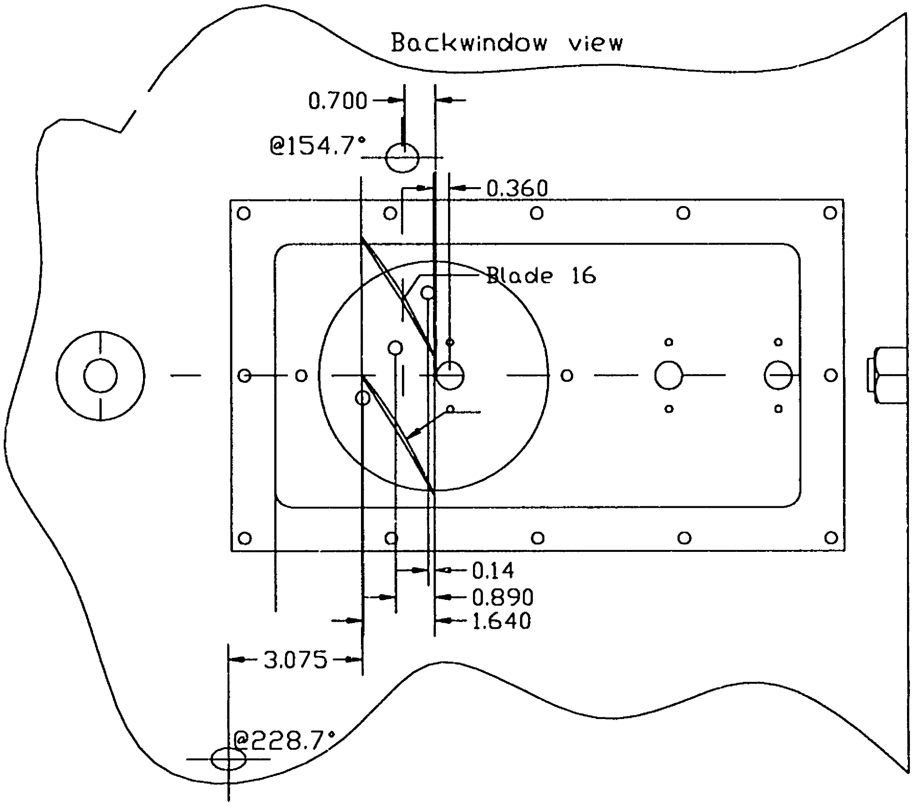

Figure 4.10 Position of wall static probes and TE/LE indicator on back side of test section

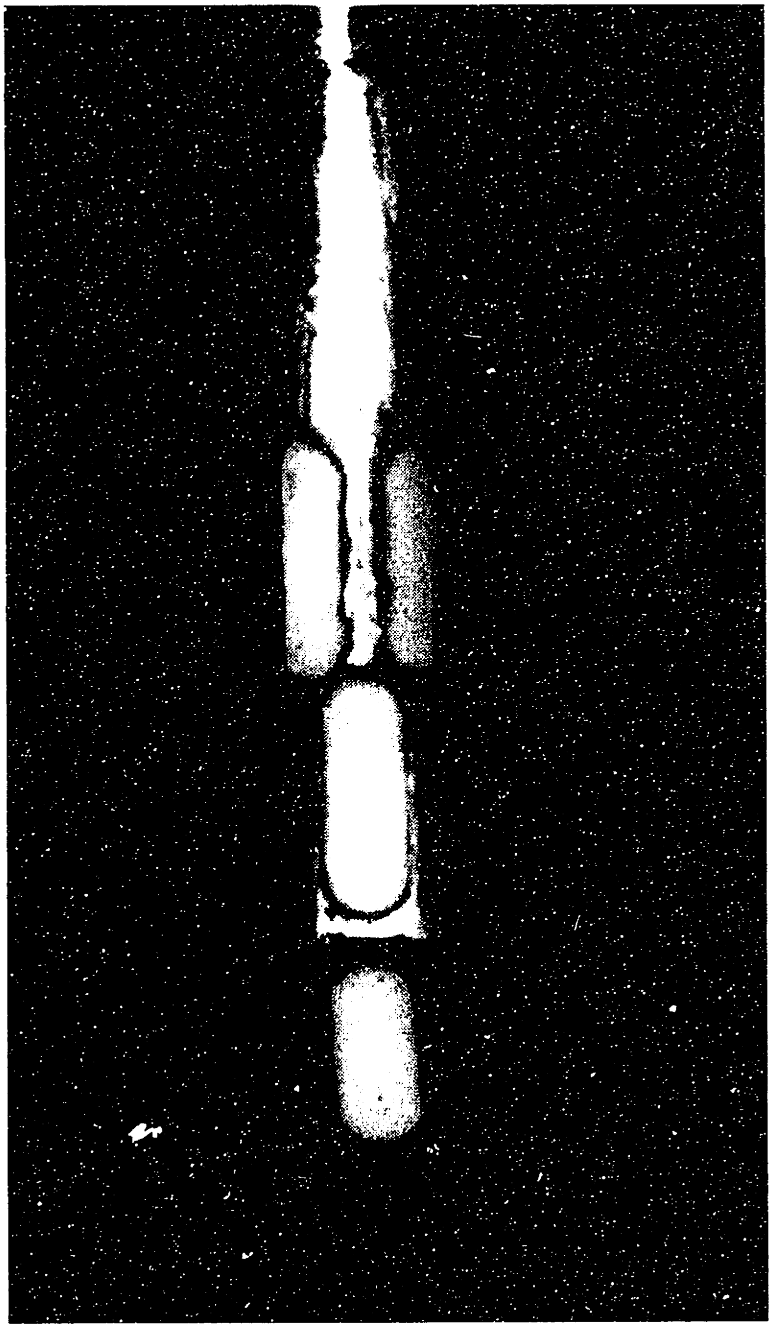

Figure 4.11 Photograph of 4 way probe

Chapter 5 Performance Measurements

5.1 Introduction

This chapter describes how measured quantities were used to calculate performance parameters, such as pressure ratio, efficiency, mass flow etc. The subscripts used in this chapter indicate the positions of the probes at the experimental facility which are shown in figure 5.1. Thus subscript 1 denotes quantities at port 1. The rotor is positioned between port 4 upstream and port 5 downstream. More details on the precise positions of the probes can be found in the experimental setup chapter.

5.2 Supply Tank Pressure and Temperature

The pressure in the supply tank is simply obtained from the transducer mounted in the tank. It is used to nondimensionalize the pressures throughout the experiment. The gas in the tank expands isentropically in the supply tank thus the supply tank temperature is obtained from:

$$T_{supply} = T_{supply}(t=0) \ [\ P_{supply}/P_{supply}(t=0)\ ]^{\gamma/(\gamma-1)} \qquad [5.1]$$

5.3 Axial Mach Number and Static Temperature at Rotor Inlet

The axial Mach number at the rotor face is determined from the pressure in port 2, 0.16 chord upstream of the rotor and the supply tank pressure:

$$M_{ax4} = \sqrt{\frac{2}{\gamma-1}\ [(\frac{P_{supply}}{P_{s4}})^{(\gamma-1)/\gamma} -1\ ]} \qquad [5.2]$$

Using M_{ax4} the static temperature at the rotor face and the accompanying speed of sound can be easily calculated:

$$T_{s4} = \frac{T_{supply}}{1+\frac{\gamma-1}{2}M_{ax4}^2} \qquad [5.3]$$

$$a_4 = \sqrt{\gamma R T_{s4}} \qquad [5.4]$$

5.4 Tip Mach Number

In most Blowdown Compressor literature the tip Mach number mentioned is based on the supply tank absolute total temperature:

$$M_{tipt} = \frac{\omega\ R_{tip}}{\sqrt{\gamma R T_{supply}}} \qquad [5.5]$$

Where ω is the rotational speed of the rotor in radians per second.
The tip Mach number based on local inlet conditions is slightly higher:

$$M_{tip} = \frac{\omega\ R_{tip}}{a_4} \qquad [5.6]$$

5.5 Temperature Ratio and Pressure Ratio of the rotor

To calculate the efficiency of the rotor the total temperature ratio and the total pressure ratio over the rotor are required. The latter is obtained by dividing the total pressure measured by the 4Way probe by the supply tank pressure:

$$PR = \frac{P_{t5}}{P_{t0}} = \frac{P_{t\ 4way}}{P_{supply}} \qquad [5.7]$$

Based on a method developed by Thompkins (ref. 5.1) the temperature ratio is calculated using the Euler equation:

$$C_p\ \dot{m}\ (T_{t5} - T_{t4}) = \dot{m}\ \omega\ r\ (v_{\theta 5} - v_{\theta 4}) \qquad [5.8]$$

Station 5 is just downstream of the rotor and station 4 is just upstream. $v_{\theta 4}$ is the swirl velocity entering the rotor and is equal to zero. This method was developed by Thompkins (reference 5.1). Earlier studies and comparisons to steady state measurements have shown this to be a reliable and accurate method of obtaining the performance of a rotor.
The Euler equation can be nondimensionlized by rearranging its terms:

$$\frac{T_{t5}}{T_{t4}} = (\gamma-1)\,\frac{r}{R_{tip}}\,\frac{\omega\,R_{tip}}{\sqrt{\gamma R T_{t4}}}\,\frac{v_{\theta 5}}{\sqrt{\gamma R T_{s5}}}\,\sqrt{\frac{T_{t5}}{T_{t4}}}\,\frac{1}{\sqrt{1+\frac{\gamma-1}{2}\,M_5^2}} + 1 \qquad [5.9]$$

$$\frac{T_{t5}}{T_{t4}} = (\gamma-1)\,\frac{r}{R_{tip}}\,M_{tipt}\,M_{\theta 5}\,\sqrt{\frac{T_{t5}}{T_{t4}}}\,\frac{1}{\sqrt{1+\frac{\gamma-1}{2}\,M_5^2}} + 1 \qquad [5.10]$$

where M_5 is the Mach number of the flow exiting the rotor in the absolute frame and $M_{\theta 5}$ is the tangential component of M_5. Both are measured by the 4Way probe just behind the blade. The above equation can be numerically solved for the T_{t5}/T_{t4} using the Newton method.

5.6 Isentropic Efficiency

The isentropic efficiency for a streamline is calculated combining the now known temperature and pressure ratio over the rotor:

$$\eta = \frac{\left(\frac{P_{t5}}{P_{t4}}\right)^{\frac{\gamma-1}{\gamma}} - 1}{\frac{T_{t5}}{T_{t4}} - 1} \qquad [5.11]$$

5.7 Rotor Mass Flow

Due to the complexity of the experiment and changes in inlet total pressure and temperature accurate mass flow measurements are very difficult to obtain. However a realistic estimate can be made using several methods. When a stator which removes all swirl, is installed, the mass flow can be obtained by using the area of the choke plate. However this requires accurate knowledge of the effective area at the choke plate which is not known when there is strong swirl in the flow through the orifice. An alternate method is to use the decay of temperature and pressure in the supply tank as a measure of the mass flow:

$$\frac{dm}{dt} = \frac{d(\rho V_{supply})}{dt} = V_{supply}\frac{d}{dt}\left(\frac{P}{RT}\right) \qquad [5.12]$$

where V, P and T are the supply tank volume, pressure and temperature. When the isentropic relation between supply tank pressure and temperature is substituted a very simple equation results:

$$\dot{m} = \frac{V_{supply}}{\gamma R T_{supply\ t=0}} \frac{d}{dt}(P_{supply}) \qquad [5.13]$$

When this method is used the mass flow is known to approximately ±5%
The casing boundary layer bleed however removes some of this mass flow so the actual mass flow through the rotor is approximately 10% smaller ($\delta=0.1$):

$$\dot{m} = \frac{(1-\delta)V_{supply}}{\gamma R T_{supply}} \frac{d}{dt}(P_{supply}) \qquad [5.14]$$

A most accurate measurement of mass flow could be obtained by integrating the axial Mach number behind the rotor while using the local total temperature and pressure ratio. The associated problem is however that this requires a complete survey over the rotor span including very close to the casing hub which is considered rather dangerous to the 4Way Probe and therefore this measurement was not performed during these sets of experiments. The last 8 percent (64-72) of the span were not surveyed and an estimate for the axial Mach number and temperature and pressure ratio at this location must be made to use this method.

5.8 Suction Mass Flow

Using a total pressure probe at the end of one of the spider legs the suction mass flow was estimated. The total pressure probe was installed in the leg with the highest pressure losses downstream of the measurement. Therefore this leg would unchoke first if the mass flow through the legs would be insufficient to choke all three legs . Based on the static pressure in the spider plenum and the total pressure at the exit of the spider leg it was easily verified that all spider legs were choked during the experiment as was intended. However determination of the bleed flow was complicated by some leakage at the rotating seal. This problem was addressed by subtracting the mass flow measured at the spider in an experiment at the identical operating point but with no suction applied from the mass flow measured at the spider legs when suction was applied.

$$\dot{m}_{spiderleg} = C_{discharge} A \sqrt{\frac{\gamma}{R}} \frac{P_{tsp}}{\sqrt{T_{tsp}}} M_{sp} \left(1 + \frac{\gamma-1}{2} M_{sp}^2\right)^{-\frac{\gamma+1}{2(\gamma-1)}} \qquad [5.15]$$

$$\dot{m}_{suction} = \dot{m}_{spider\ leg\ suction} - \dot{m}_{spider\ leg\ no\ suction} \qquad [5.16]$$

After correcting for the leakage through the rotating seal the suction mass flow per blade was estimated to be 0.6%±0.1 of the mass flow through a blade.

References:

5.1 Thompkins, W.T. Jr., "An Experimental and Computational Study of the flow in a Transonic Compressor Rotor", MIT-GTL Report No. 129, 1976.

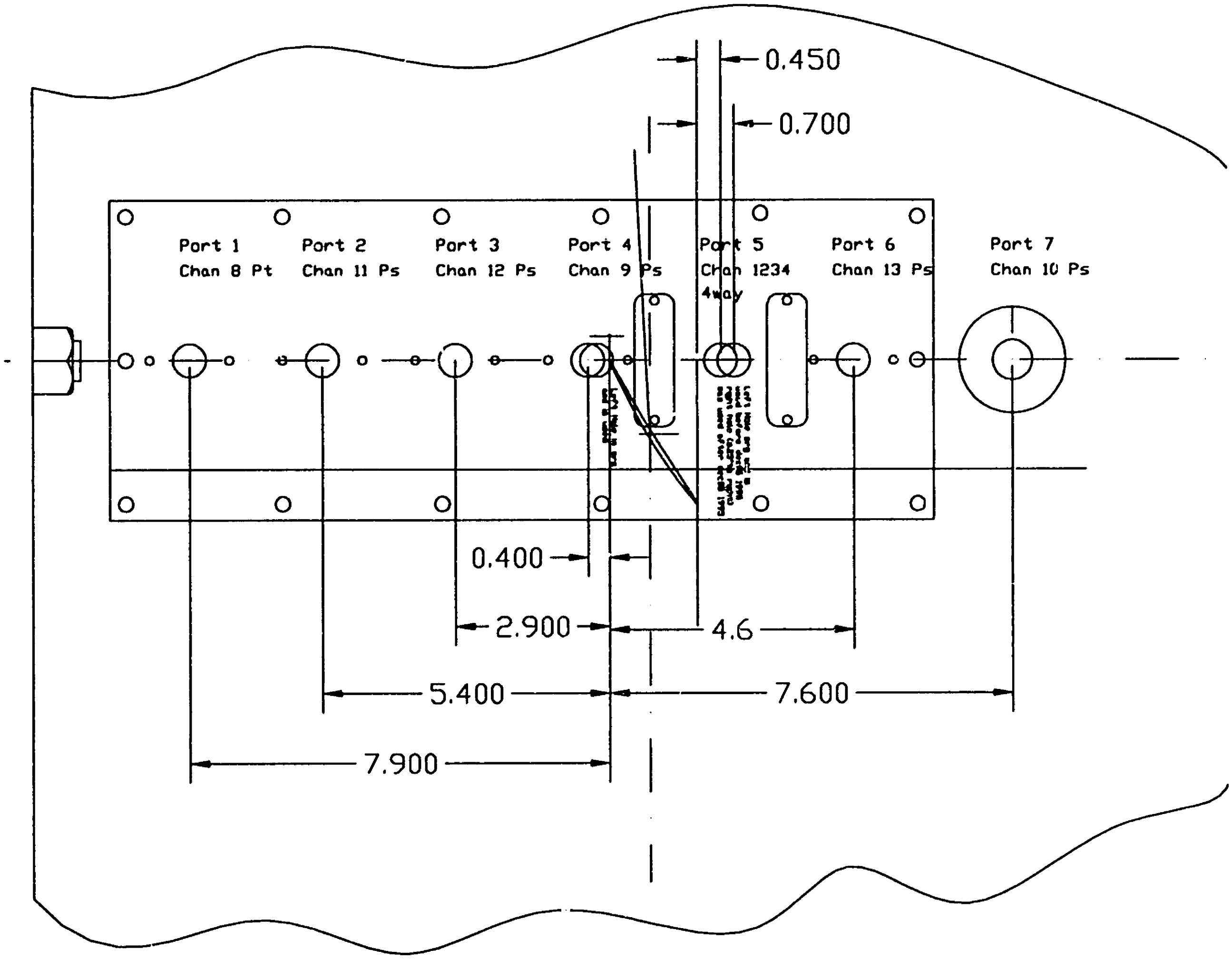

Figure 5.1 Positions of probes and port relative to rotor. Dimensions in inches.

Chapter 6 Computational Fluid Dynamics

6.1 Introduction

During this project extensive use has been made of MISES (reference 6.1). MISES is a quasi 3D coupled viscous inviscid numerical solver developed by Prof. M. Drela and H. Youngren at M.I.T.. It can calculate the flow on a meridional plane (usually similar to a conical plane in an axial compressor) through a rotating blade row. It consists of an inviscid Euler solver coupled to an integral boundary layer scheme which includes a transition prediction. The Euler equations and boundary layer equations are solved simultaneously, and are fully coupled via U_e and δ^*. Details on running the code can be found in reference 6.1. An early version of the MISES code was altered by the author to incorporate suction. Later versions were modified by Willy Ziminsky and Ali Merchant. The latest version is able to model multiple blades while some of the blades have suction. Input variables are $C_Q=\dot{m}_{bleed}/\dot{m}_{tot}$, chordwise position of bleed, length of bleed slot, and specification of sucked blades. To run MISES in the quasi 3D mode however the meridional plane has to be specified, along with the rotational speed and the change in stream tube height (measured in the radial direction). To accomplish this a streamline curvature code was used written by Larry Smilg (reference 6.2) based on the approach of Hearsey (reference 6.5).

6.2 Streamline Curvature Code

The streamline curvature code is described in detail in reference 6.2. The shape of the inlet, rotor and exit were inputted to the grid generator supplied with the streamline curvature code written by Larry Smilg. Some general comments and advice on using the code can be found in appendix D.

The design case was modeled by the streamline curvature code. Rotor losses were set to 10%, total temperature over the rotor to 1.16 and the inlet Mach number was set to 0.41 which is equivalent to a constant rotor axial inlet Mach number of 0.55 and a mass flow of 40 kg/sec using close to standard air inlet conditions ($T_{ambient}$=300 K, $P_{ambient}$=1.013 10^5 Pa). The design case corresponds to a throttle plate diameter of 17.21" and a tip speed of M=1.2. The resulting total pressure ratio is 1.6. The resulting grid which forms streamlines is shown in figure 6.1. Mach and static pressure contours are presented in figures 6.2-6.4.

6.3 Application of Streamline Curvature Solution to MISES

The converged streamline curvature grid was used to generate the streamline radius and height files MISES needs for its quasi 3D calculations. The inlet Mach number, rotation number and non dimensional pressure ratio which are required by MISES, were calculated based on the Mach and pressure distribution of the streamline curvature solution. The details of these processes are described in appendix E. Using the generated files MISES was run for streamlines entering the rotor at R/R_t=0.7, 0.8, 0.9 and 1.0 at design point. The Mach number distribution for the streamline at which most of the wake data was taken are shown in figure 6.5 And 6.6. Additional results are presented in appendix E.

6.4 MISES Modifications

The standard MISES v 2.3 was modified by Ali Merchant to include suction on the airfoils. The modifications are identical to the modifications which were made to the airfoil design code MSES and are described in the Master Thesis of Ali Merchant (reference 6.4). Basically, mass removal is simulated by decreasing the amount the inviscid Euler grid is offset away of the blade while simultaneously the boundary layer integral equation is locally modified to include wall-normal velocities, decreasing the moment thickness θ and indirectly the displacement thickness δ^*, thus simulating suction into the blade.

6.5 Modeling of Flow with Suction on a Fraction of Blades in Rotor

In order to qualitatively simulate the effect of 5 modified blades in a base rotor, MISES was modified to be able to accommodate multiple blade passages and individual blade boundary layer control. As is discussed in detail in appendix E, multiple not identical passages increase the required grid size enormously because the grid has to allow propagation of the disturbances which are not identical in each blade passage, upstream. This results in a long grid and therefore large grid. As a result the available computer equipment in the laboratory limited the analysis to 6 blade passages. Results are discussed in the Discussion of Experimental Results chapter.

References:

6.1 M. Drela, H. Youngren. A user guide to MISES 2.3, December 1995, Massachusetts Institute of Technology, Computational Aerospace Sciences Laboratory

6.2 L. Smilg. Design of a high pressure ratio fan stage to take advantage of boundary layer suction. Master's thesis, Department of Aeronautics and Astronautics, Massachusetts Institute of Technology, 1994.

6.3 W.S. Ziminsky. Design of a high pressure ratio transonic compressor stage with active boundary layer control. Master's thesis, Department of Aeronautics and Astronautics, Massachusetts Institute of Technology, 1996.

6.4 A. Merchant. Design and analysis of supercritical airfoils with boundary layer suction. Master's thesis, Department of Aeronautics and Astronautics, Massachusetts Institute of Technology, 1996.

6.5 R.M. Hearsey. A revised computer program for axial compressor design. Aerospace Research Laboratory Report ARL-TR-75-0001, Wright Patterson AFB, Dayton, Ohio, January 1975

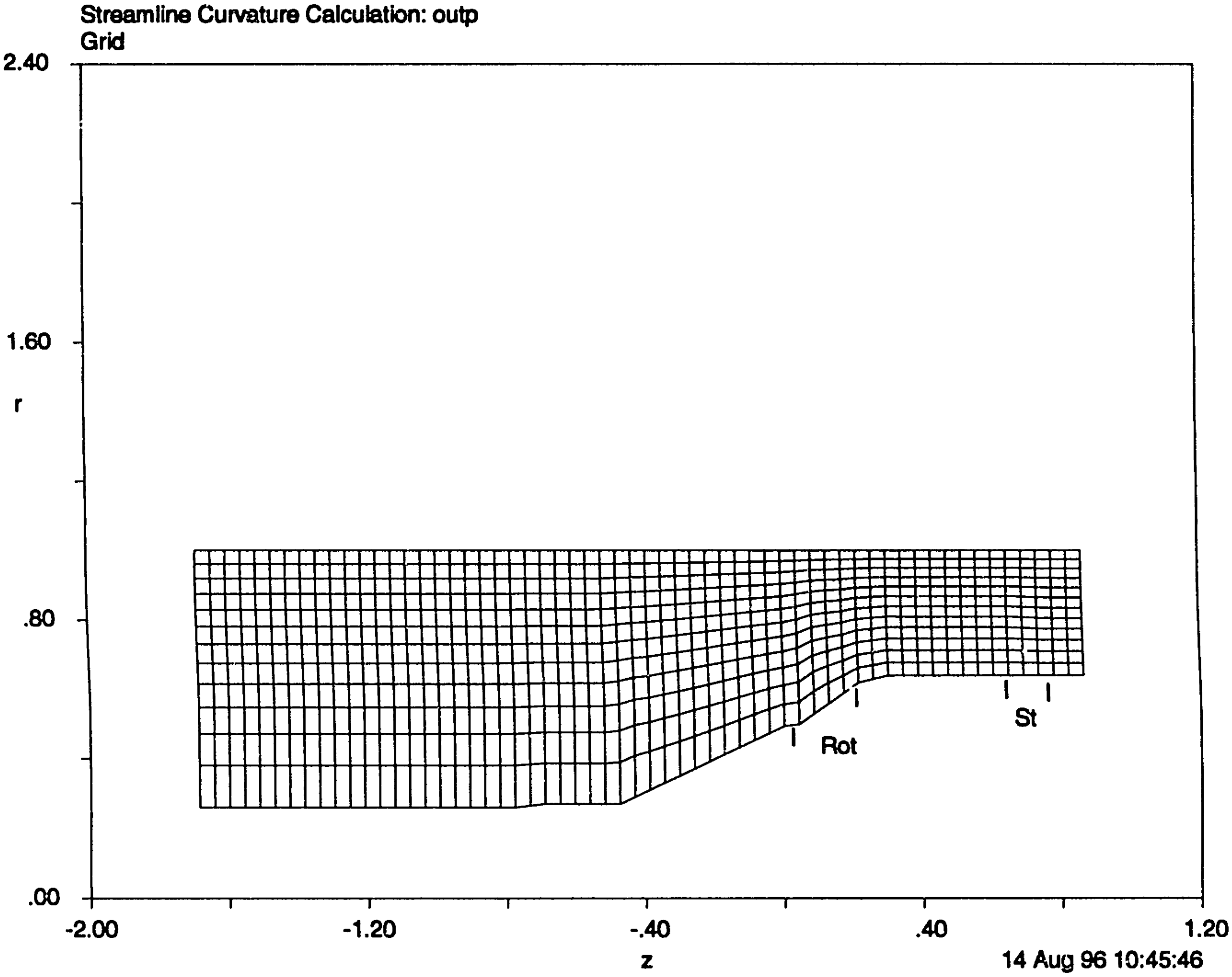

Figure 6.1 Resulting streamline grid for design streamline curvature case

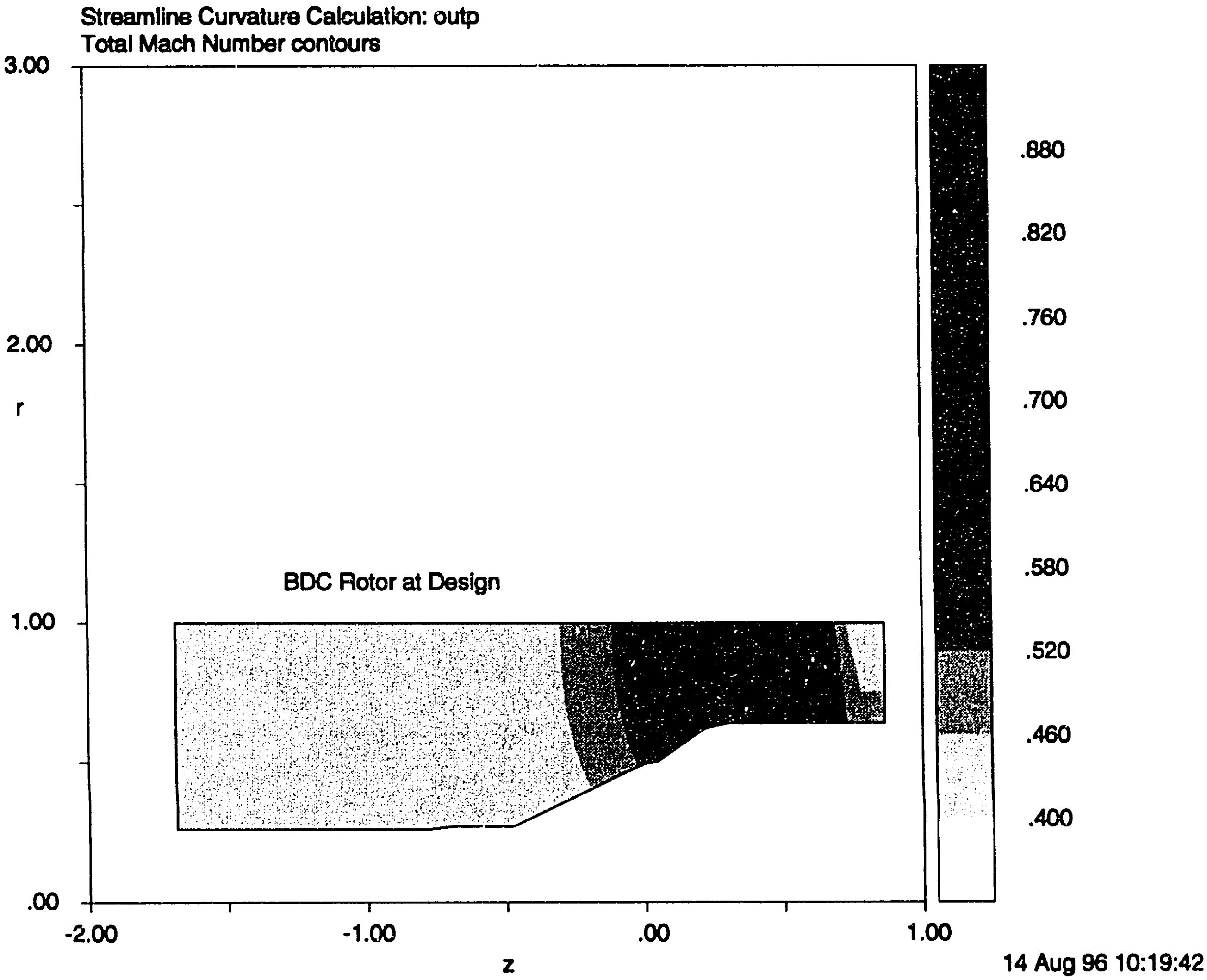

Figure 6.2 Total Mach number contour for design streamline curvature case

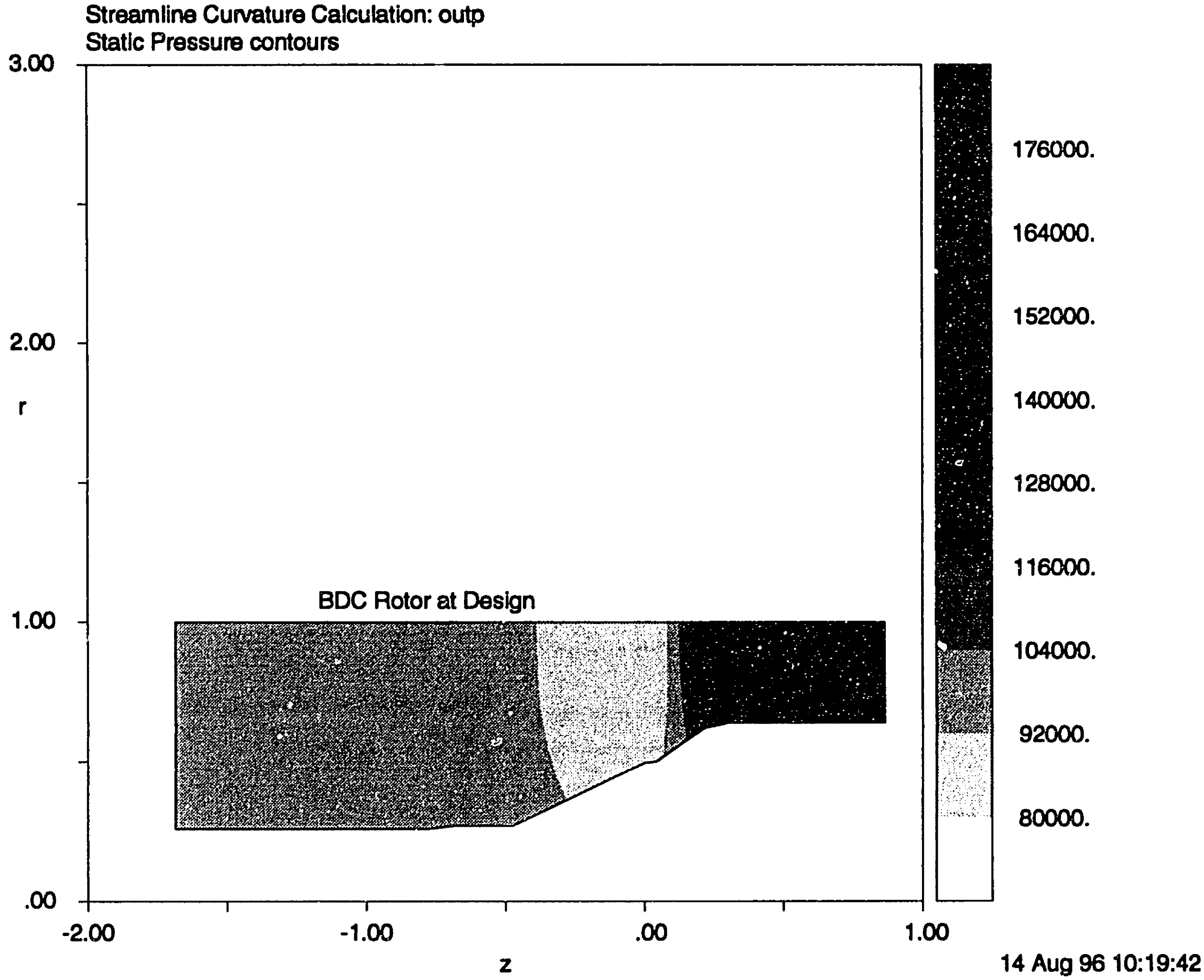

Figure 6.3 Static pressure contours for design streamline curvature case

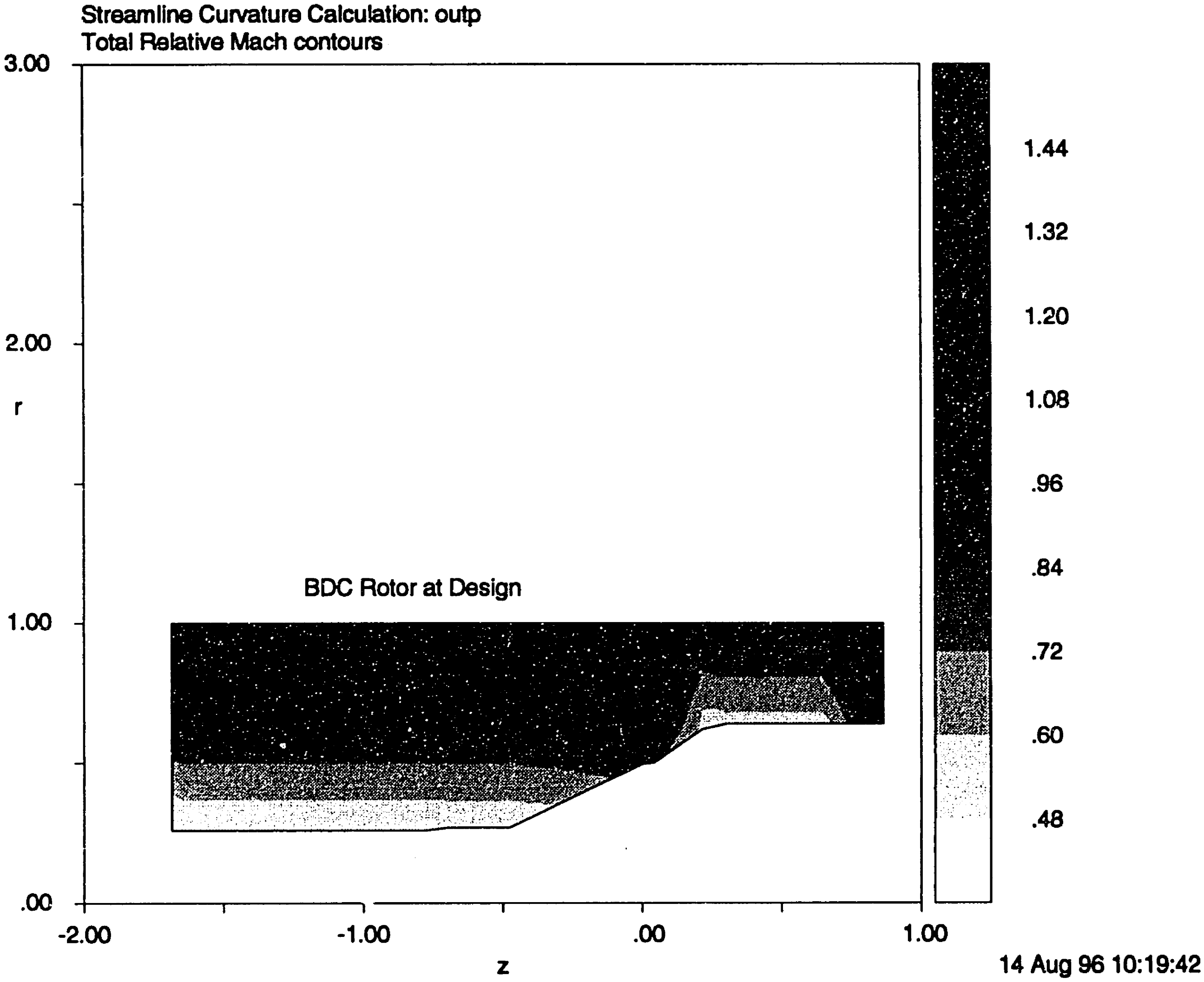

Figure 6.4 Total relative Mach contours for design streamline curvature case

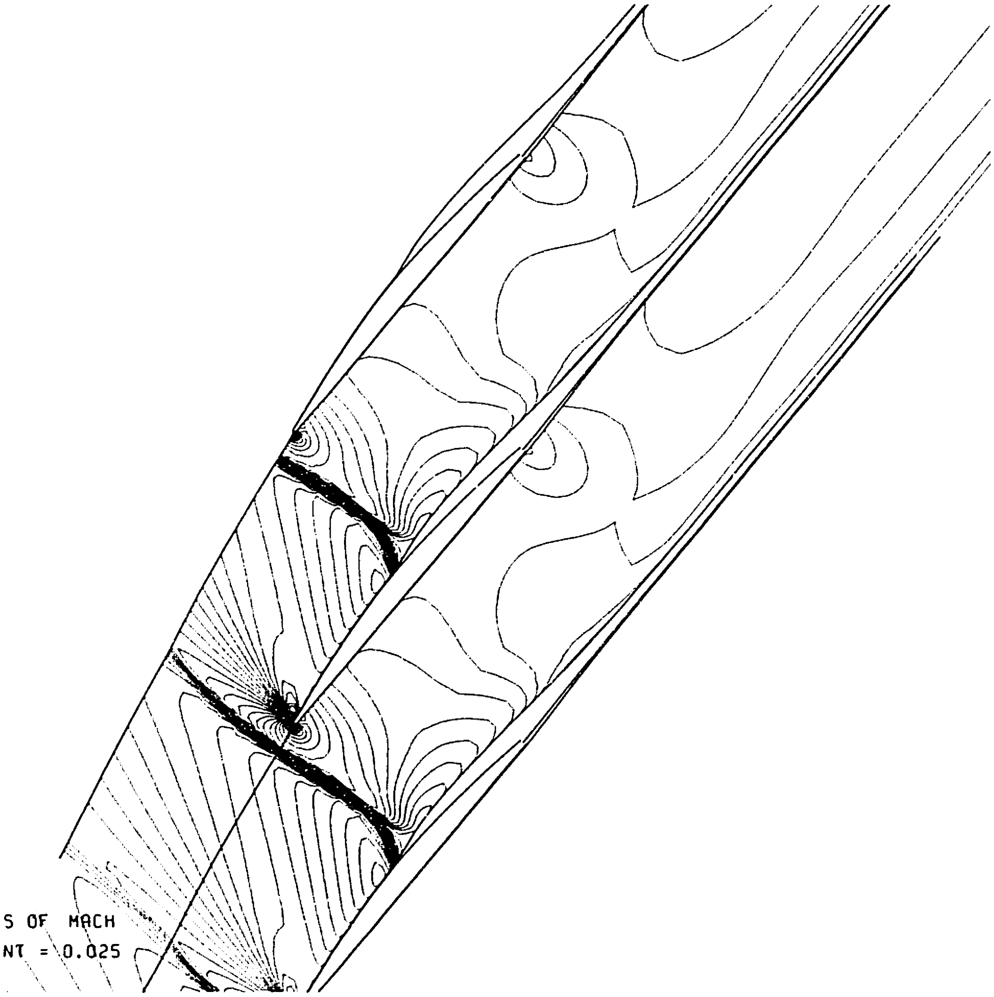

Figure 6.5 Mach contours for R/R_t=0.80 -0.85 at design point

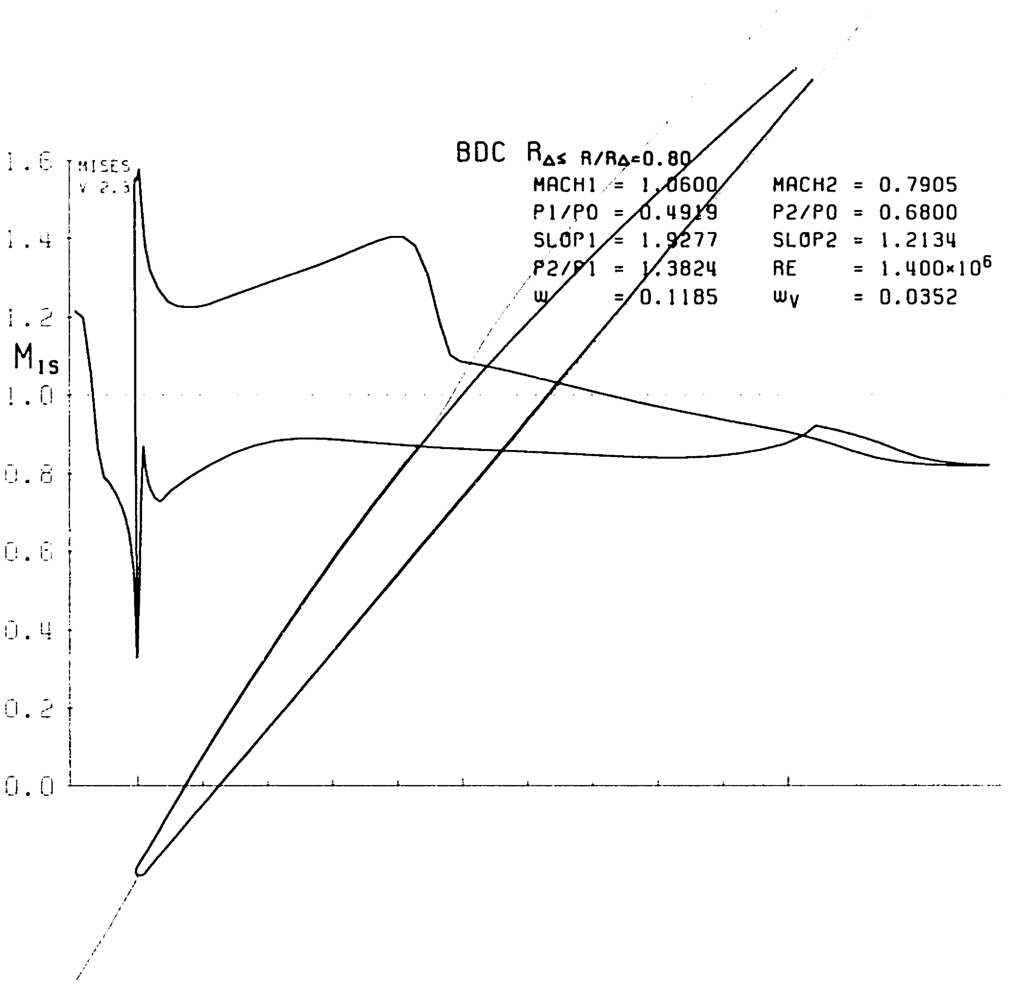

Figure 6.6 Mach number distribution on blade surface for R/R$_t$=0.80 -0.85 at design point

Chapter 7 Discussion of Experimental Results

7.1 Introduction

As was described in detail in the experimental setup chapter the significant information is obtained using high frequency static pressure transducers on the compressor casing upstream and downstream of the rotor, and the 4Way probe which allows the wakes to be studied. Reliable wake information is not available for the tip and the hub region. Out of fear of damaging the 4Way probe, the probe was never moved very close to the hub. Reliable wake traces are not available in the tip region due to the high radial gradients in the desired quantities relative to the resolution of the probe. However the probe produces wake data with sufficient resolution away from the direct tip region (top 3 %) and the hub.

The notation in this chapter of the different pressure traces etc. is based on the position of their transducer at the experiment. Sup denotes supply tank, P_{s4} denotes static pressure at port 4 etc. As can be seen in the different graphs in the experimental setup chapter the rotor is positioned between port 4 and port 5 thus all numbers 4 and lower denote upstream quantities.

It also is important to note that the blades which have the suction scoops are blades 1, 23, 22, 21 and 20. They pass the transducers in this order so blade 1 is the leading blade. To stress the fact that these blades have the scoops they are usually denoted with an S instead of the regular # in the graphs.

Often the data is presented using so called ensemble averages. This simply means that the probe was positioned at a fixed radius and that the data point at some rotational position was obtained by averaging the values measured at that rotational position for several (different) rotations. This highlights features in the flow that are correlated to peripheral variations in the rotor, the difference between blades with and without suction in particular. These variations are obscured by unsteadiness in the real-time traces. For example figure 7.1a was made by ensemble averaging the time trace in figure 7.3. It was found that a minimum of 4 rotor revolutions were required to obtain a pattern of variations in the rotor geometry. Adding more revolutions does not noticeably change the pattern. The ensemble average graphs in this chapter use 5 or 6 rotor revolutions.

7.2 Presentation of Results

The data to be discussed were acquired from two different rotor configurations, sucked and without suction, and two operating points.

The term <u>baseline</u> denotes the original rotor with 23 identical blades operating at design corrected speed and choke area. <u>Design point</u> denotes the sucked rotor operating at identical conditions. <u>Highly loaded</u> refers to the sucked rotor operating at a similar pressure ratio but reduced speed which moves the operating point closer to the stall line.

While analyzing the experimental results, the effect of suction was found to be strongly affected by the operating point of the rotor. While at the so called design point the wakes of the sucked blades did not appear very different from the other blades, their signatures became very distinct when the loading was increased, allowing suction to make the difference. Because of this, the data presented here stems from the more highly loaded case unless specified otherwise.

In order to have consistent notation,

7.2.1 Tip Region Wall Statics and Mid Span Wakes

By combining the pressure traces measured at the casing upstream of the rotor as seen in figure 7.1 one can reconstruct the shock structure at the tip of the blades by drawing crosses at the steep pressure rise over the shock and connecting them. The result is illustrated in figure 7.2. One of the first things noted as an effect of suction, was a change in this shock structure upstream of the 5 sucked blades. Suction caused a significant change in the strength of the shockwaves and changed the angle relative to the axial direction of some of the shock waves. These effects were accompanied by a 5% drop in static pressure upstream of the 5 sucked blades as can be seen in figure 7.3. Also, the wall statics indicated a 1% decrease in static pressure aft of the sucked blades. The wake data which was measured at 86% span (hub/tip at rotor outlet is 0.64) which corresponds to the center of the scoop, shows a similar trend; A high static pressure behind the blades just preceding the sucked blades is followed by two passages with a low static pressure after which the flow recovers to normal (figure 7.4). In addition to the static pressure distribution, the wakes show several other characteristic features which are illustrated in figures 7.5-7.8. The area just aft of the first and second sucked passages typically shows inferior performance. The total pressure in the relative frame is low which results in a low isentropic efficiency. The fifth sucked passage typically has performance similar to the unsucked part of the rotor. The group of three or four blades preceding the 5 sucked blades always exhibit superior performance compared to the blades out of the region of influence of the sucked blades. This group combines a high static exit pressure with a normal turning in the relative frame but a high relative total pressure and therefore high isentropic efficiency.

7.2.2 Operating Point Dependence

As mentioned earlier, the operating point of the compressor was found to have a mayor impact on the influence of suction. This became clear when two experiments with an identical choke area but a different rotational speed were compared. Because the resulting total pressure ratios of both experiments were very similar, the lower rotational speed resulted in moving the operating point of the compressor to the left on the compressor map. Therefore the operating point moved closer to the stall line and the compressor was more highly loaded. At this more highly loaded operating point the velocity defect in the wakes of the non sucked blades was on average 50% higher compared to the design point case. Comparing the ensemble averages of the absolute total pressure aft of the compressor at 86%, a remarkable difference was noted. In the design point experiment the 5 sucked blades do not distinguish themselves. But in the more highly loaded experiment the difference is dramatic as is illustrated in figures 7.10 and 7.11. The flow coming off the suction surface of the sucked blades exhibits a higher absolute total pressure and a significantly higher turning in the relative frame which indicates that the flow exits the blade at an angle very close to the blade angle of the suction surface at the trailing edge. Of all five sucked blades, the third and fourth exhibit the most interesting behavior. Their wakes have lower velocity deficits and higher turning, both indicators for superior boundary layer properties. The core flow of these sucked passages incurs lower shock losses which results in a higher efficiency. Figure 7.12 summarizes the observed features in a schematic.

7.2.3 Stall Behavior

At the end of every experiment the baseline rotor typically enters a stall. The pressure in the dump tank increases until it is too high to keep the flow choked at the choke plate. Therefore the corrected mass flow decreases while the corrected speed of the rotor does not change. The rotor moves up the speed line and approaches the stall line and stalls. In the experiments with suction applied the rotor behaves differently as can be seen in figure 7.13. The rotor without suction the mass flow drops significantly before the rotor stalls while in the case with suction the rotor stalls more abruptly. Because the pneumatic valve opened slightly later in the suction experiment its time scale is shifted by the amount of the delay (approx. 18 msec).

7.3 Analysis of Results

7.3.1 Upstream Flow Field

In order to get a better qualitative understanding of the flow behavior with suction MISES was modified as described in the CFD chapter to accommodate 6 blade passages of which three consecutive blades were sucked. This number of blades was chosen due to computer equipment limitations, a larger number of blade passages proving impractical. It was considered sufficient for modeling the upstream flow because the experimental data (figure 7.2) indicated that it required two sucked passages for the flow to adjust followed by two "normal" sucked blades and a fifth sucked blade to initiate the change back to normal blades which required two additional passages. This brings the total to 3 unsucked and 3 sucked passages. To model the flow behavior aft of the cascade a much higher number of blades was found to be necessary, so the CFD model does not reproduce the features of the downstream flow.

The quasi 3D CFD analysis was found to simulate the low static pressure region just upstream of the sucked blades caused by the flow turning into the sucked blades and therefore expanding its stream tubes. Similar to the experimental data the low pressure region upstream of the rotor is produced by a shockwave followed by a strong expansion wave as seen in figures 7.14 and 7.15. The model was unsuccessful however in predicting the correct strengths of the shockwaves. Probably this is a result of the fact that the shocks at the tip are affected by interaction with the casing boundary layer.

Based on the results of the 6 blade analysis and detailed analysis of the data one can conclude that mass removal results in the sucked blades wanting to swallow more flow than the normal blades surrounding them and to turn the flow more. This results in a higher axial Mach number (M_4) as can be seen in figure 7.13a. Every time the 5 blades pass the transducer the axial Mach number increases. To allow this the shock system upstream of the sucked blades has to adjust. Also because the patch of 5 blades is surrounded by normal blades the flow around the 5 blades will try to resist the additional turning by setting up the high pressure region behind the blades preceding the patch. This results in a pressure gradient which resists the additional turning that the sucked patch wants to do. All these features combine to give a strong shock just upstream of the leading edge of the first sucked blade, followed by a very strong expansion which initiates the low static pressure region in front of the 5 blades, followed by a weak shock. The next 3 sucked blades have shock waves slightly stronger than normal. The adjustment of the shock system is

concluded by a weak shock followed by a even weaker expansion and a region of 2 blade passages where the static pressure is slightly higher than normal.
The strong shock combined with the even stronger expansion diverts the flow into the first sucked passage while signaling the flow further upstream to also turn into the patch.

The shockwaves upstream of the cascade are relatively weak causing very small losses in total pressure, therefore to get a qualitative understanding of the flow it is acceptable to assume isentropic flow. Under this assumption we can directly use the Prandtl-Meyer relationships to tie changes in static pressure to variations in Mach number and flow angle. Applying these relations to the static pressure at the inlet of the cascade, one can deduce a 2.5 degree change in flow angle by the strong shock /expansion combination. It also follows that the strong shock puts the first sucked blade at a very high incidence causing it to shed a larger wake. The large expansion also puts the flow in the first sucked passage at a low incidence removing the need for a strong shock to turn the flow. The turning is attenuated over the following sucked blades and a region with high static inlet pressure follows the patch signaling a mass defect to correct for the mass increase over the 5 sucked blades.

7.3.2 Wake Information

Analysis of wake traces shows a high static pressure region at the trailing edge of the blades preceding the 5 sucked blades. The total pressure in the relative frame just aft of the trailing edge of these blades exhibits a similar pattern. A high total pressure region aft of the blades preceding the patch of sucked blades is followed by one passage with a low total pressure region, one with an intermediate value and two sucked passages with a high relative total pressure. As discussed, in the tip region the patch of 5 blades tries to over turn the flow. Because the 5 sucked blades are embedded in 18 regular blades the regular blades resist this extra turning. This is done by setting up a static pressure gradient aft of the blades which balances the desire to overturn the flow. The result of this mechanism is that the shocks in the passages leading the 5 sucked blades are slightly pushed forward decreasing the amount of expansion on the suction surface therefore decreasing the Mach number entering the passage shock and the associated shock losses. The first two of the sucked blades are spoiled by the shock system attempting to adjust to the new characteristics of the 5 sucked blades. The next two and sometimes three sucked blades exhibit behavior similar to that of a rotor with all blades sucked. Over the following blades the flow adjusts back to normal.
The two sucked blades that appear to be representative of a fully sucked rotor have a higher total pressure recovery than the average baseline blade, and have wakes which exhibit more turning and a lower velocity deficit.
Because no data is available the shock structure in the passage at this mid span location one can only speculate about it. Based on the experiments discussed in the literature, it is hypothesized that at the more highly loaded case the bow shock moves upstream due to the higher loading while the passage shock stays attached to the scoop at the suction surface. This pulls the passage shock backwards and makes it more oblique. Therefore the shock becomes less strong which accounts for the lower losses.

7.3.3 Properties of a Fully Sucked Rotor

When analyzing the data from this experiment, one of the first questions which comes to mind is, how does this experimental data extrapolate to a fully sucked rotor? The answer to this question lies in the wake and casing data. The shock structure and pressure traces at the casing show that the static pressure upstream of the cascade requires two passage to adjust to the sucked blades, stays constant over three passages, after which the readjustment process starts. The associated shock structure requires two shocks to adjust but is followed by three shockwaves with similar shock strengths and shock angles. In the case of the wakes the indications are not as strong. The core flow tends to support the trend from the upstream flow while the wakes do not give a clear answer. However, although the case is not watertight, the author believes that the passages associated with the third and the fourth sucked blades give an excellent representation of the core flow properties of a fully sucked rotor and a fair indication of its wake properties.

If the properties of the third and fourth blade are extrapolated to a fully sucked rotor this rotor will tend to pass more mass flow and will have wakes with more turning in the relative frame and less velocity deficit.

7.4 Concluding Remarks

From the wake data it is clear that suction modified the characteristics of the blade row locally at the representative sucked blades. The sucked blades have a shock system which results in lower losses in the representative passages. But even more important, the sucked blades show behavior at the highly loaded operating point which is similar to that of all blades for the lightly loaded case. The wakes have less velocity deficit and show an increase in turning. These results suggest that applying suction to all blades of this rotor might significantly improve its performance, even without a change in design to take advantage of the higher loading that suction should enable.

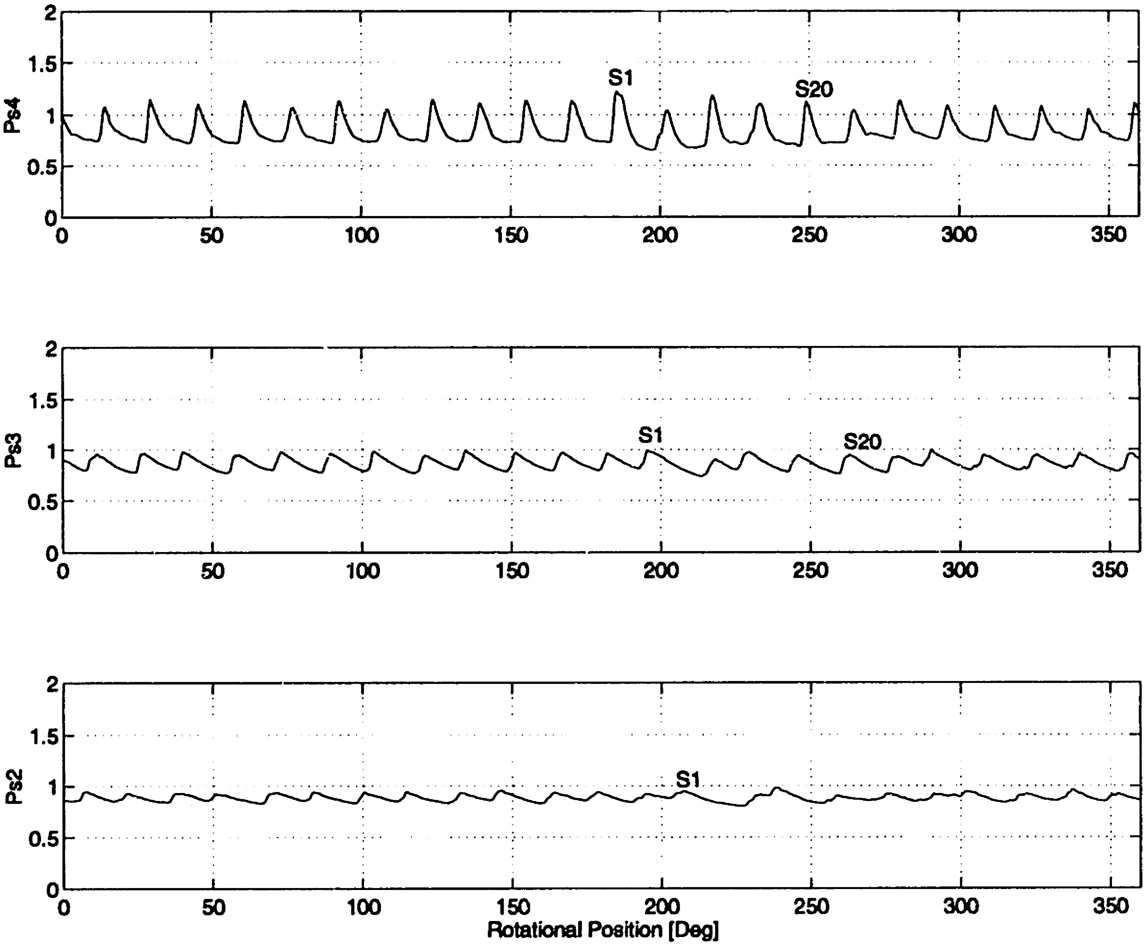

Figure 7.1 Static pressure upstream of rotor normalized by total inlet pressure (P_{s4} 0.16 chord, P_{s3} 0.95 chord and P_{s2} 1.73 chord upstream)

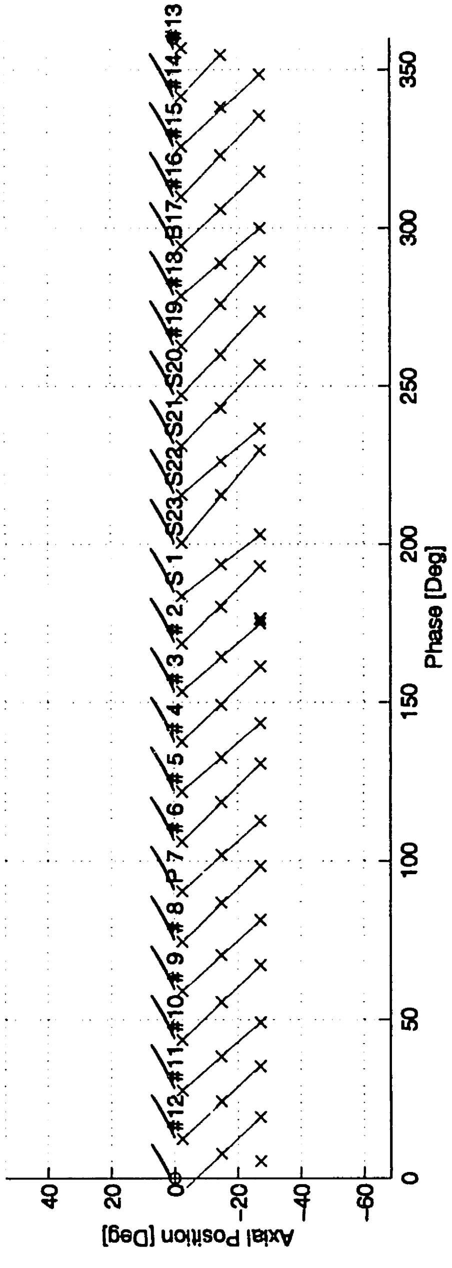

Figure 7.2 Shock structure upstream of rotor

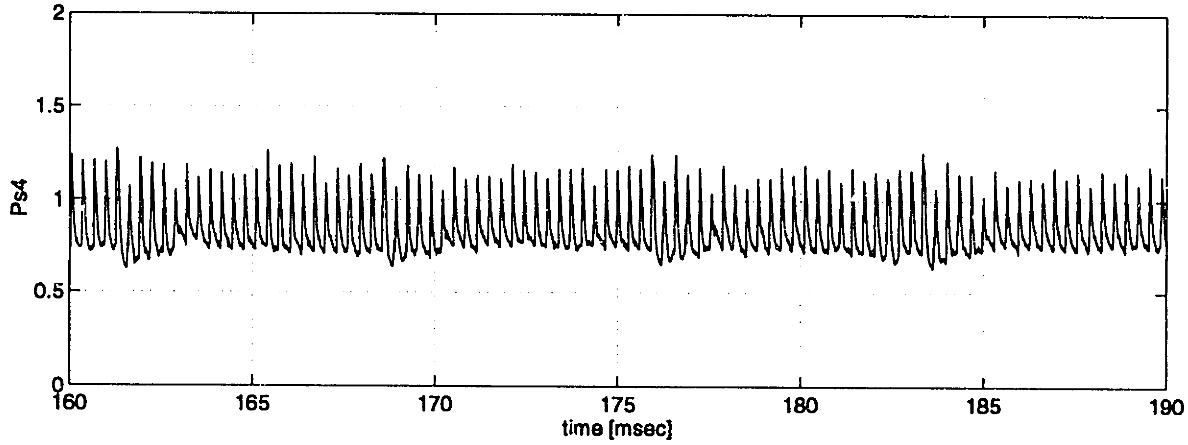

Figure 7.3 Static pressure as function of time just upstream of the rotor for 4 revolutions

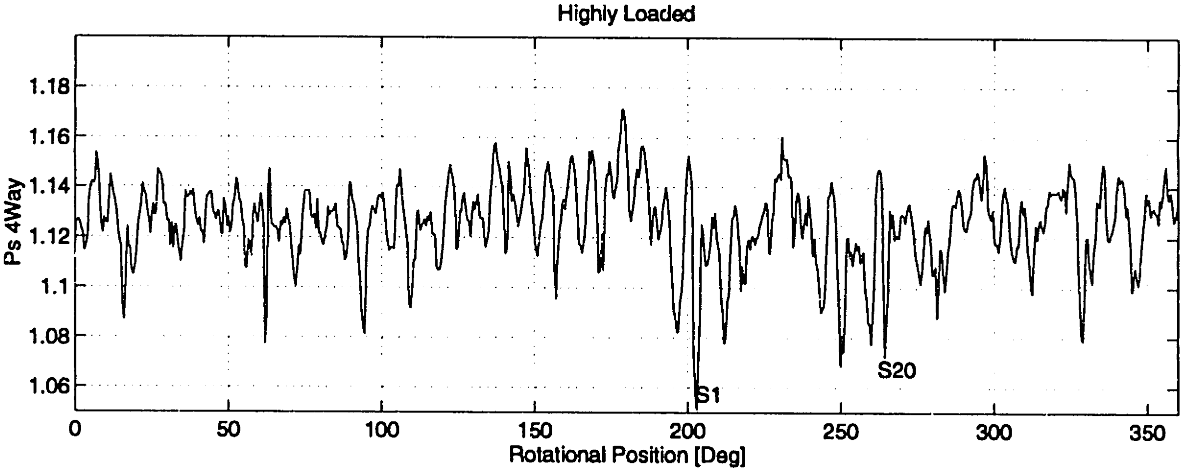

Figure 7.4 Static Pressure at trailing edge at 86% span.

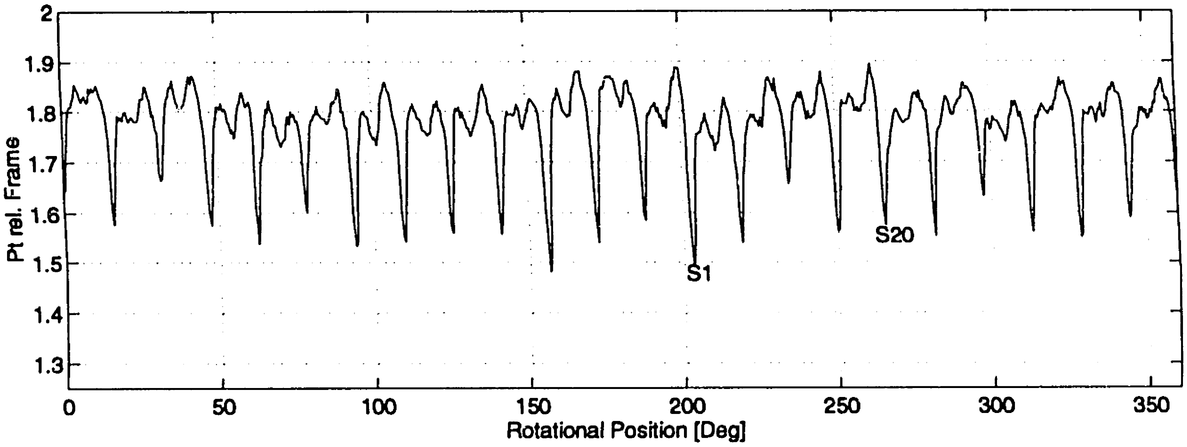

Figure 7.5 Relative stagnation pressure behind rotor at 86% span

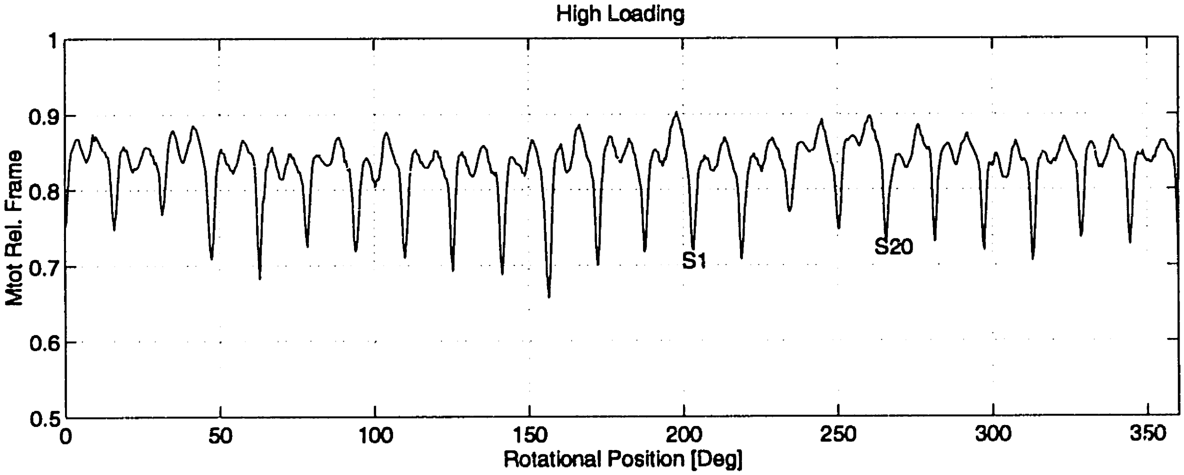

Figure 7.6 Total Mach number behind rotor at 86% span

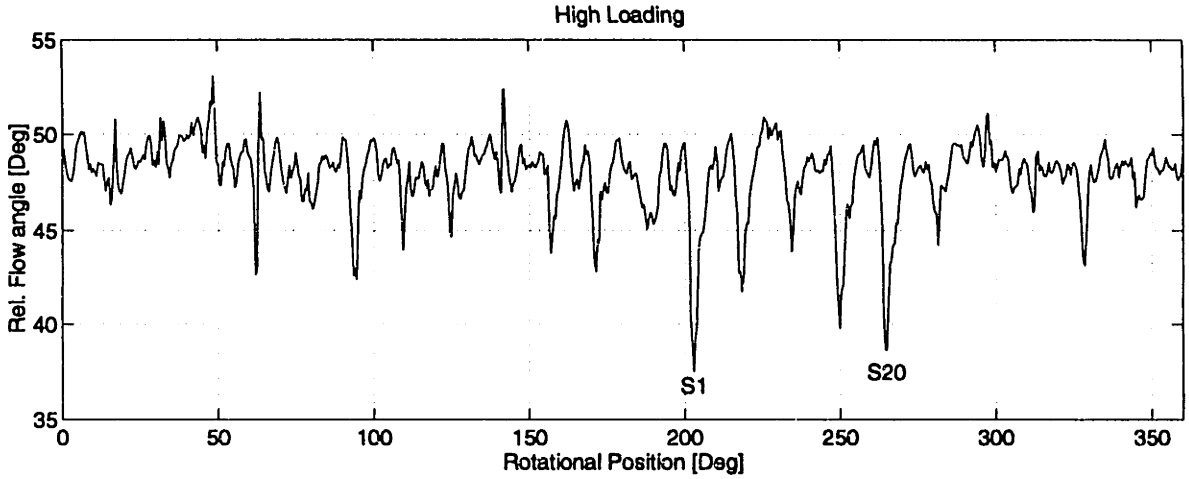

Figure 7.7 Relative flow angle behind rotor at 86% span

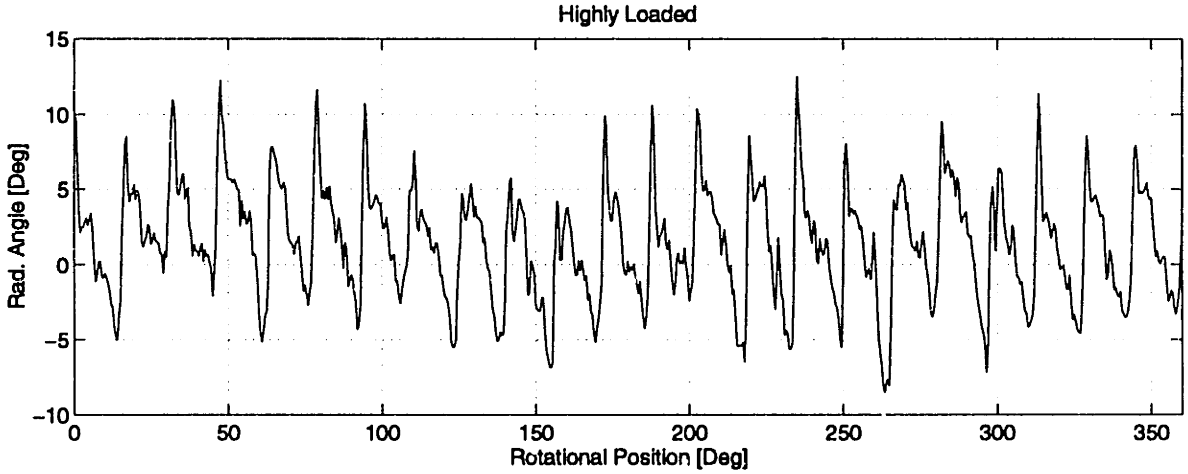

Figure 7.8 Radial angle behind rotor at 86% span

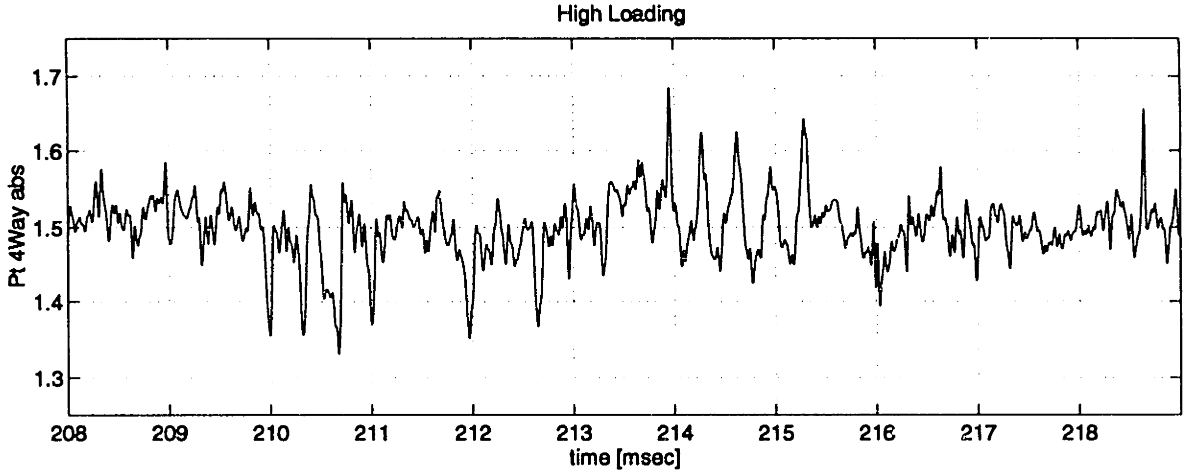

Figure 7.9 Time traces of absolute stagnation pressure behind rotor at 86% span

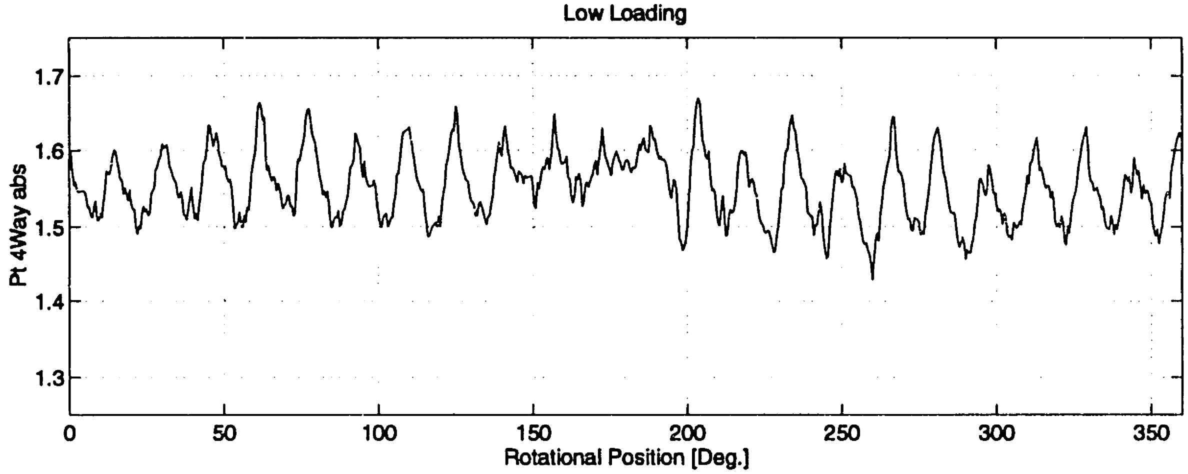

Figure 7.10 Absolute stagnation pressure behind rotor at 86% span, low loading

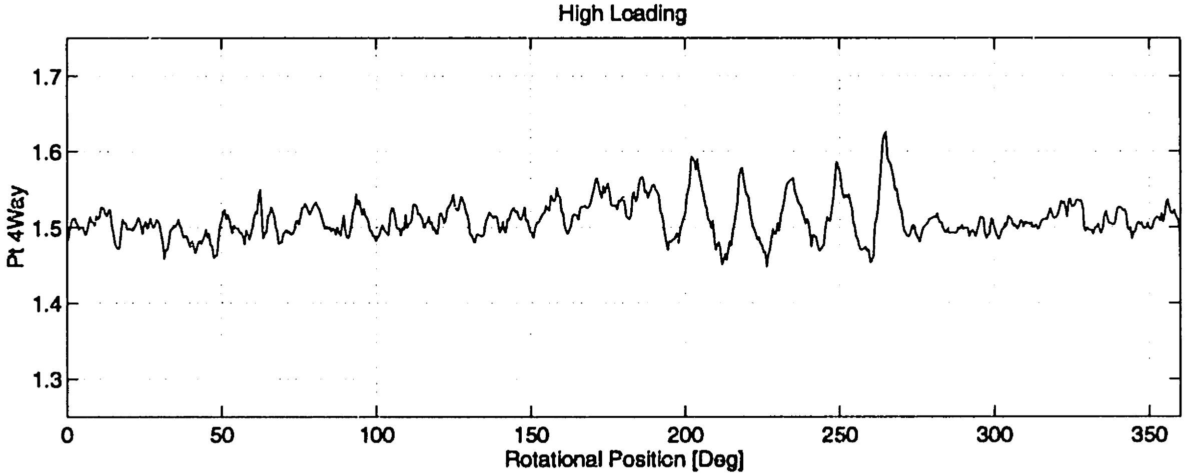

Figure 7.11 Absolute stagnation pressure behind rotor at 86% span, high loading

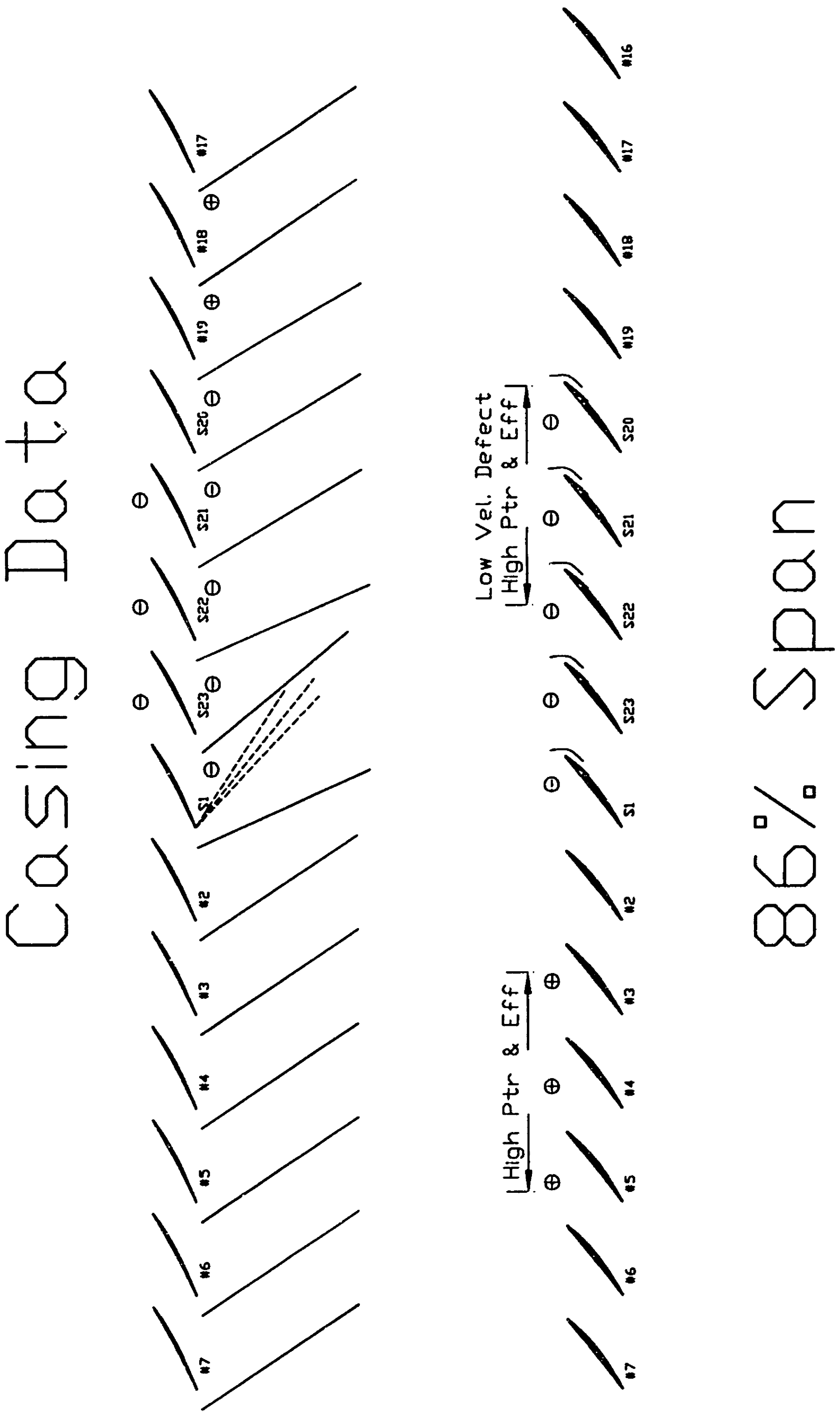

Figure 7.12 Schematic of observed flow features

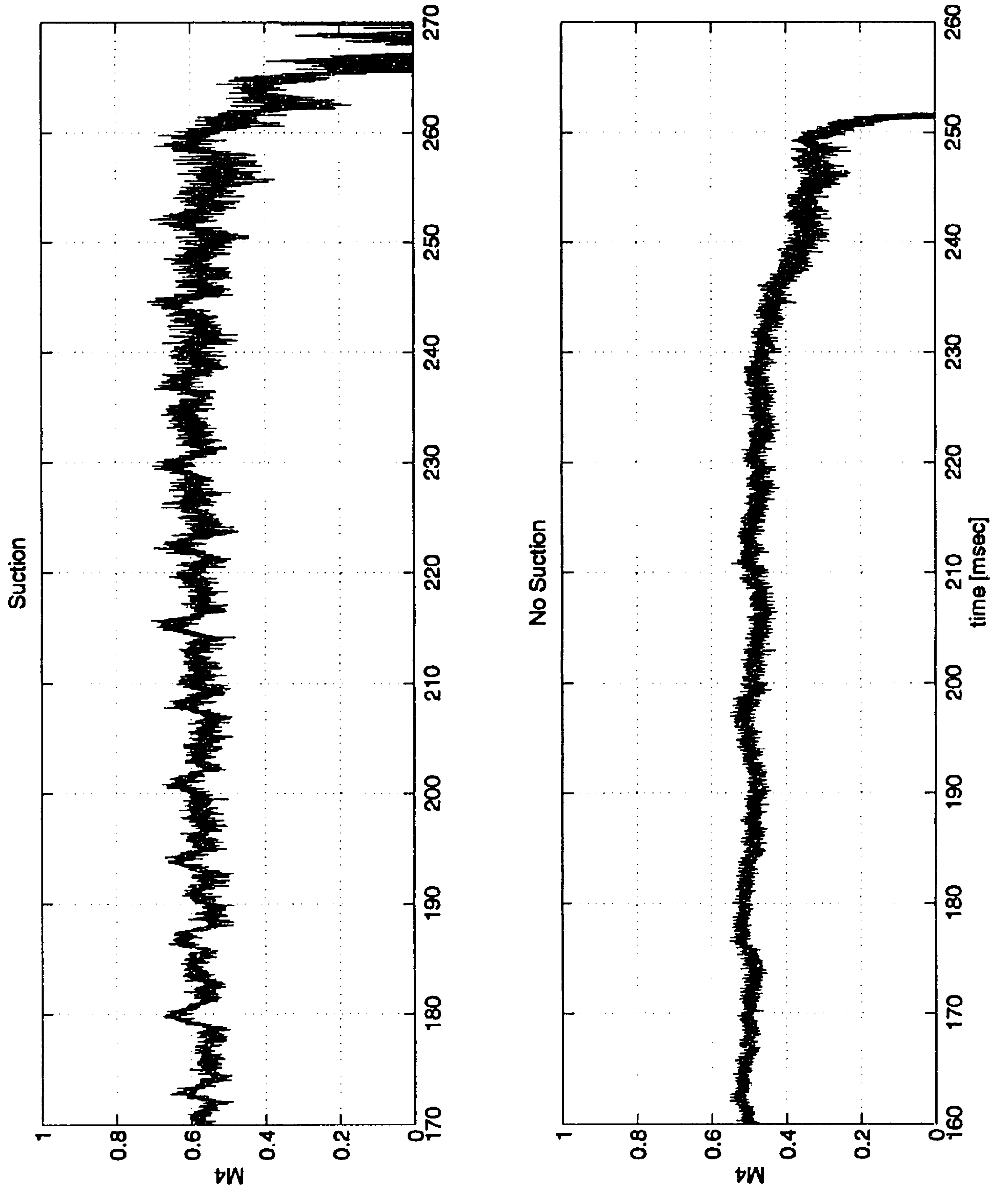

Figure 7.13 Effect of suction on stall behavior

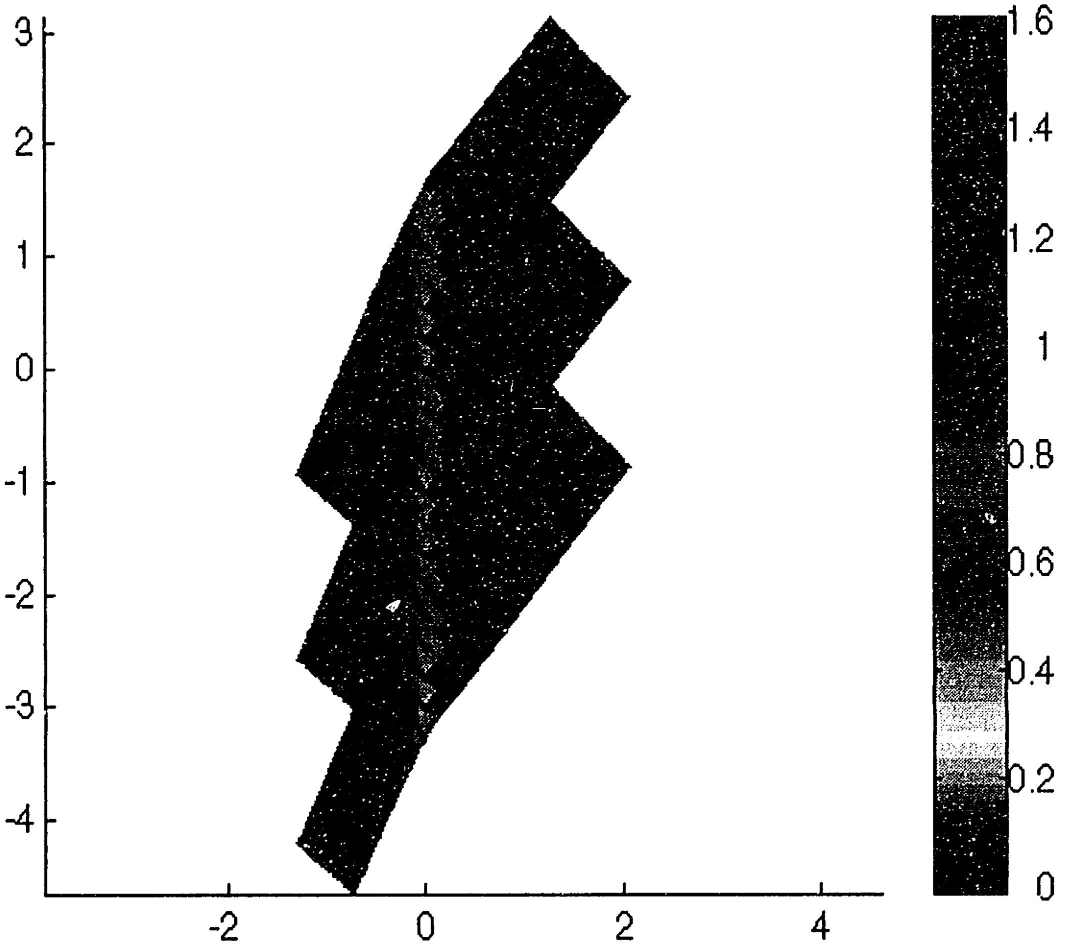

Figure 7.14 Pressure distribution of 6 blade analysis

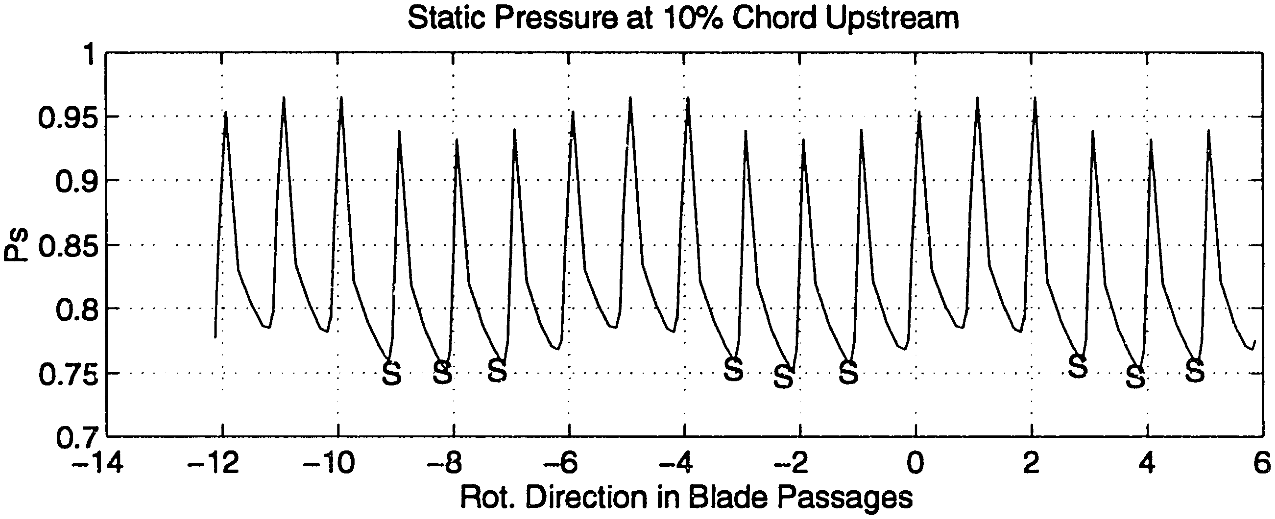

Figure 7.15 6 Blade analysis showing low static pressure in front of sucked blades

Chapter 8 Implications for Future Designs

8.1 Impact on Design Process

Application of suction alone will not significantly improve the performance of a fixed design rotor if the design is highly developed. As noted above, suction on all blades might significantly enhance the rotor tested but its design is not highly refined so that it exhibits considerable larger losses than fully developed rotors.

In some cases suction may actually deteriorate its overall performance because it may moves the shock to a position where the incurred shock losses are higher. In order to obtain considerable gains in more refined designs, boundary layer control has to be an integral part of the design philosophy. In a design without boundary layer control, one is limited by the diffusion at the end of the suction side of the blade. This has a serious impact on the design of the whole blade: because transonic compressor blades require small leading and trailing edge radii and have a fairly flat pressure surface, additional thickness or a higher slope of the suction surface at the point of impingement of the passage shock increases the turning required at the end of the suction surface where the flow is subsonic. This increases the diffusion at the end of the suction surface. Thus for a given maximum diffusion the designer is limited in his design choices when he designs the supersonic part of the chord. Suction has the capability to relieve these limits, providing the designer with a larger design space.

8.2 Different Design Approaches

The transonic compressor blade designer might use the higher allowable diffusion to design a blade with no expansion or even pre compression on the front part of the suction surface. This will weaken the passage shock and make it easier to control so that he can use the remaining part of the suction to control the higher diffusion.

In one application of this concept the suction at the shock boundary layer interaction would be such that the boundary layer coming out of the interaction zone is capable of handling the high diffusion without suction aft of the shock boundary layer interaction. So all suction is concentrated in the shock boundary layer interaction where it avoids separation due to the pressure jump and provides the following subsonic diffuser with a healthy boundary layer.

One can take this concept also to the opposite extreme by weakening the passage shock by pre compression to the point that the boundary layer will pass it without separating and concentrate all the suction on the aft part of the blade to control the boundary layer during the diffusion process. Thus, all available kinetic energy in the boundary layer is used over the supersonic part of the chord and the shockwave. Although the boundary layer emerges from the shock boundary layer interaction on the verge of separation, the boundary layer suction ensures no problems during the subsonic diffusion.

Which approach is more advisable depends on the operating condition of the blade row. When the inlet relative Mach number is high, the second approach will become very hard to implement and the issue of shock stability has to be addressed. But at low inlet Mach numbers the simplicity of the second approach is tempting. The suction and the shock boundary layer interaction are separated.

Both approaches result in thicker blades with the complementary advantage of having more internal flow area available to transport the removed boundary layer fluid. This of course is very desirable from structural and system design points of view.

As was seen in the literature review section, and especially suction using a scoop, has the capability to set the position of the shock to a certain extent. This can be used to ensure the shock is positioned at the most advantageous position at design. In addition it is also beneficial to the stability of the shock system in the passage.

8.3 Concluding Remarks

Boundary layer control can only provide a significant improvement in performance if the designer makes full use of the additional capabilities it provides. However while concentrating on the details of blade design he has to keep the big picture in mind. It may become necessary to accompany boundary layer control on the blade surface with some form of casing treatment because the boundary layer on the casing may become the weakest link in the chain when the pressure ratio in the machine increases due to more highly loaded blades enabled by boundary layer control on the blade surfaces.

Chapter 9 Conclusions and Recommendations

The effect of suction was found to be strongly dependent on the operating point of the compressor. While at design point the wakes of the sucked blades did not appear very different from the other blades, their signatures became very distinct when the loading was increased allowing suction to make a difference.

At the highly loaded operating point the third and the fourth blade which are thought to be indicative for the behavior of a fully sucked rotor, obtained lower pressure losses in the core fluid and higher turning in the wakes resulting in a higher efficiency.

The partly sucked rotor exhibited a more abrupt stall behavior.

However in order to make significant improvements in performance, boundary layer suction has to be an integral part of the design philosophy. The design has to take full advantage of the capabilities of suction.

Appendices

Appendix A Experimental setup

A.1 Description of Blowdown Compressor Facility Piping

Because it took the author and his partner Jed Dennis a considerable amount of time to figure out the piping in the Blowdown Compressor Facility, a description is included here. In principle piping is used for five purposes:

1) Evacuation of the dump and the supply tank
2) Filling of the supply tank with the test gas
3) Measurement of pressure of the supply and the dump tank
4) Recycling of the test gas
5) Removal of the suction fluid

A schema of all piping available on the facility in February 1995 is shown in figure A.1. In this drawing all pipe diameters are drawn to the same scale and all valves are given a letter which corresponds with the letter on the spacer ring attached to the valve on the rig.

A.1.1 Evacuation of Supply and Dump Tank and use of the Vacuum Pump

All 3 inch diameter piping is used to evacuate the supply and dump tank. This is done by closing all valves which are opened to ambient. Be aware that the shaft itself also has an by oil pressure actuated seal to separate the test section from the motor which is at ambient pressure. The seal can be actuated by pressurizing the little oil reservoir mounted to the outside wall up to approximately 20-40 Psi. The reservoir can be refilled by unscrewing a bolt on top of the reservoir. Vacuum pump oil can be used for this purpose. The plastic tubing and the seal can be refilled with oil by opening the tube end connected to the top of the seal while the reservoir is full and pressurized. Keep this end open until a steady stream of oil indicates that all the air is removed from the system.

Before a typical experiment the oil in the vacuum pump is checked. This can simply be done by checking the little glass window on the side of the pump. The oil level is supposed to fill half or more of the glass window. The oil is available directly from the supplier Stokes. A manual for the pump containing the address is available in one of the cabinets. Next, the cooling water for the pump is turned on. The valve is positioned directly next to the pump on the floor. The next step is to check that the exhaust of the pump is not blocked by making sure that valve G is open and F is closed. Finally the pump can be started by pushing the switch next to the pump on the outside wall. At present, the minimum pressure the pump can achieve is around 15 millitorr. (1 torr=1 mmHg, 760 torr=1 atm). By opening the large valves K and L the supply tank and the dump tank are evacuated. Typically pressures around 0.35 torr can be reached for the supply and the dump tank when all mayor leaks are closed. Leak finding is done by listening or by spraying acetone on a suspected connection while monitoring the thermistor gauge while the pressure is lower than 1 torr. A clicking sound signals that the pump is operating at very low pressure.

Best results were achieved by the author when the system was evacuated before the bolts between the test section and the dump tank were tightened. Sometimes it is hard to insert these bolts because the holes do not line up. Use an old very large screwdriver and insert it through the holes. When the tip barely touches the dump tank flange, a very large moment can be applied and the flanges can be easily forced to line up.

A.1.2 Filling of the Supply Tank with Test Gas

After closing valve F and evacuating the supply and the dump tank, valves K and T are closed. The gas mixture is mixed using the equipment mentioned in reference A.1 and seen in figure A.2. The valve separating the cylinder shaped reservoir on the wall and the vertical heat exchanger on the wall (CC) is closed. Next, the valve between the Freon tank and the reservoir (AA & BB) is opened and the reservoir starts to fill. This process can be expedited by heating the Freon tank a little with a heat gun. When the level in the glass watch tube reaches the first mark, the reservoir contains sufficient Freon and the Freon tank is closed off (AA & BB). The vertical heat exchanger is heated by a mixture of hot water and cold water and the user must make sure in advance that sufficient hot water is available. Often it necessary to increase the thermostat on the hot water heater and to not start the heating process too early in order not to run out of water during the filling process. This will manifest itself by a drop of the heat exchanger temperature which can be viewed on the console. The water leaving the Freon heat exchanger is used to heat the argon heat exchanger positioned in the bottom of the console. Additional hot water can be added before the water enters the argon heat exchanger. Before the filling process starts, solenoid A is opened (up) and solenoid C is closed (down) and switch D is positioned down. Both regulators (Argon bottle and Freon flowmeter) are set to 15 PsiG and the heat exchanger is heated to approximately 40-50 C. The gas valve between the Freon heat exchanger and the flowmeter (DD) and the valve between the argon bottle and the console (GG) are closed. The valve between the Freon reservoir and the heat exchanger (CC) is opened and the liquid Freon enters the heat exchanger. Next, the valve on the argon bottle (HH) is opened. During the next step the mixing is started by opening the valve next to the Freon flow meter (DD) and the valve separating the argon regulator form the console (DD) simultaneously. Adjust both regulators in such way that the pressures at both flow meters indicate 15 PsiG. Adjust the valves mounted on the console under the plexiglass in such way that the large argon flowmeter indicates 61% and the small Freon flowmeter indicates 58% (for Freon 12/Argon). Adjust the temperature in both heat exchangers to yield an equal gas temperature of approximately 30 C at both flow meters. During this process the mixed gas is dumped. When the system is set up right this is no longer necessary and the tank can be filled without any spillage. By toggling switch D on the console solenoid A is closed and C is opened simultaneously allowing the mixture to enter the supply tank.

In principal all 0.5 inch tubing in the facility is used for transporting test gas to the tanks. Note that opening solenoid B allows gas from the supply tank to flow to the dump tank or vice versa. Also note that some of the solenoids have the tendency to be leak-free only in one direction.

A.1.3 Measurement of Pressure in Supply and Dump Tank

The pressure in the supply tank can be measured using various gauges.

a) Open valve U and close valve T. The large gauge on the left side of the console will read the supply tank pressure in torr (760 torr=101325 Pa). At the time of writing this gauge reads 10 torr higher than the actual pressure.

b) Open U, T and close S. Both gauges in the console will read the supply tank pressure.

c) Use one of the transducers in the supply tank.

d) Close I and H and open J. Connect a McLeod or other gauge at the open end half inch tube.

e) While pumping, close P and open N and O and read the pressure on the installed vacuum

thermistor gauge next to valve O.
Similarly, the pressure in the dump tank can be measured by the same gauges.
All 0.25 Inch tubing on the experiment except for the cooling water for the 4Way probe, is used for measurement of system pressures.

A.1.4 Recycling of the Test Gas

All equipment between and including valve E and F is added for the benefit of being able to recycle the test gas. This is done by cooling the heat exchanger between E and F and opening valve E, F and L simultaneously with closing valve G after an experiment while running the vacuum pump. For the benefit of the test gas it is advisable to evacuate the volume between E and F before filling the supply tank for the first time. The filter is installed to remove the vacuum oil from the test gas while the heat exchanger condenses the oil before it enters the filter.

A.1.5 Suction Mass Piping

All piping in the 1 to 1.5 Inch diameter range was added for suction fluid removal. It transports the fluid exiting the spider legs to the suction dump tank. Valve R should be closed at all times except when testing the suction system for leaks. It can be closed by inserting rubber coated aluminum plates in the unions between the pipes separating the suction dump tank from the rest of the facility.

A.2 Speed of Sound Device

In order to be able to verify the gas mixture before the run, a special device was developed based on an idea of Prof. Ingard. It consists of a 24 Inch (0.61 m) long 3/4 Inch diameter copper tube ending on both sides in a small 3.5 x 3 Inch diameter plenum as seen in figure A.4, A.5. One of the plenums contains a simple Radio Shack speaker (8 Ohm / 0.2 Watt). The opposite side has several valves to empty and fill the plenum. A simple Radio Shack omnidirectional condenser microphone which has a reasonable flat frequency response between 20 Hz and over 10 kHz is mounted in the middle of the 24 Inch tube. A modified Radio Shack radio was used to generate white noise which was fed to the speaker in order to excite the tube. The on both sides seemingly open-ended tube will be excited at its natural frequency (f_n) and its multiples (f_k). Maximum amplitude will occur in the middle where the microphone is positioned. Using a Hewlett Packard spectrum analyzer these multiples of the natural frequency can be determined.
Now, the speed of sound can be easily calculated using $\lambda=2*l=2*24$ Inch=1.22 m, and the wave number k:

$$a_k=\lambda_1 .\ f_k/k= 1.22 * f_k/k$$

For example $f_1=218$ Hz, $f_3=655$ Hz and $f_5=1040$ Hz. Calculating the speed of sound using the first natural frequency yields: $a_1=1.22*218/1=265.9$ m/s. Using the third natural frequency we obtain $a_3=1.22*655/3=266.4$ m/s, or using the fifth $a_5=1.22*1040/5=253.8$ m/s. Traditionally, the third mode provides the most reliable measurement.

A.3 Position Instrumentation

A.3.1 4Way Probe Translator

In order to be able to translate the 4Way probe during the experiment and to minimize the time the very fragile probe is exposed to the flow, the probe is mounted on a pneumatic translator capable of shooting the probe to the hub in less than 40 msec as seen in figure A.3.

The translator consists of two gas reservoirs which can be individually vented into a drive piston by the means of pulsed solenoids. This way the probe can be shot in and be retracted at remarkable speeds. The position of the probe is measured using a LDVT (4 inch Trans-Tek 0245-0000) which is a position indicator using induction instead of the traditional resistance a potentiometer uses. This enables a clearer signal during fast movements.
Calibration is done by measuring the output voltage for several known positions.

A.3.2 Valve position indicator

In the summer and fall of 1994 a new pneumatic valve was developed for the Blowdown Compressor by professor Kerrebrock, Willy Ziminsky, professor Durali and Chris Brown. This valve substitutes the aluminum diaphragm which formerly separated the supply tank and the tube containing the rotor. In order to measure the performance of this actuator a 38 inches long translating potentiometer was installed. Using a 5 Volts power supply, the potentiometer (58.5 kOhm) is used as a voltage splitter. The voltage between the moving leg and one of the outer points of the resistor is measured by the data acquisition system. Calibration is achieved by measuring the voltage when the valve is closed and when the valve is fully open (19 Inches back).

A.3.3 Magnetic Encoder

The original electrical motor and assembly of the Blowdown Compressor facility which was used during this set of experiments, has a 115 teeth tooth wheel mounted on its shaft. One of the 115 teeth is replaced by a tooth of a different material. Every time a tooth passes the installed magnetic pick-up it generates a sine wave. The special tooth generates a higher amplitude sine wave which establishes the rotational position of the rotor. The signal generated by the magnetic pick-up can be directly recorded by the AD system without any amplification and is a useful tool for checking the rotational speed of the rotor

A.3.4 Optical Encoder

The optical encoder (BEI MX-21) is an improvement over the magnetic index. It simply consists of two disks, a LED and two photo electrodes. One disk contains one line which signals the rotational position of the rotor. The second disk contains 400 lines which enables a finer rotational position once the zero is set by the 1/rev disk. It outputs 3 basic signals: a once per revolution pulse, called I, a 400 pulses per revolution signal called A and a signal called B which is identical to A but has a 90 degree phase lag. A and B can be combined to provide a 800/rev signal. The specification sheet of this encoder that also contains its wiring diagram is available in the Blowdown Compressor Bible.

A.4 Firing Mechanism

The firing mechanism is quite complex and therefore will be discussed here. It is positioned in the top box of the console containing the power controls for the motor. It receives the 400/rev and 1/rev optical index signals as inputs. It outputs a 5 volt TTL which triggers the experiment. The 400/rev signal is used for determining the speed of the rotor and the number of blips per second is indicated digitally. For example, the design speed of the MIT rotor of 167 rev/sec will correspond to 167*400=66800 on the indicator. Before a run, all systems in the test cell are armed and the door is closed. The design speed at which the experiment is supposed to start is inputted using the rotating numbers. The large power switch on the wall is set to on. Before the electrical motor can be used, the shaft oil seal has to be turned on. Failing to do so will result in the ringing of a bell in the motor console. Remember, the oil seal is turned on by providing it pressure using an argon or nitrogen bottle and flipping the switch next to the reservoir. The rotor is spun by flipping both switches below the rotating Variac controls, setting the current in the field (right side) to approximately 5 amperes and starting to increase the current in the winding (left side) itself. Values to approximately 80-90 amperes are allowed. In the case of no red light or there is no other reaction: the fuse is probably gone. Simply reset the appropriate fuses (3 linked together) in the fuse box next to entrance to the Blowdown Compressor test cell.

The motor receives nearly no cooling air so long operation will result in overheating and destruction of its precious bearings. During the spin-up the winding current will decrease and the controls have to be turned to keep it high.

The firing mechanism is initiated by keeping the small toggle switch on the indicator first left for 1 second and then right for approximately 4 seconds. You will hear a click and see the set design speed for a moment on the indicator. When the rotor exceeds its design speed, all power to the rotor is turned off by rotating the dials back, not flipping the switch! It is important to make sure there is enough time between turning off the power and the start of the experiment to avoid noise in the instrumentation. The final arming is done by pushing the small black button on the left of the box while the rotor is slowing down. Once this button is pushed and the set speed is reached, the box will send a TTL pulse to the experiment in the test cell. However there is one more option to the process. When the toggle switch on the bottom of the box is set to Tach & Strobe, the box will not fire on the moment supreme but wait until the 1/rev occurs. This makes sure the rotor is always in the same position when the experiment starts and this can be very useful. This option is usually used.

It is essential that the input signal the box receives are truly close to a TTL (5 Volt). If this is not the case the counter will not read correctly at speeds above approximately 50000 counts/Rev.

A.5 Data Acquisition System

Data is acquired using three 333.0 kHz, 8 channels PC-based data acquisition cards. The cards are manufactured by ADTEK (Analog Digital Technology, 31324 Via Colinas, Suite #105, West Lake Village, California 91362, (818) 597 8211). The cards have a 12 bit AD converter. Using accompanying software, the analog operating range of the individual channels can be set: -10 to 10 Volts, -5 to 5 Volts, -2.5 to 2.5 Volts and -1.25 to 1.25 Volts. For example: using the -5 to 5

Volt, a zero Volt input signal will result in 2048, -5 Volt in 0 and 5 Volt in 4095. During the data acquisition the data is stored in the RAM of the computer. When the software gets the opportunity, it is written to disk. To ensure operation of the data acquisition system, it is important to note a few things which often cause problems. Make sure that the clocks of all boards are connected. Always take data before an experiment to ensure there is sufficient disk space. Make sure the data file does not have the same name as the configuration file. Do not enter the test cell when the computer is still taking data for a calibration. Always restart the computer before taking serious data to avoid weird memory problems. Always manually check that all AD boards operate correctly by using the view data option and checking that the AD board is not locked resulting in 4095 for all channels regardless of the real input signals.

A.6 Explosive Diaphragms

Prior to the development of the Blowdown Compressor fast acting pneumatic valve in the summer of 1994, explosive diaphragms were used to separate the supply tank from the rest of the facility. A thin 20 mils thick non heat treated aluminum sheet was cut in 8 equal pie pieces (see figure ?) using plastic explosives. The plastic explosives are made by Dupont and sold under the name Deta Sheet trade. They come either in thin sheets or as "spaghetti" on a roll. When the sheets were used, thin strips were cut. The strips or a piece of spaghetti were applied to the diaphragm in a 8 spoked star using double adhesive tape . In addition to the thin cutting strips a small circular piece of explosive sheeting was applied to the center of the start to improve the propagation to the spokes. In the top of the tunnel a standard dynamite explosive cap was mounted and a relatively wide strip of explosive sheet connected the center of the star with the detonator. The bursting of the diaphragm was initiated by a TTL pulse which discharged a capacitor sending a high current to the detonator to start the explosion. The explosion propagates from the detonator through the thick strip to the center of the diaphragm. From there it propagates into all the spokes and ideally cuts the diaphragm into 8 lobes. The lobes are pressed inward by the supply tank pressure. The non annealed state of the aluminum prevents the lobes from bending back.

The problems associated with this process are numerous: A very experienced technician is necessary to obtain good strips. The preparation usually took a complete morning and once the system was put in a place, no last minute changes or corrections could be made because of safety concerns. The result was an elaborate process which only yielded a successful 8 lobe diaphragm once. Because of the low success rate higher than necessary explosive charges were used. This resulted in pieces of aluminum of the diaphragm being send through the rotor which is spinning at full speed with possible damage to the rotor or one of the probes in the casing.

Fortunately, the fast acting pneumatic valve finally solved all these problems.

References:

A.1 Kerrebrock, J. L., The MIT Blowdown Compressor Facility, MIT Gas Turbine Report 108, Sept 1975.

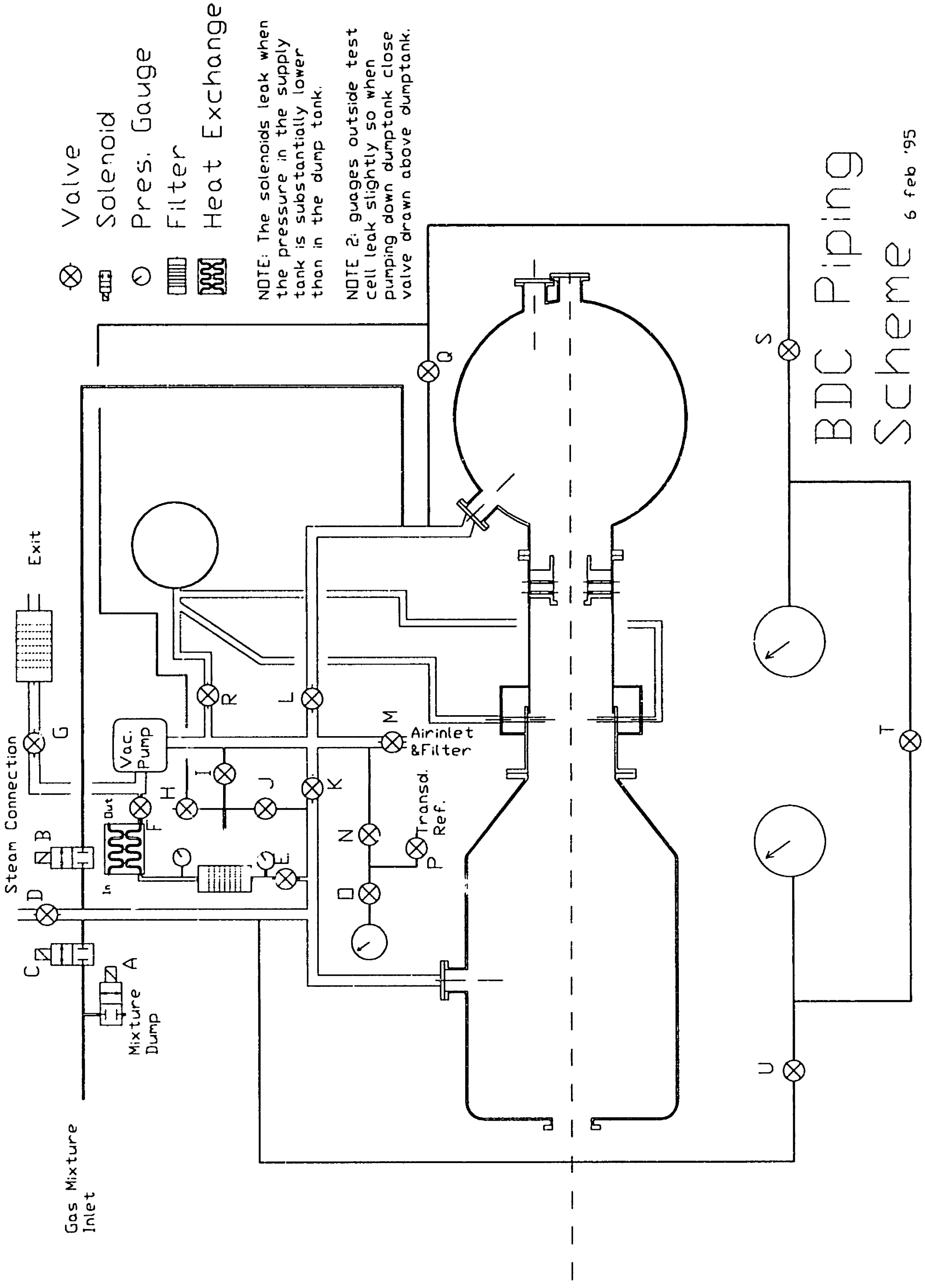

NOTE: The solenoids leak when the pressure in the supply tank is substantially lower than in the dump tank.

NOTE 2: guages outside test cell leak slightly so when pumping down dumptank close valve drawn above dumptank.

Figure A.1 Schematic of piping in Blowdown Compressor Facility

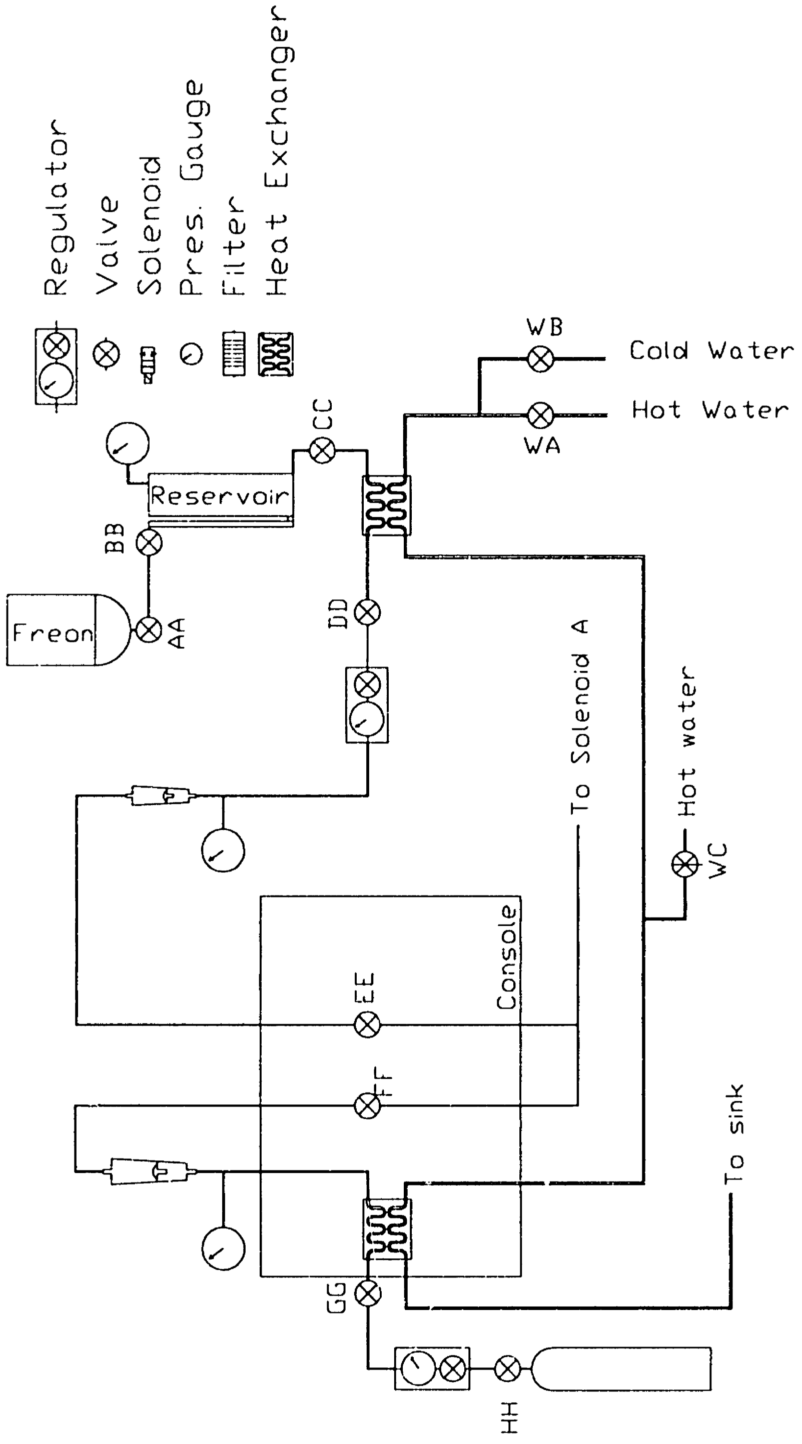

Figure A.2 Schematic of equipment used to mix gasses

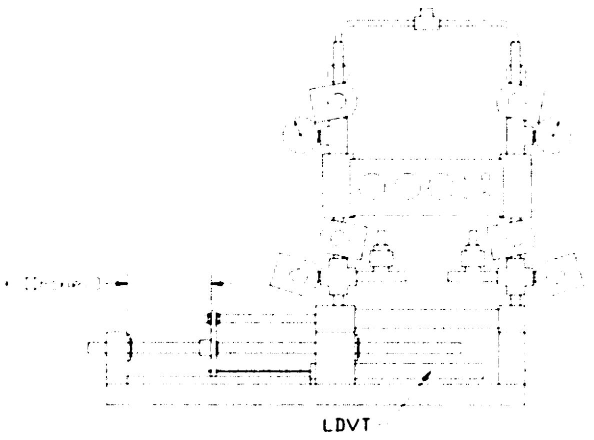

Figure A.3 Scaled drawing of 4Way probe translator .

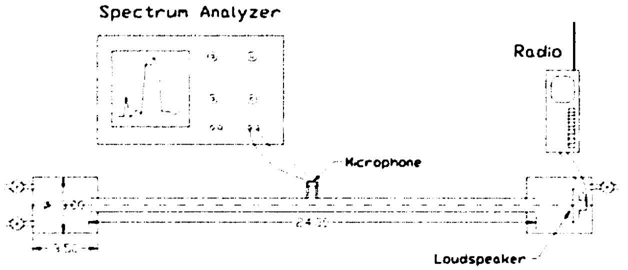

Figure A.4 Scaled drawing of the speed of sound device

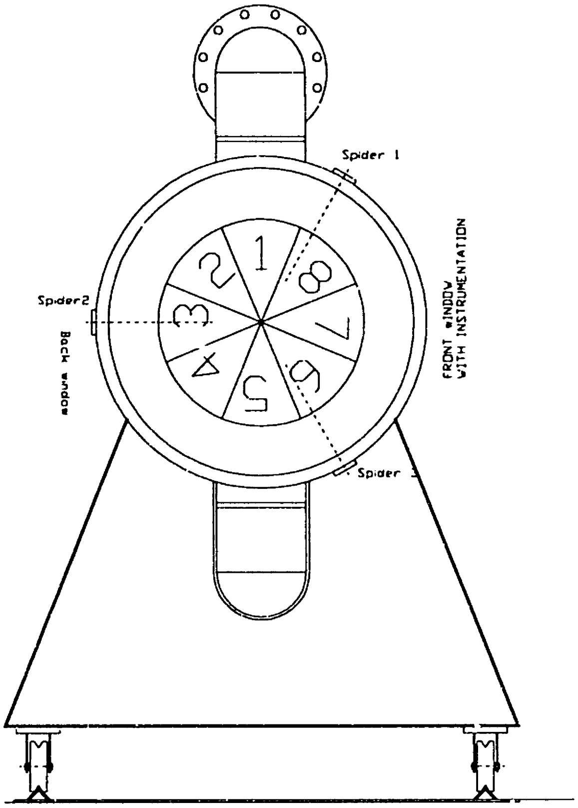

Figure A.5 Scaled drawing of the diaphragm illustrating numbering

Appendix B Fabrication of Boundary Layer Scoop Blades

For this experiment 5 blades of the aero elastic Blowdown Compressor rotor were modified. The blades were taken out of the disk and channels as specified in the drawings (figures B.1 - B.3) were milled in the aluminum blades. The boundary layer is scooped by the graphite scoop, enters the blade on the suction surface, diffuses while going from the suction side to the pressure side and enters the cavity on the pressure side. It flows radial inwards via 3 parallel channels and leaves the blade for the disk just above the spring pins which hold the blade as seen in figure B.4. The flow enters a cavity in the back of the disk which is sealed by a ring mounted on the back of the disk as illustrated in figure B.5. A 0.540 Inch hole connects the cavity behind each blade with the front of the disk where it enters the system to remove the fluid out of the rotating system. The resulting shape of the blade is shown in figure B.6.

After the completion of the modification of the disk and the milling of the 5 blades, the scoop itself had to be fabricated. The scoop would be essentially a plate as thin as possible facing a high speed flow while experiencing very high centrifugal forces. In order to avoid flutter effects and minimize the centrifugal forces, a very stiff and light material was required and therefore graphite was chosen.

Using graphite epoxy required the production of molds: one mold to represent the internal geometry of the scoop and one for the external geometry of the scoop. This was achieved by casting a real blade in silicone compound (Castall S-1284 Fast A/B clear Silicone Rubber compound). The real blade was removed and the resulting mold was used to cast two copies of the real blade. This was necessary because no extra real blades were available. To one of the copies the external shape of the scoop was added. To the second the internal shape, thus the shape of the channel through which the air will flow, was added. The molds are shown in figure B.7. Each resulting blade was cast in silicone. The resulting negative mold for the internal geometry blade was used to copy that blade but now made out of heat resistant Devcon High Temperature Mold Maker C1. So at this stage we have a negative mold which contains the external geometry of the blade and a blade made out of heat resistant mold maker which has the internal geometry of the scoop added to it. When this blade is put into the negative mold just the space taken by the scoop remains vacant. Thought was given to use the real modified blade for a mold because it would facilitate this whole process considerably. But this proved impractical because the high curing temperature of the epoxy would affect the heat treatment of these 7075-T6 blades and might stress relieve them thus changing their geometry.

The scoop (figure B.9) itself consists of 7 layers of 5 mils thick AS4-3501-6 39% net-resin pre impregnated graphite epoxy and a layer of 0.75 Oz/yard^2 fiber glass (figure B.8). The layers were oriented to maximize axial stiffness. The fibers of the top layer were aligned with the flow and the subsequent layers were given a small plus and negative angle to minimize thermal stress and deformation. Because of the awkward shape of the scoop, the final orientation and shape of the layers was obtained on a trial and error basis. The molds to cut the different layer of the scoop are shown in figure B.10.

After the seven layers were laid up, a layer of the very thin fibre glass was put on top of the most outer layer. This was done to give the most outer layer which formes the knife edge of the scoop, some strength in the direction perpendicular to the flow direction. Because at the knife edge all fibers face the flow, without the fiber glass the layer would break and crack axially.

The completed lay up was put in the mold between the mold itself and the Devcon blade after spraying mold release on all parts of the blade and mold. The mold was inserted in a strong aluminum box in which the mold itself was cast. The box was placed on an aluminum plate and covered and sealed with special heat resistant plastic and tape. The space between the plate and the plastic was connected to a vacuum pump and evacuated to avoid air bubbles and to press on the mold. The whole assembly was placed in an oven in the machine shop of the Gas Turbine Laboratory and cured 1 hr at 240 F, and 5 hrs at 350 F.

The next step was to remove the cured scoop out of the molds, clean it up and glue it to the modified aluminum blade with a layer of the thin glass fiber impregnated with Eccobond 45 clear between the scoop and the aluminum blade to improve the fit and the bond strength. This assembly was put back in the negative mold and cured at room temperature while pressed. Finally, the scoop was cut to have the knife edge on the specified position and polished. The result is shown in figure B.11.

The only task remaining was to close up the channels on the pressure side of the blade. This was accomplished by first making a cover using a regular blade as a mold. In order to make the cover as thin as possible while not deforming under load, the glass fiber cloth (2 Oz./yard^2, see figure B.8) was reinforced with loose graphite fibers perpendicular to the channels in the blade. The mold blade was sprayed with Eccoslip 122S mold releaser after which the graphite fibers were put in places and covered with two layer glass fiber cloth (0/90) impregnated by Epoxy Patch epoxy. Both cloth layers had the fibers aligned in the radial and perpendicular to radial direction..After curing the cover was removed from the regular blade, roughed and using clear Epoxy Patch glued on the slotted blade. Finally, the blade was polished to obtain a smooth shape.

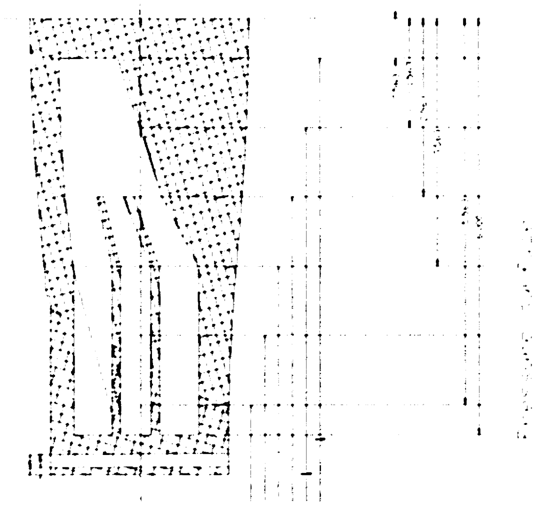

Figure B.1 Specification of channels in pressure surface

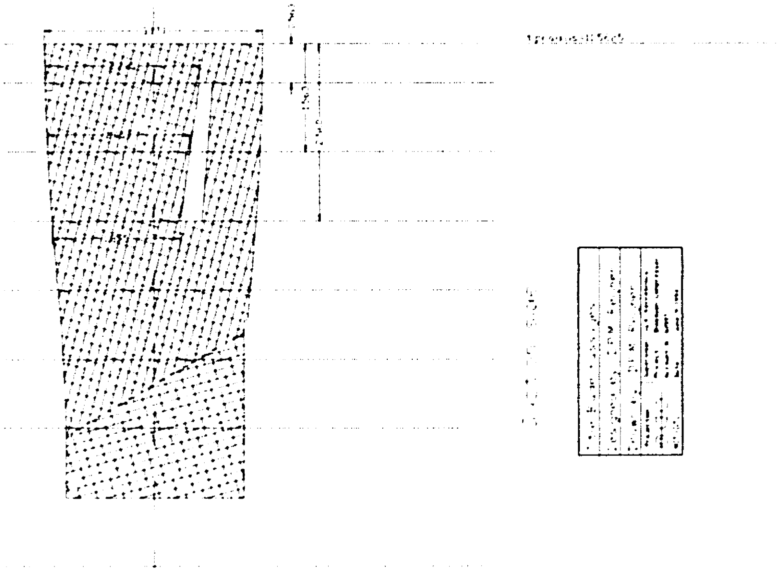

Figure B.2 Specification of slot in suction surface

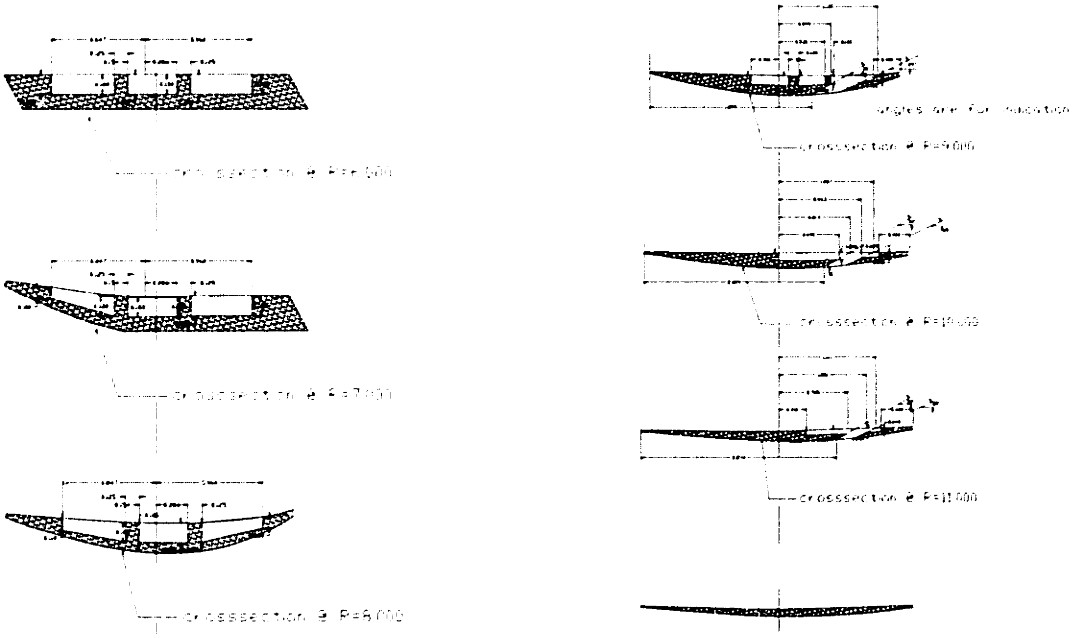

Figure B.3 Cross section of modified blade

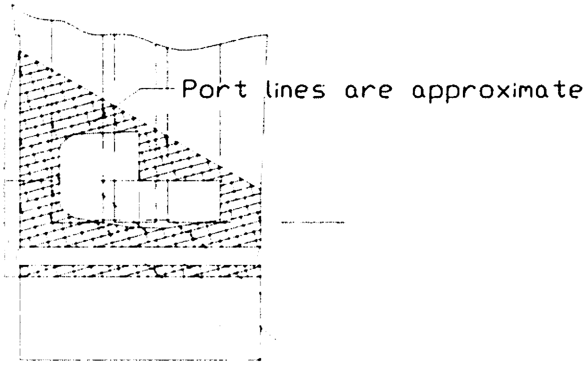

View E-E

Figure B.4 Transition between blade and root

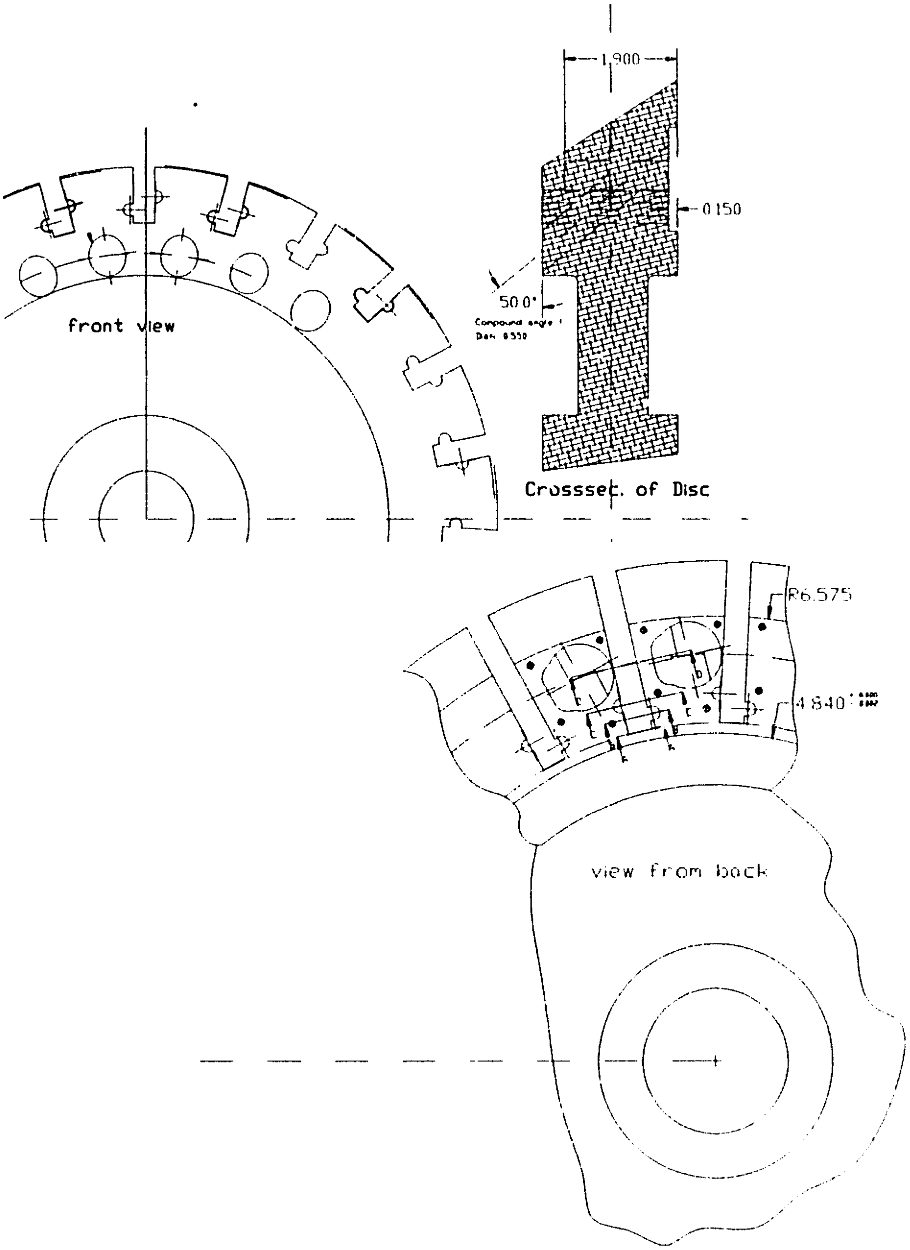

Figure B.5 Cavity and channels in rotor disk

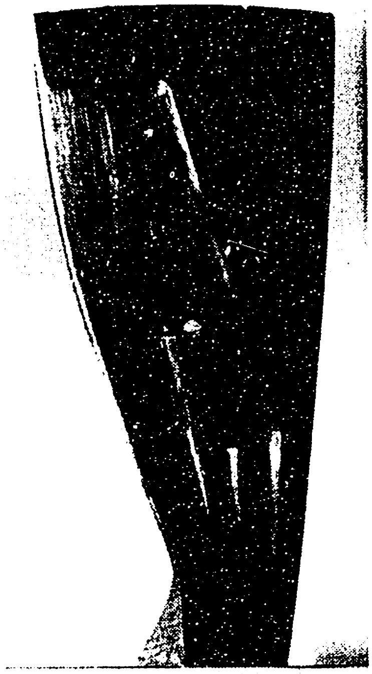

Figure B.6 Channels in pressure side of blade

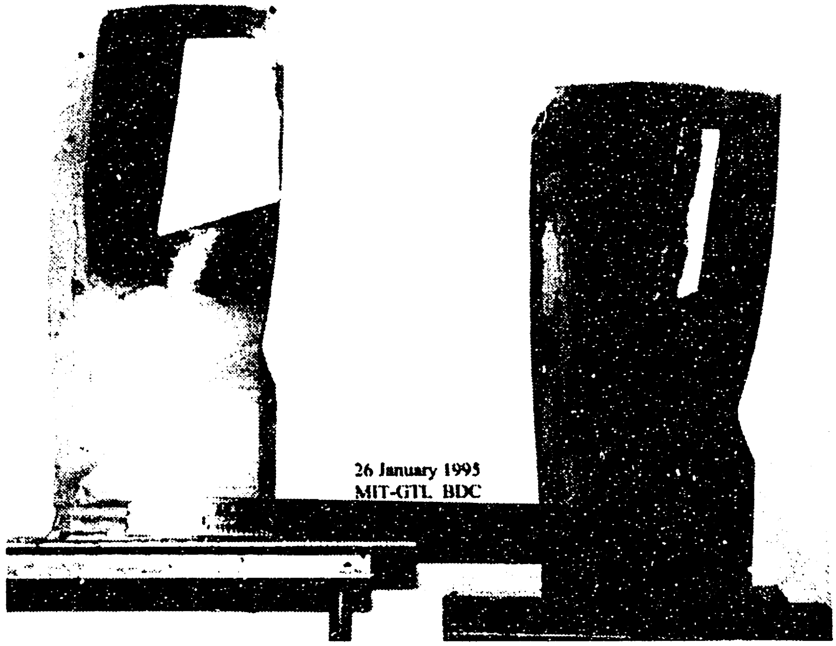

Figure B.7 Mold for external (left) and internal geometry (right)

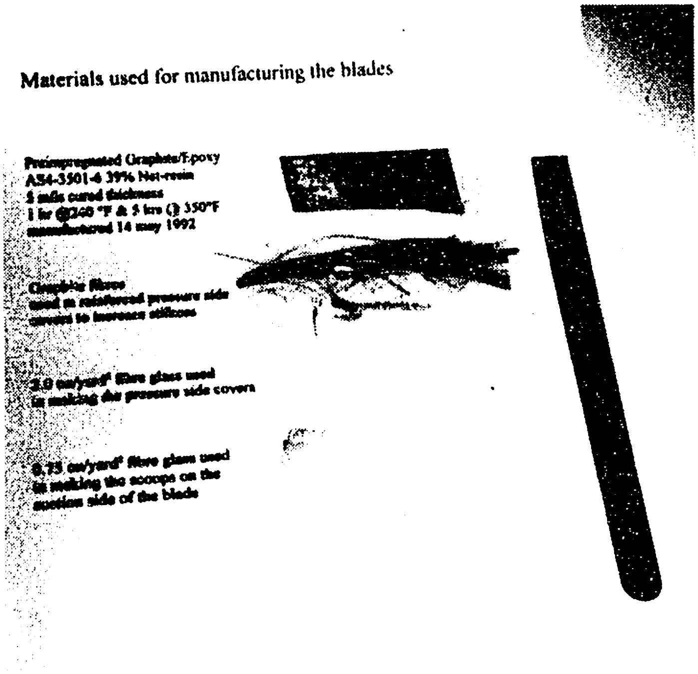

Figure B.8 Materials used to make scoop and cover

Figure B.9 Boundary layer scoop before being bonded to blade

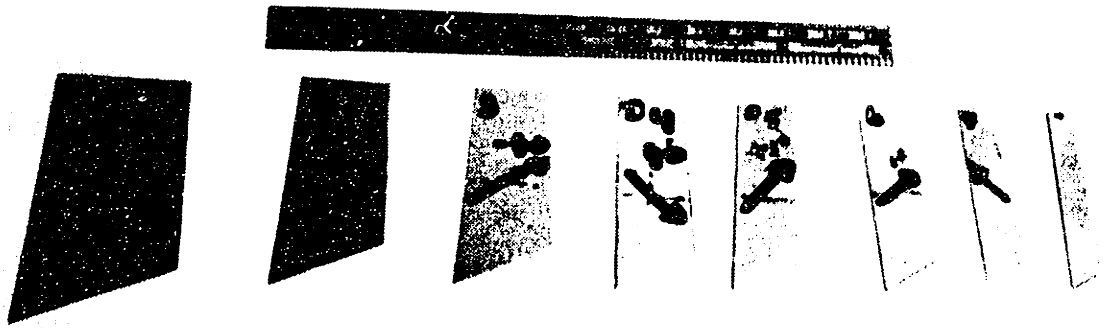

Figure B.10 Molds used to cut layers

Figure B.11 Suction side of resulting blade

Appendix C 4Way Probe

C.1 Introduction

The concept of the 4Way probe was developed at the M.I.T. Gas Turbine Laboratory in the mid seventies. Basically, a probe was required to do real time simultaneous measurements of the unsteady flow Mach number, stagnation pressure and angle behind high speed turbo machinery blades. In order to achieve the high frequency response, small transducers mounted directly in the flow were needed. A photograph of the resulting design is shown in figure C.1.

The probe features 4 silicon diaphragm type transducers mounted on a elliptical shaped cylinder 45 degrees angles to the mean flow. One transducer (referred to as P_1) directly faces the flow and measures a pressure very close to the total pressure. A second and third diaphragm are mounted slightly aside and 45 degrees up, resp. down of the first one. The fourth diaphragm is mounted on a 45 degree wedge cut at the end of the cylinder. When facing the probe front side which houses the transducers and pointing the wedge side to your left (similar to mounting the probe in the windtunnel in the usual way), transducer 2 is the bottom transducer.

The four transducers measure four pressures which can be converted using a suitable calibration into a total pressure (P_t), static pressure (P_s), tangential (θ) and radial angle (ϕ). This can easily be seen when considering that the P_1 & P_4 provide radial angle information, P_1 & P_2/P_3 provide static and total pressure information, and P_2 & P_3 provide the tangential angle. Using P_t, P_s, θ and ϕ, the flow Mach number and its components can be determined using geometric relations and definition of total pressure.

C.2 Physical Description of Probe

C.2.1 Geometry and Frequency Response

For later reference, detailed drawings of the newly built (November 1995) 4 way probe are included in the back of this appendix. See figures C.18-C.26. The tolerances on the head of the probe and the extension are all less than ±0.5 mils.

As can be seen in the drawings, the elliptical tip body of the probe is 130 mils x 170 mils with the 130 mils semicircle facing the flow. (1 mil is a thousand of an inch which equals 2.54 E-5 meter.) These dimensions were basically set by the size of the silicon transducers.

It is important to note the size of the probe relative to the feature one is trying to measure. The Blow Down Compressor rotor has a diameter of 23.135 Inches (0.587 meter), 23 blades, a streamline constant chord of 3.140 Inches (0.082 meter), a hub to tip ratio of 0.64 at the exit of the fan, a solidity (chord/blade spacing) of 1 at the tip and a rotational speed of 167 rev/sec. This means that the probe fills 1/25 of a blade spacing at the tip and 1/16 at the hub. So the probe is small compared to the blade spacing and even comparable to the wakes, which typically fill around 20% of the blade passage in this kind of rotor. Using a simple model described in reference C.1 the frequency response can be estimates based on the blade velocity and the geometry of the probe. Transducers 1, 2 and 3 are mounted approximately 65 mils apart, which enables the good spatial resolution of the tangential angles, P_s and P_t. The fourth transducer is approximately 200 mils away from the other three because of geometric constraints. To obtain P_s,

P_t, ϕ and θ all four pressures are used. Given that the natural frequency of the transducers is in excess of 200 kHz, as is described below, the frequency of the disturbance which can be accurately resolved is determined by the speed at which the disturbance is convected over the probe and the size of the sensing area of the probe. This is the maximum distance between two transducers, which is approximately twice the diameter (d=3.3 mm) of the probe. So f_{max}=U/(2*2d)=25 kHZ. Where U is the rotor tip speed: 167 rev/s*π*0.58=300 m/s. This turns out to be 6.5 times the blade passing frequency. Because the tangential angle measurement is virtually uninfluenced by the radial angle and thus by the pressure of the transducer 4, the characteristic length for this measurement is only one probe diameter which yields a frequency of 50 KHZ.

C.2.2 Specifications of Transducers

Transducers of the type Kulite XCQ-093-25D were mounted on the probe. These are 0.036x0.036 and 0.020 inches thick. After being mounted and electrically hooked up, the transducers were covered with a thin layer of silicone to provide some form of protection to the transducers and a thermal insulation. To improve the insensitivity to thermal drift even more, the probe head is water cooled, to prevent it from heating up while in vacuum.
The recent transducers have a natural frequency in excess of 200 kHz, and have excellent thermal compensation, in strong contrast with the earlier versions. The drift was measured to be about 1%/100 Deg F which coincides with the specifications given by the manufacturer in table C.1. The drift during the experiment was determined by doing a run with the reference pressure line connected to the dump tank which means that the pressure difference over the diaphragm is zero before and after the run. This way the drift over the time of the experiment could be obtained. 900 msec after the start of the experiment, the drift was measured to be 280 , 110, 150 and 45 Pa. This yields a thermal drift of less than 0.8% over a time span nearly 4 times that of the experiment.

C.2.3 Probe Material

The probe head is made of a special NiFe alloy which thermal expansion coefficient is close to that of the silicon transducers. This is done to avoid thermal expansion problems.
The alloy is named ALLOY 42 and was obtained from Scientific Alloys Inc, P.O.Box 523, 379 Old Hopkinton Road, Westerly, R.I. 02891, tel: (401) 596 4947. Made following ASTM F 30 specifications and cold finished it has the following composition in percents:
C 0.004, P 0.007, S 0.009, Si 0.18, Mn 0.44, Ni 40.45, Co 0.04, Cr 0.09, Al 0.003, Fe balance.
Its coefficient of thermal expansion was measured to be: 25°C - 300°C 4.24 10^{-6} in/in/C

25°C - 350°C 4.77 10^{-6}
25°C - 400°C 5.87 10^{-6}
25°C - 450°C 6.97 10^{-6}

by the manufacturer.

C.3 Calibration Procedure of 4Way Probe

C.3.1 Calibration of 4Way Probe

The current Blow Down Compressor 4Way probe (made November 1995 together with an identical twin for the Blow Down Turbine) was calibrated by Boeing at Boeing Field using their experimental setup during the first week of June 1996. This setup is shown in figure C.2. The probe was mounted in a holder which could rotate in two directions. The probe was immersed in a 1 Inch (0.0254 meter) diameter jet exhausting to ambient air as seen in figure C.3. Preceding the nozzle of the jet was a 3.055 Inch diameter settling chamber where P_t^* and T_t were measured. These are the values mentioned in the data received from Boeing. Using these values Boeing calculated their estimates of the free jet Mach number. However, the P_t^* is not the real P_t of the flow because it is measured using a simple wall pressure tap in the settling chamber. Using the area ratio of the nozzle and the ambient pressure P_p, P_t^* was corrected for the flow velocity in the settling chamber and the real free jet Mach number and P_t were obtained. In the following equations P_p denotes P_t^* (plenum pressure) and P_j denotes free jet pressure (ambient pressure). A_j is the area of the nozzle and A_p is the cross sectional area of the plenum.

$$M_j = \sqrt{\frac{\left(\frac{P_p}{P_j}\right)^{\frac{\gamma-1}{\gamma}} - 1}{\frac{\gamma-1}{2}\left[1-\left(\frac{P_p}{P_j}\right)^{-\frac{2}{\gamma}}\right]\left(\frac{A_j}{A_p}\right)^2}} \qquad [C.1]$$

$$P_t = P_j\left(1+\frac{\gamma-1}{2}M_j^2\right)^{\frac{\gamma-1}{\gamma}} \qquad [C.2]$$

During the calibration the ambient pressure, the pressure in the plenum and the temperature in the plenum were measured in addition to the four 4Way probe transducer pressures. This brings the number of quantities measured for each sample to 7.

The probe was tested for seven different free jet Mach numbers: 0.0981, 0.3156, 0.4076, 0.5045, 0.6023, 0.7017, 0.9187.

For each Mach number 21 tangential angles (θ) were set: -26.0, -22.0, -18.0, -14.0, -12.0, -10.0, -8.0, -6.0, -4.0,-2.0, 0.0, 2.0, 4.0, 6.0, 8.0, 10.0, 12.0, 14.0, 18.0, 22.0, 26.0.

In addition 13 different radial angles (ϕ) were set: -20.0, -16.0, -12.0, -9.0, -6.0, -3.0, 0.0, 3.0, 6.0, 9.0, 12.0, 16.0, 20.0.

So for each Mach number setting 13 x 21 = 273 different sample points were taken. Which totals for all Mach numbers to 1911 different sample points.

C.3.2 4Way Probe Algorithm

The objective of the 4Way probe algorithm is to predict the P_t, P_s, tangential and radial angle for a given P_1, P_2, P_3 and P_4. This is achieved in the following manner: Using P_t, P_s, P_1, P_2, P_3, P_4 one tries to find nondimensional variables which are preferably only sensitive to θ or ϕ and not to the Mach number. Another important property the variable needs is monotonic behavior with θ or ϕ. This ensures that only one value of the variable corresponds to each value of θ or ϕ. If possible, one prefers to have variables which are only a function of measured pressures P_1, P_2, P_3 and P_4. This omits iteration steps and makes the calibration logarithm more stable and faster. Historically (reference C.1 and C.2) the following variables were used:

$F_{23}=(P_2-P_3)/((P_2-P_1)+(P_3-P_1))$
$Cp_4=(P_4-P_s)/(P_t-P_s)$

$Cp_1=(P_1-P_s)/(P_t-P_s)$
$Kp_2=(P_2-P_s)/(P_2-P_1+P_3-P_1)$
$Kp_3=(P_3-P_s)/(P_2-P_1+P_3-P_1)$
$H_{23}=(P_t-P_s)/(P_2-P_1+P_3-P_1)$

F_{23} is an excellent choice because it nondimensionalizes the pressure difference between transducer 2 and 3, which is very sensitive to the tangential angle, by a first order guess of the dynamic head ($P_2-P_1+P_3-P_1 \approx -2q$) . Remember P_1 is very close to the total pressure for angles around zero, and the surface pressure around a cylinder in inviscid potential flow reaches the ambient pressure at 42 degrees ($(P-P_\infty)/\rho=\frac{1}{2}U^2(1-9/4\sin^2(\theta))$) away from the flow direction. So the average of the two diaphragms at flow angles below 45 degrees is a very good first estimate of the static pressure. As said before F_{23} does not require any iteration because it only involves quantities measured during the experiment. As a result, F_{23} only has a very small dependence on radial angle and Mach number and is extremely sensitive in θ. F_{23} will be used to obtain the tangential angle.
Cp_4 will be used to obtain the radial angle ϕ but in a less simple way. It depends directly on P_t and P_s, which are not measured directly during the experiment. It is also not independent of θ, because P_t has to be used.
Because of the above described problems with Cp_4 the author changed the code to use Cp_4^* instead of Cp_4. Cp_4^* uses the same first order estimates for the static and total pressure as F_{23} yielding the following definition:

$Cp_4^* = (P_4 - \frac{1}{2}(P_2+P_3)) / (P_1 - \frac{1}{2}(P_2+P_3))$

This provides slightly better results and faster iterations.

The resulting variables are chosen to facilitate the determination of P_t and P_s without experiencing singularities!(at θ 22.5 degrees $P_1=P_2$, $\phi=22.5$ $P_1=P_4$, etc.) For a given θ, ϕ and Mach number, the 4 additional nondimensional variables (Cp_1, Kp_2, Kp_3, H_{23}) are determined and can obtained in the calibration data base. Cp_1 and H_{23} combine to provide P_t:

$$P_t = P_1 + H_{23}(1-Cp_1)(P_2-P_1+P_3-P_1) \qquad [C.3]$$

The static pressure can be obtained by using either Kp_3 or Kp_2. However, the best results are obtained when the average of both static pressures is used. This eliminates problems due to non monotonic behavior of Kp_2 & Kp_3 at high tangential angles.(at high positive θ P_1 is too close to P_2, and at high negative θ P_1 is too close to P_3):

$P_s^{**} = P_2 - Kp_2\,(P_2 - P_1 + P_3 - P_1)$
$P_s^{***} = P_3 - Kp_3\,(P_2 - P_1 + P_3 - P_1)$
$Ps = \frac{1}{2}(P_s^{**} + P_s^{***})$ [C.4]

At this point two nondimensionalized coefficients (F_{23} and Cp_4^*) can be determined based on the 4 measured pressures for a sample point during the experiment of interest. The same can be done for each data point taken during the calibration. Because the Mach number, tangential and radial angle are known during the calibration, curves can be generated for F_{23} as functions of θ for a constant Mach number and radial angle. Similarly curves of Cp_4^*, Cp_1, Kp_2, Kp_3 and H_{23} as function of ϕ for constant tangential angles and Mach numbers can be generated. See figure C.4-C.10. If M and ϕ were known during the experiment, θ could be simply obtained by interpolation using the F_{23} vs θ and the known value of F_{23}. Because F_{23} was chosen to have a minimal dependence on M and ϕ, even using a calculated guess for M and ϕ will provide a very reasonable answer for θ. Therefore an iteration is used to determine θ, ϕ, P_s and P_t. So using a guess for P_t, P_s ($M=f(P_s,P_t)$) and ϕ, θ is obtained. Subsequently the obtained θ and guessed Mach number are used when interpolating Cp_4^* vs θ and obtaining θ. When θ, ϕ and M are known the additional 4 nondimensional variables (Cp_1, Kp_2, Kp_3, H_{23}) can be obtained from the calibration database enabling calculation of P_t and P_s using equations C.3 and C.4. As a last step the Mach number is recalculated based on the (new) P_t and P_s and is used as an input for the next iteration.

Summarizing, the following procedure is used to obtain the angles and P_t & P_s during a run:

1) Estimate P_t & P_s (Use P_t=P_1, P_s is lowest of P_2 & P_3)
2) Calculate total Mach number based on P_t & P_s
3) Calculate F_{23c} & Cp_{4c}^*
4) Start iteration
5) Assume radial angle (ϕ) is zero
6) Determine F_{23} as function of tangential angle (θ) for given ϕ and Mach number
7) Interpolate and find θ for calculated F_{23c}
8) Determine Cp_4^* as function of ϕ, for given θ and Mach number
9) Interpolate and find ϕ for calculated Cp_{4c}^*
10) Determine F_{23} as function of tangential angle (θ) for given ϕ and Mach number
11) Interpolate and find Θ for calculated F_{23c}
12) Determine Cp_4^* as function of ϕ for given θ and Mach number
13) Interpolate and find ϕ for calculated Cp_{4c}^*
14) For given θ, ϕ and Mach number retrieve Cp_1, Kp_2, Kp_3, H_{23} from database
15) Calculate new static pressure using equation C.4
16) Calculate new total pressure using equation C.3
17) Calculate new Mach number
18) Check difference between old and new static pressure, if too large goto 4)
19) Calculate components of Mach number using ϕ and θ

Usually the logarithm converges in 3 to 6 iterations. On average every 1000 samples require less than 40 seconds on the 80486-50MHz used. So the whole process takes about half an hour per experiment.

C.4 Limitations, Accuracy and Error analysis.

Unfortunately, the program does not succeed in recovering every angle and P_t & P_s exactly. The higher the dynamic head, the larger the errors in P_t and P_s become due to the $\gamma/(\gamma-1)$ factor in the equation which determines the Mach number. In addition it was found that transducer 2 (and therefore F_{23}) does not increase monotonically between $\theta=2$ and $\theta=6$ degrees for Mach numbers 0.3,0.4 and 0.5 for many radial angles as can be seen in figures C.5-C.7. This means that the algorithm cannot determine a value between 2 and 6 degrees when this behavior occurs. Fortunately, these Mach numbers are rather low and the tangential angle rather high. The mean flow the probe tries to resolve during the experiment is in M=0.6 to 0.8 and θ= -10 to -5 range and is thus unaffected. The errors because of this and the ambiguity of the algorithm are illustrated in figures C.11 and C.17.

Unfortunately, the data taken by the data acquisition system also contains noise. All transducers which were expected to see high frequency pressure fluctuations were not filtered using an analog filter. When no digital filter is applied after obtaining the data, the noise is approximately ±0.8% during the experiment.

It is interesting, however, what influence this noise has on the obtained results. To analyze this an error analysis was performed. For a typical rotor outflow Mach number of 0.7 and the probe lined up with the mean flow, ±1% noise (with no coherence assumed) will lead to the following possible errors $d\theta=\pm1$deg, $d\phi=\pm2$deg, dPt=0 to 1%, dPs=-2.8% to 1.2%. When examining the data, however, the errors seem much smaller, which can be due to the noise affecting all 4 transducers approximately equally. Because the calibration procedure is non-dimensionalized and mainly measures pressure difference, an up spike in all transducers results in small errors.

During the experiment the 4Way probe is translated using a pneumatic translator. At the end of the translation the probe is stopped by letting run into a soft rubber stop. Because a significant deformation of the rubber stop occurs, during these set of experiments the probe was never translated very close to hub out of fear of damaging the probe by hitting the hub. Thus no wake data is available for radial position under 70% span.

Because of the size of probe and especially the distance between the transducer on the tip and the 3 other transducers the probe suffers errors in area were very strong radial gradients exist. Because of this the probe is not able to predict radial angle in these regions. This effects results in measured radial angles at the tip which would lead the flow into the casing wall while the wall is of course imposing a no radial flow condition at the casing. This can be simply explained by the fact that the tip transducers sees the total pressure outside the casing boundary layer while the other 3 transducer are fully submerged in the casing boundary layer and therefore see the low total pressure. Because of the higher total pressure on the tip the probe is fouled in believing that there is a (mean) radial flow.

References:

C.1 Gertz, Jeffrey B., "Unsteady Design-Point Flow Phenomena in Transonic Compressors", p.10-18, GTL Report No. 188, 1986.

C.2 Figueriedo, W.A., "Spherical Pressure Probe for Retrieving Free Stream Pressure and Directional Data", 1977.;

C.3 Analog Digital Technology, "AD-830 user's manual", acquired Jan. 1993.

Dimensions in Inches	0.036 x 0.036 square 0.020High
Pressure range	25 Psi Differential
Burst pressure	75 Psi
Over Pressure	50 Psi
Max excitation	15 VDC
Residual Unbalance	± FSO
Comb. Non-lin.& Hyst.	0.5% FS BFSL
Sensitivity at Vexc=10 VDC	4 mVolt/Psi D
Comp. Temperature range	35 deg F to 235 F
Repeatability	0.1%
Natural Freq.	200 kHz
Thermal sensitivity shift	1%/100 deg F

Table C.1 Source Kulite Semiconductor Products Bulletin KS-1000D & personal comm. Specifications of XCQ-093-25D

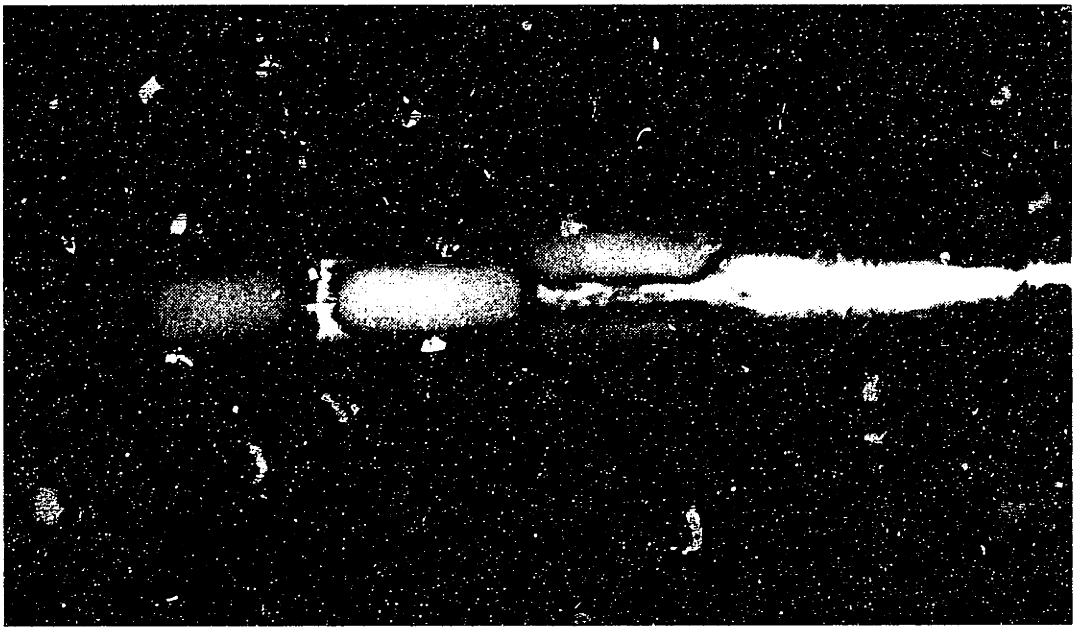

Figure C.1 Photograph of 4Way probe (November 1995 Built identical (Turbine) probe is shown)

Figure C.2 Probe Test Facility at Boeing Field

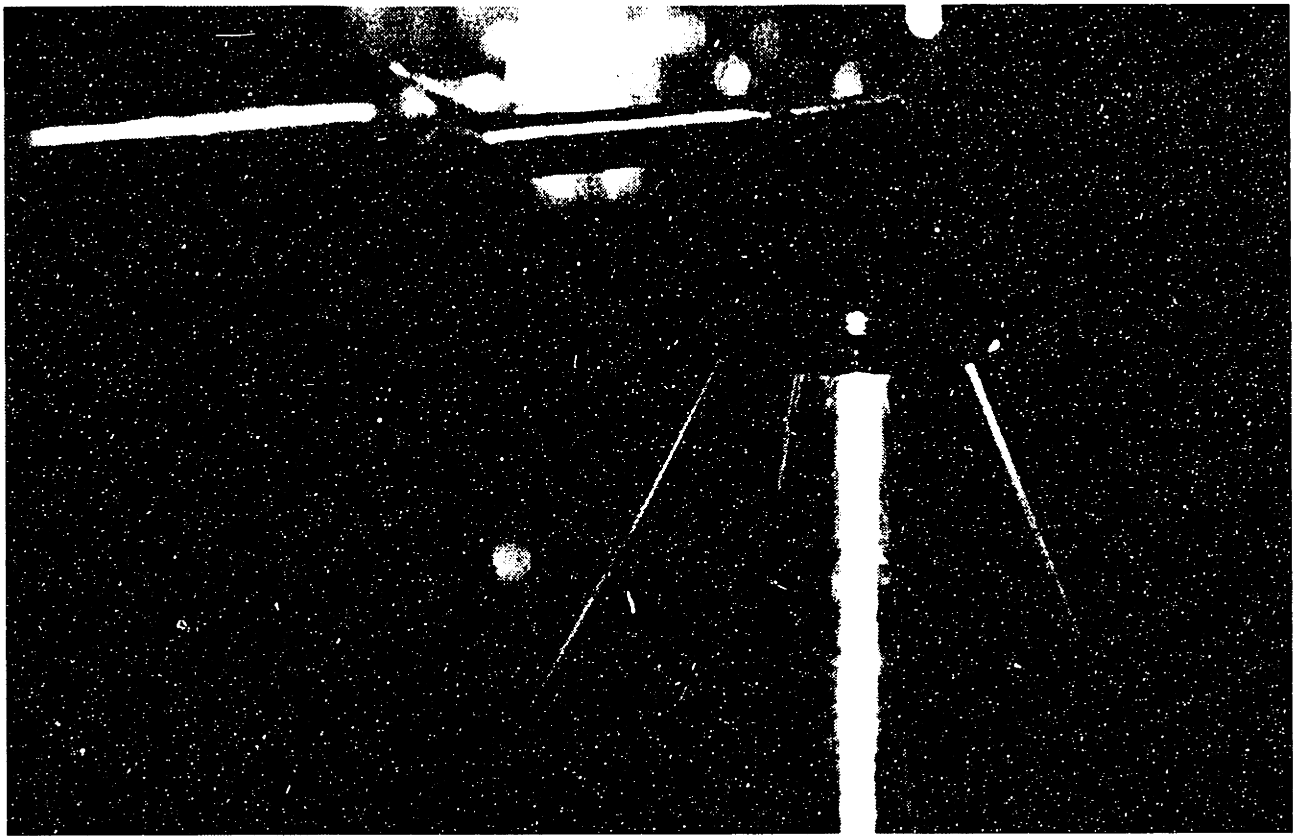

Figure C.3 Detail of 4Way Probe Head in Free Jet

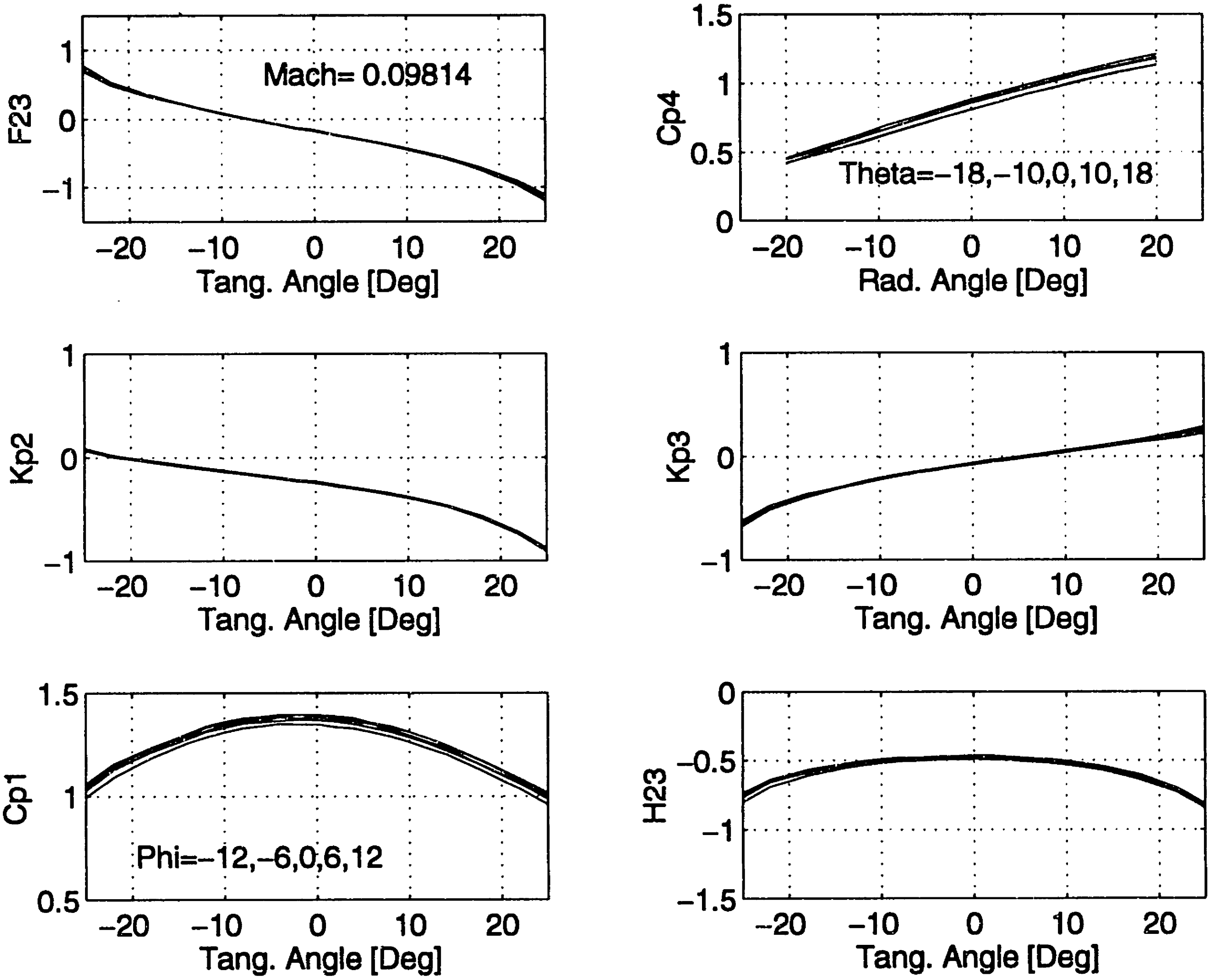

Figure C.4 F_{23}, Cp_4, Cp_1, Kp_2, Kp_3 and H_{23} as function of θ and ϕ for M=0.10

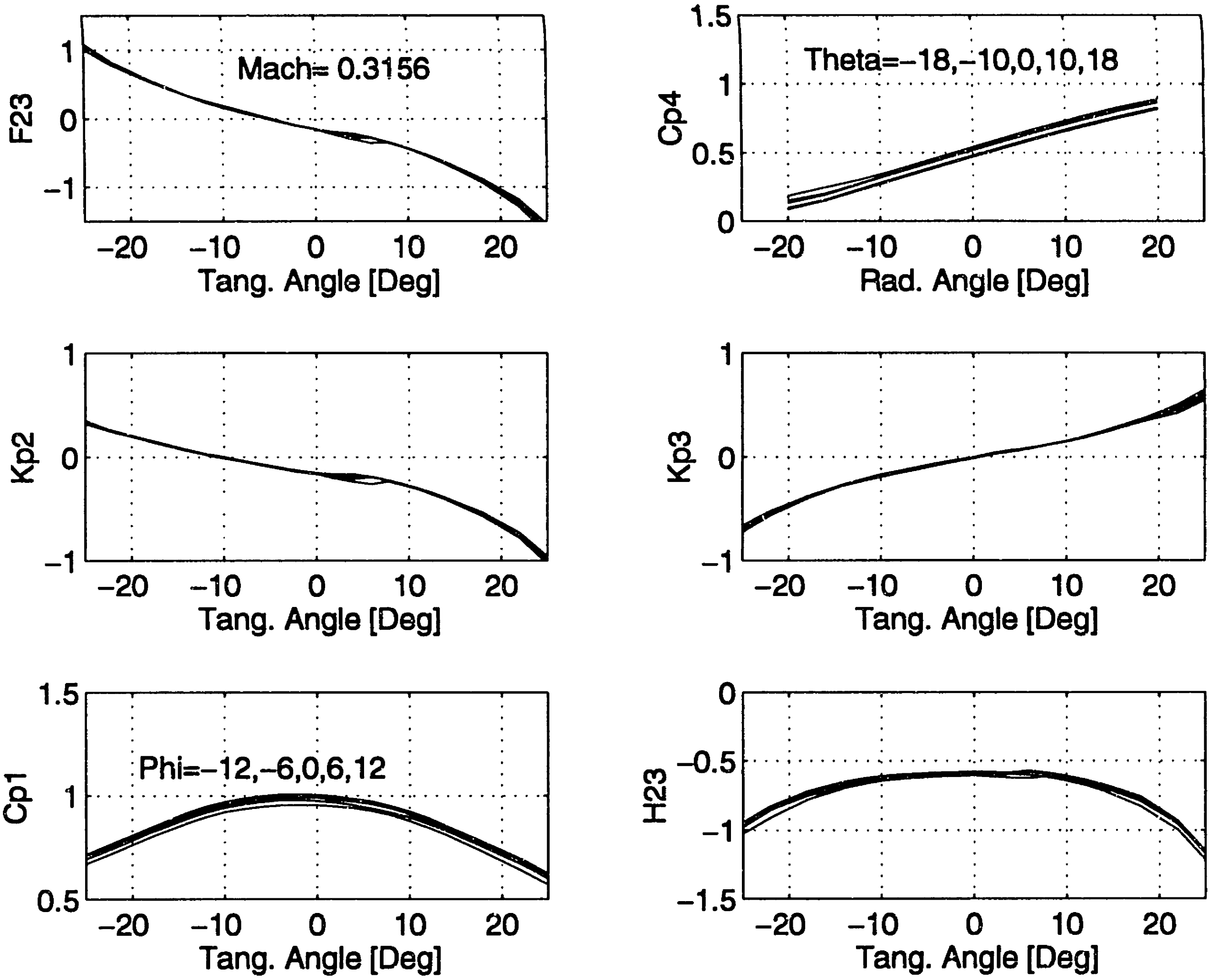

Figure C.5 F_{23}, Cp_4, Cp_1, Kp_2, Kp_3 and H_{23} as function of θ and ϕ for M=0.32

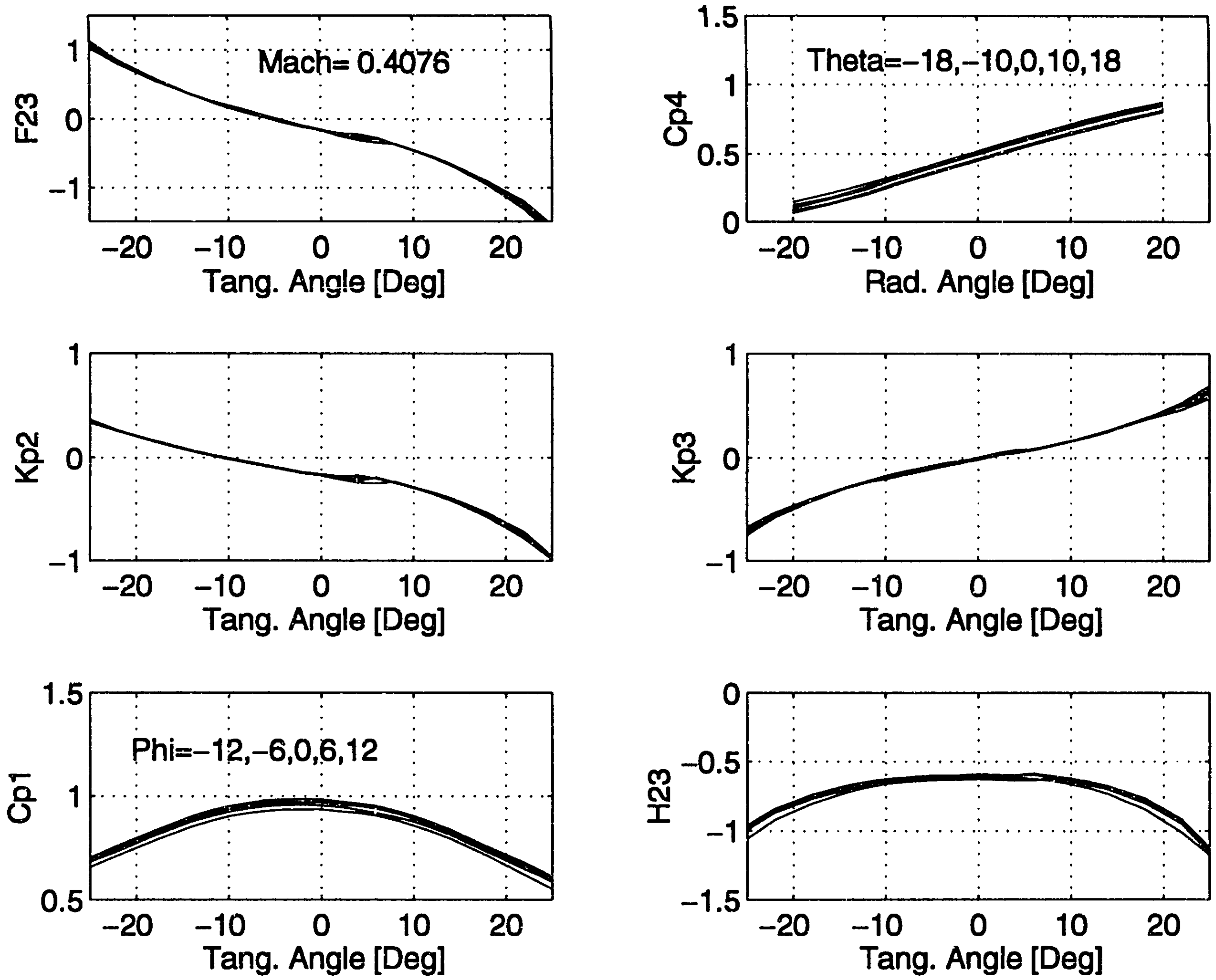

Figure C.6 F_{23}, Cp_4, Cp_1, Kp_2, Kp_3 and H_{23} as function of θ and ϕ for M=0.41

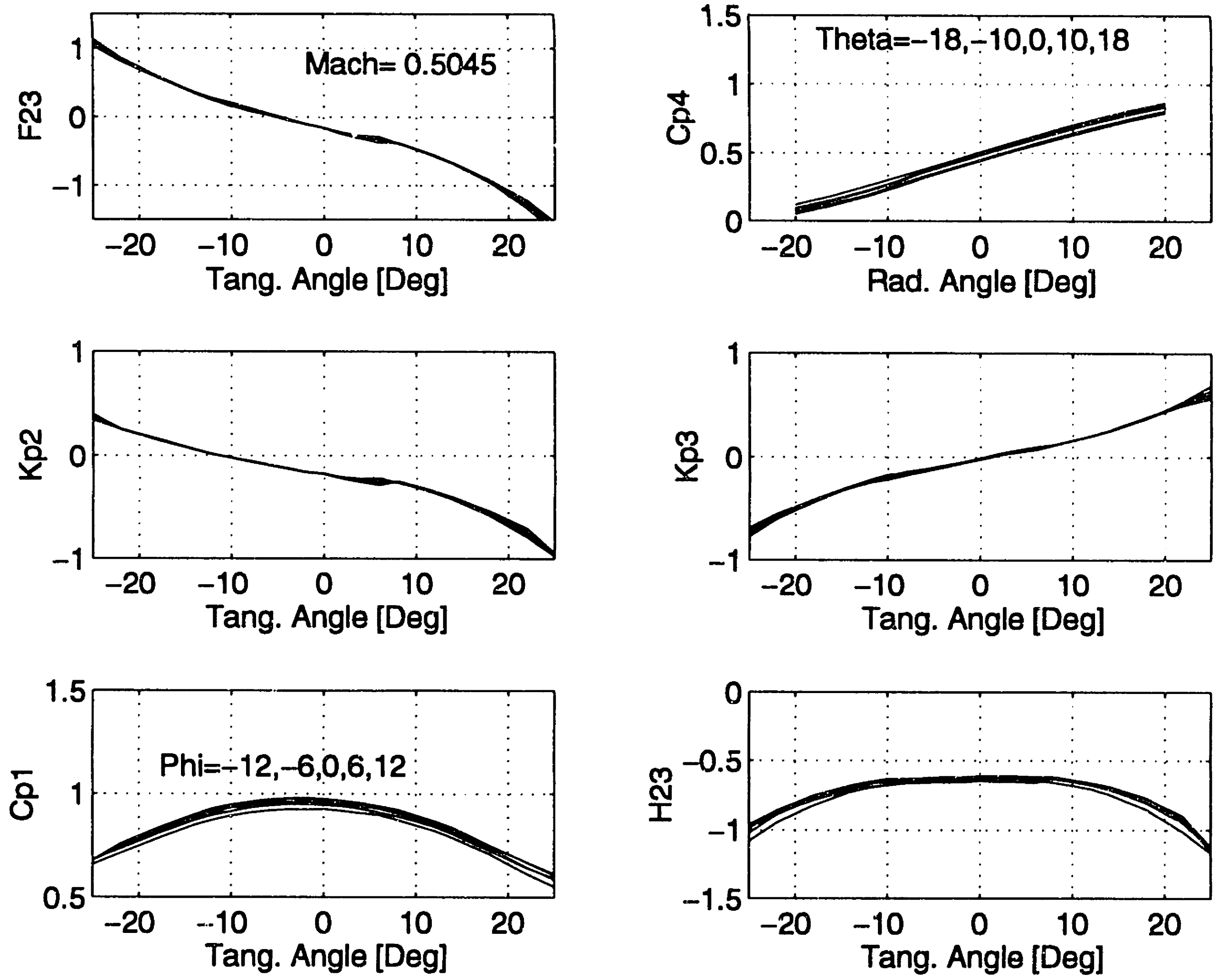

Figure C.7 F_{23}, Cp_4, Cp_1, Kp_2, Kp_3 and H_{23} as function of θ and ϕ for M=0.51

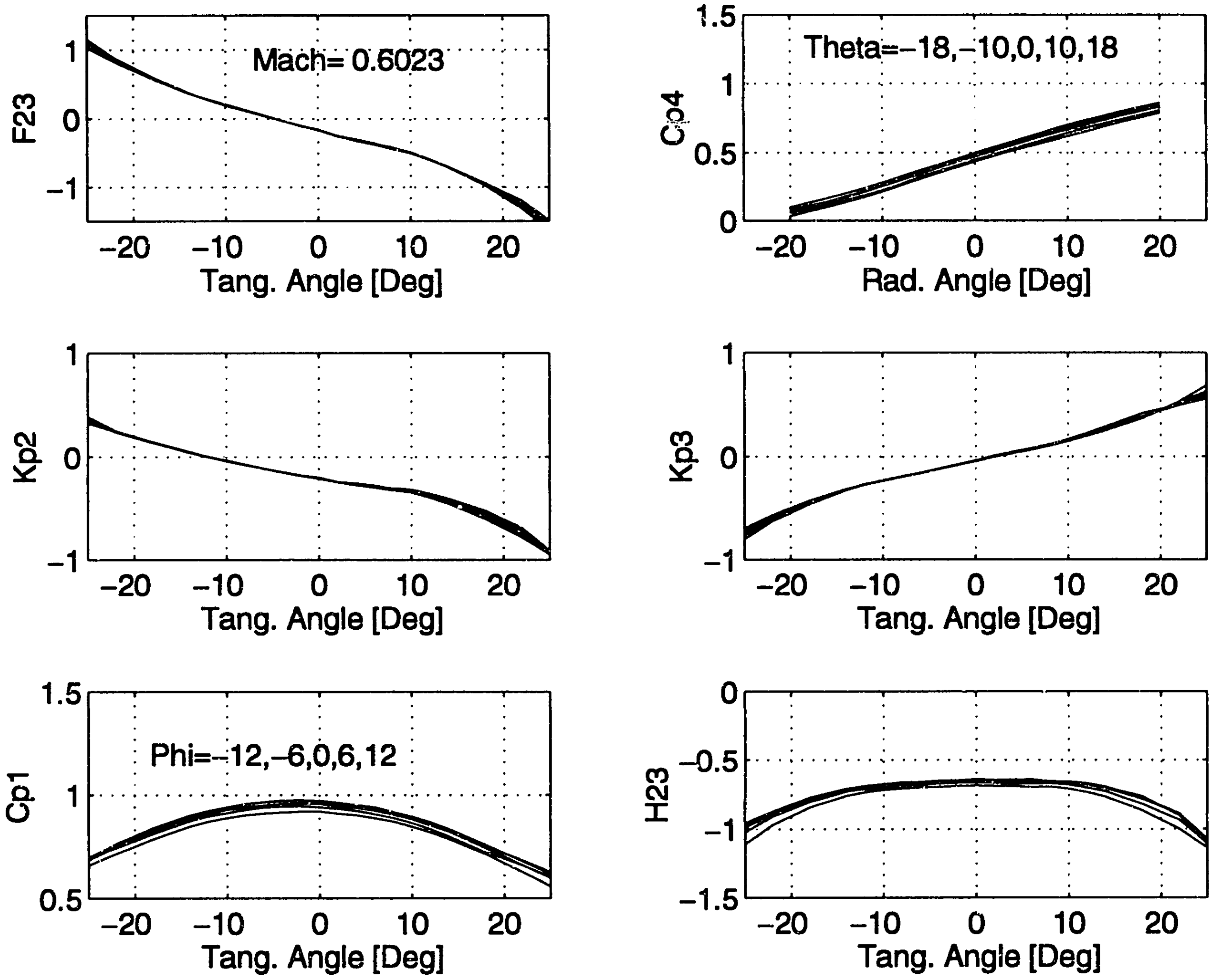

Figure C.8 F_{23}, Cp_4, Cp_1, Kp_2, Kp_3 and H_{23} as function of θ and ϕ for M=0.60

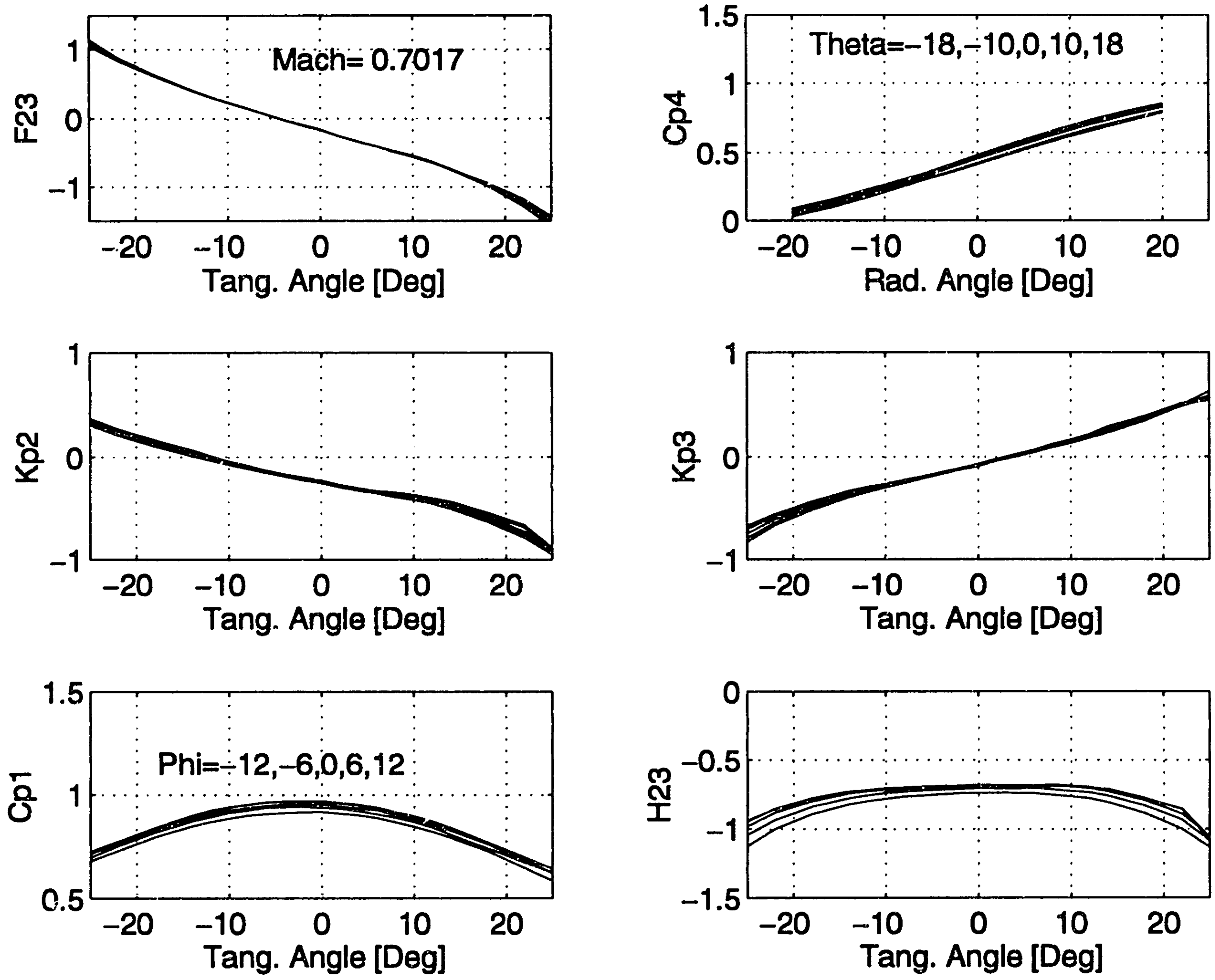

Figure C.9 F_{23}, Cp_4, Cp_1, Kp_2, Kp_3 and H_{23} as function of θ and ϕ for M=0.70

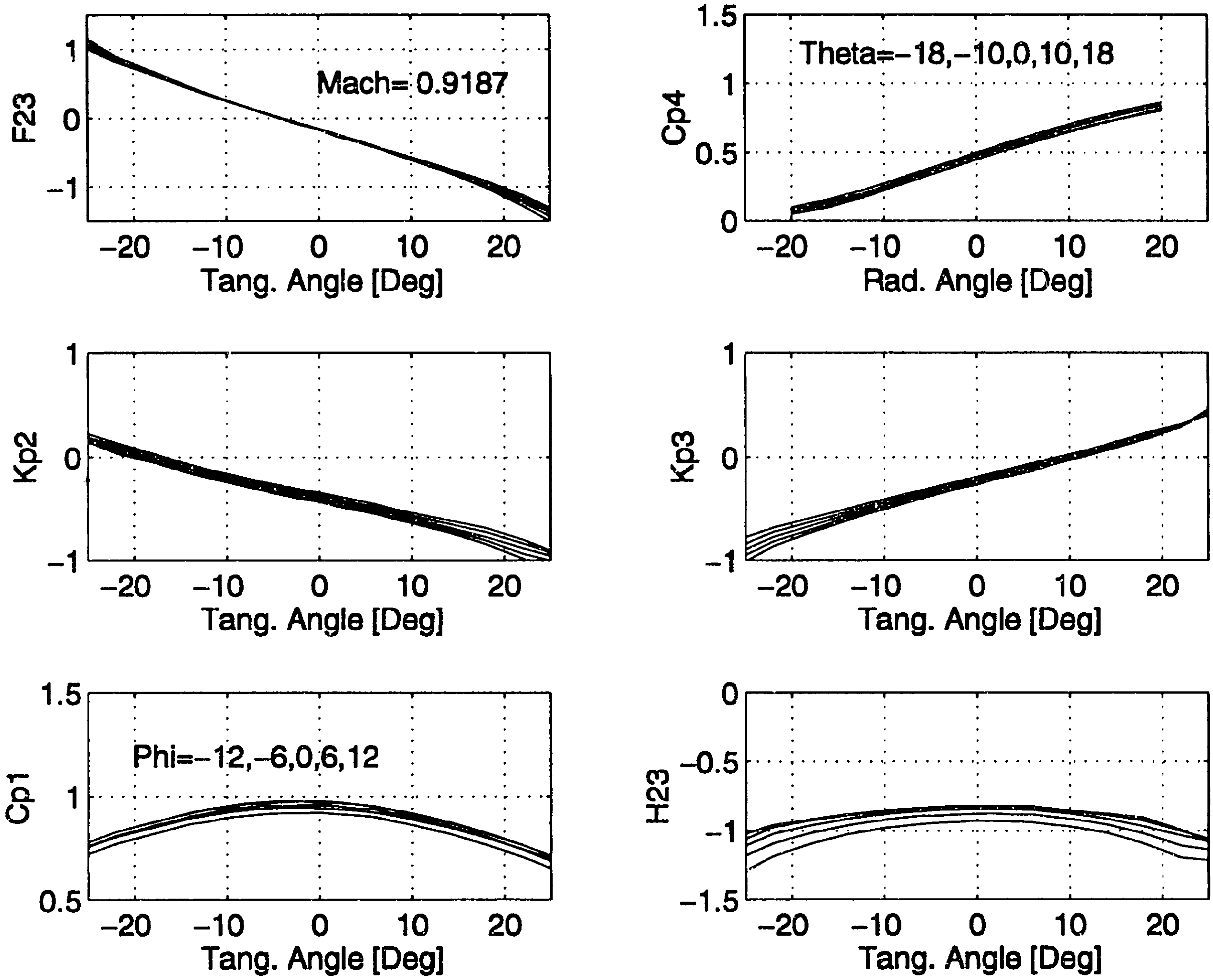

Figure C.10 F_{23}, Cp_4, Cp_1, Kp_2, Kp_3 and H_{23} as function of θ and ϕ for M=0.92

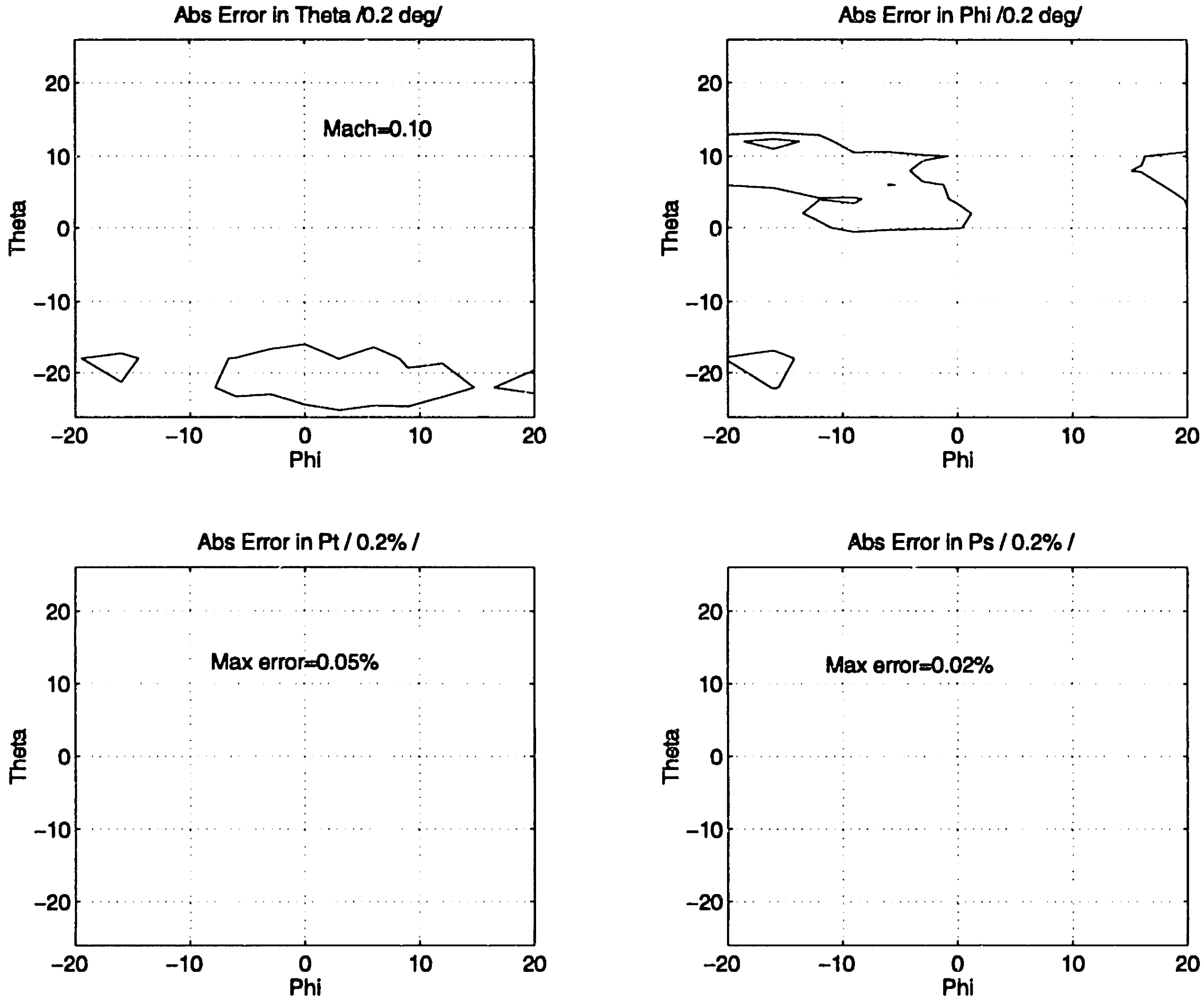
Abs Error in Theta /0.2 deg/

Abs Error in Phi /0.2 deg/

Abs Error in Pt / 0.2% /

Abs Error in Ps / 0.2% /

Figure C.11 Errors in predicted θ, ϕ, Pt and Ps as function of actual θ and ϕ for M=0.10

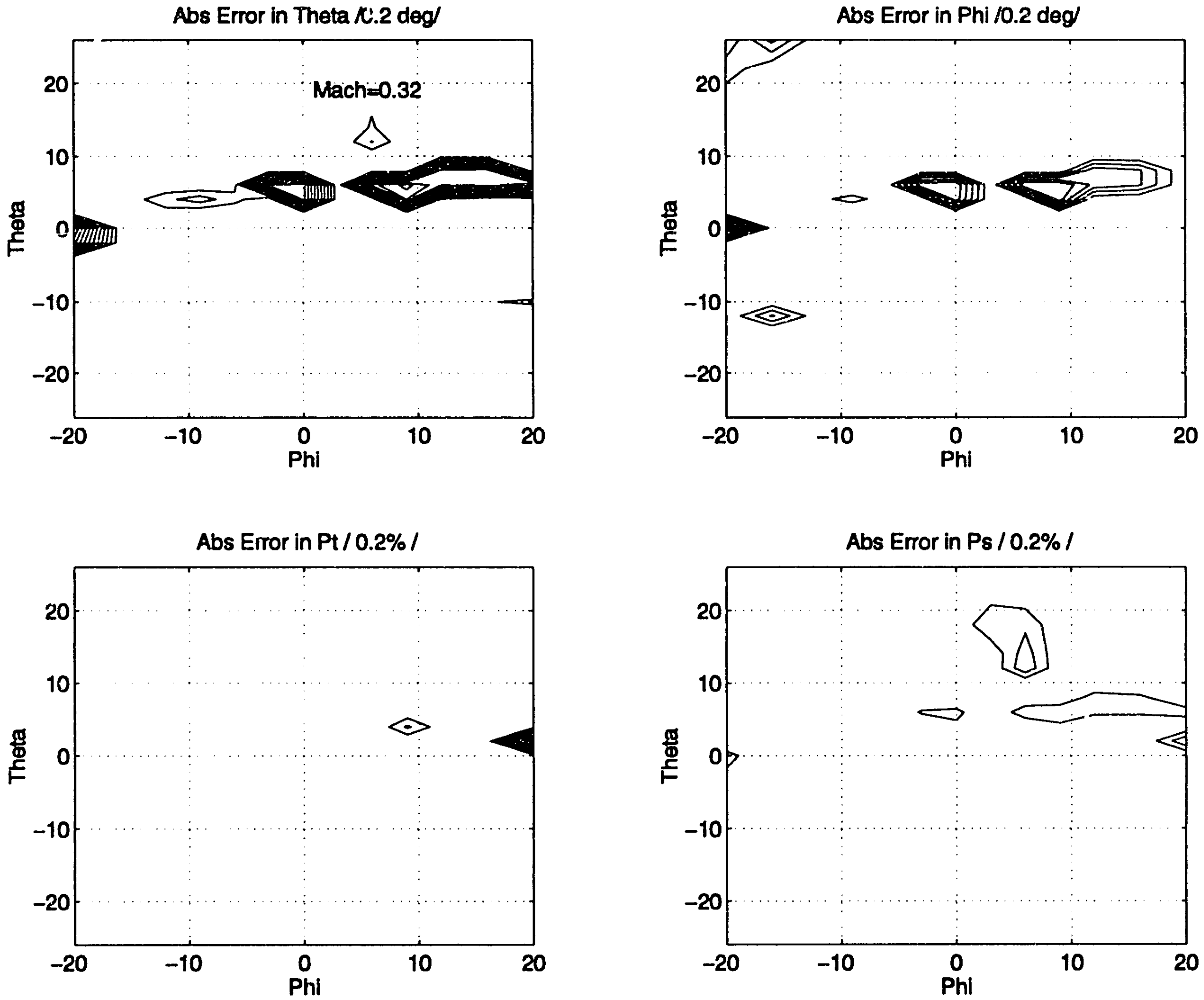

Figure C.12 Errors in predicted θ, ϕ, Pt and Ps as function of actual θ and ϕ for M=0.32

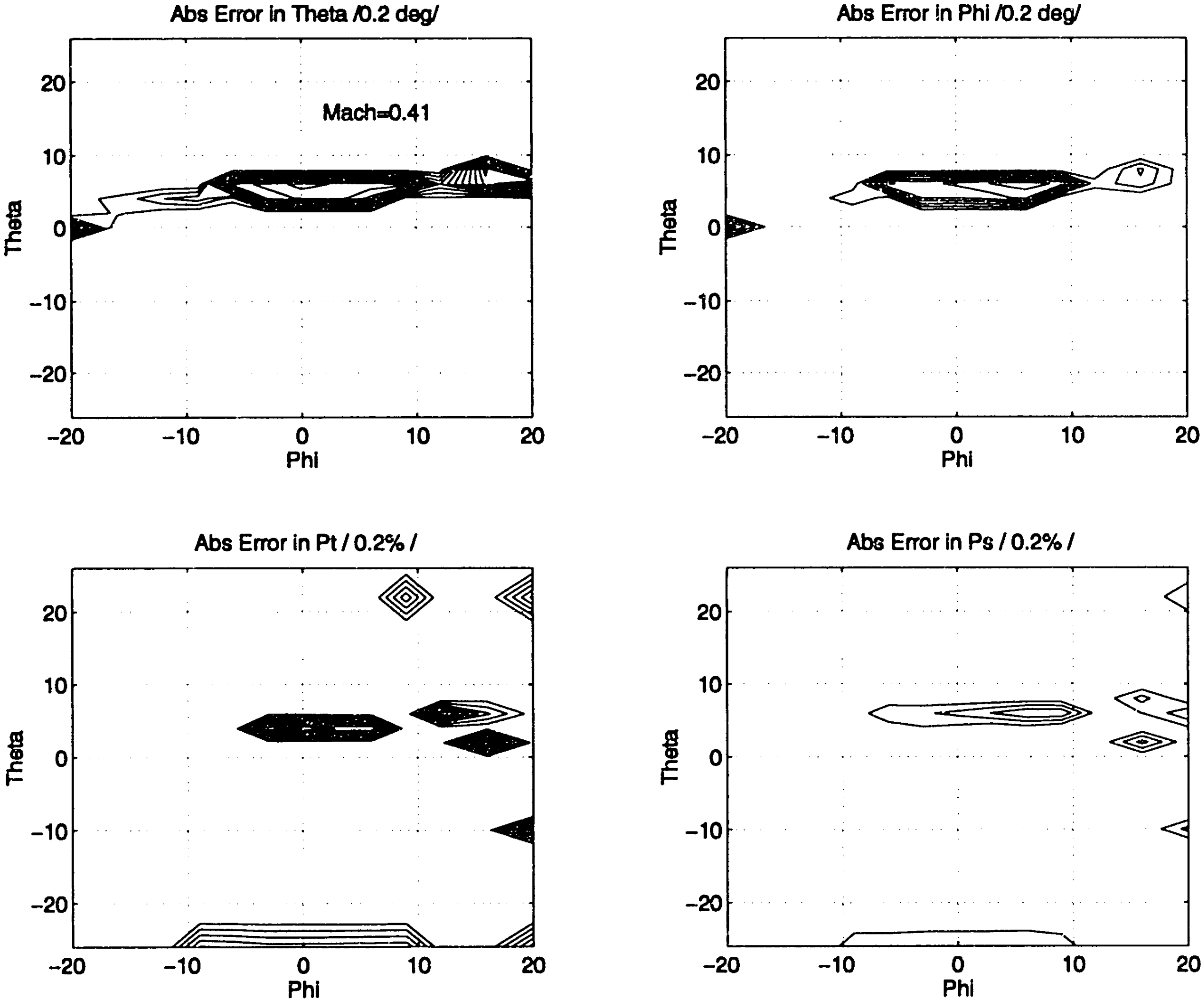

Figure C.13 Errors in predicted θ, ϕ, Pt and Ps as function of actual θ and ϕ for M=0.41

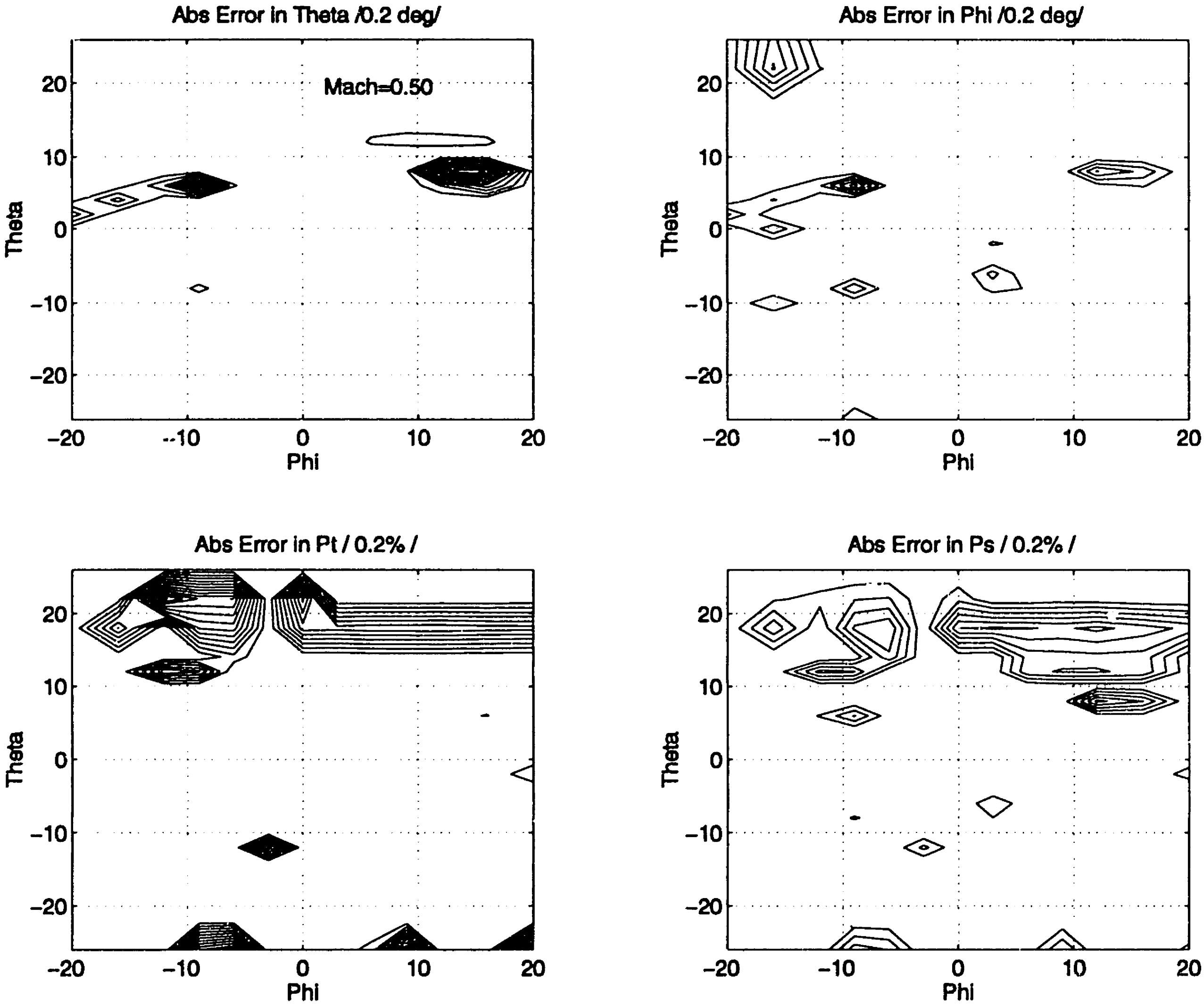

Figure C.14 Errors in predicted θ, ϕ, Pt and Ps as function of actual θ and ϕ for M=0.51

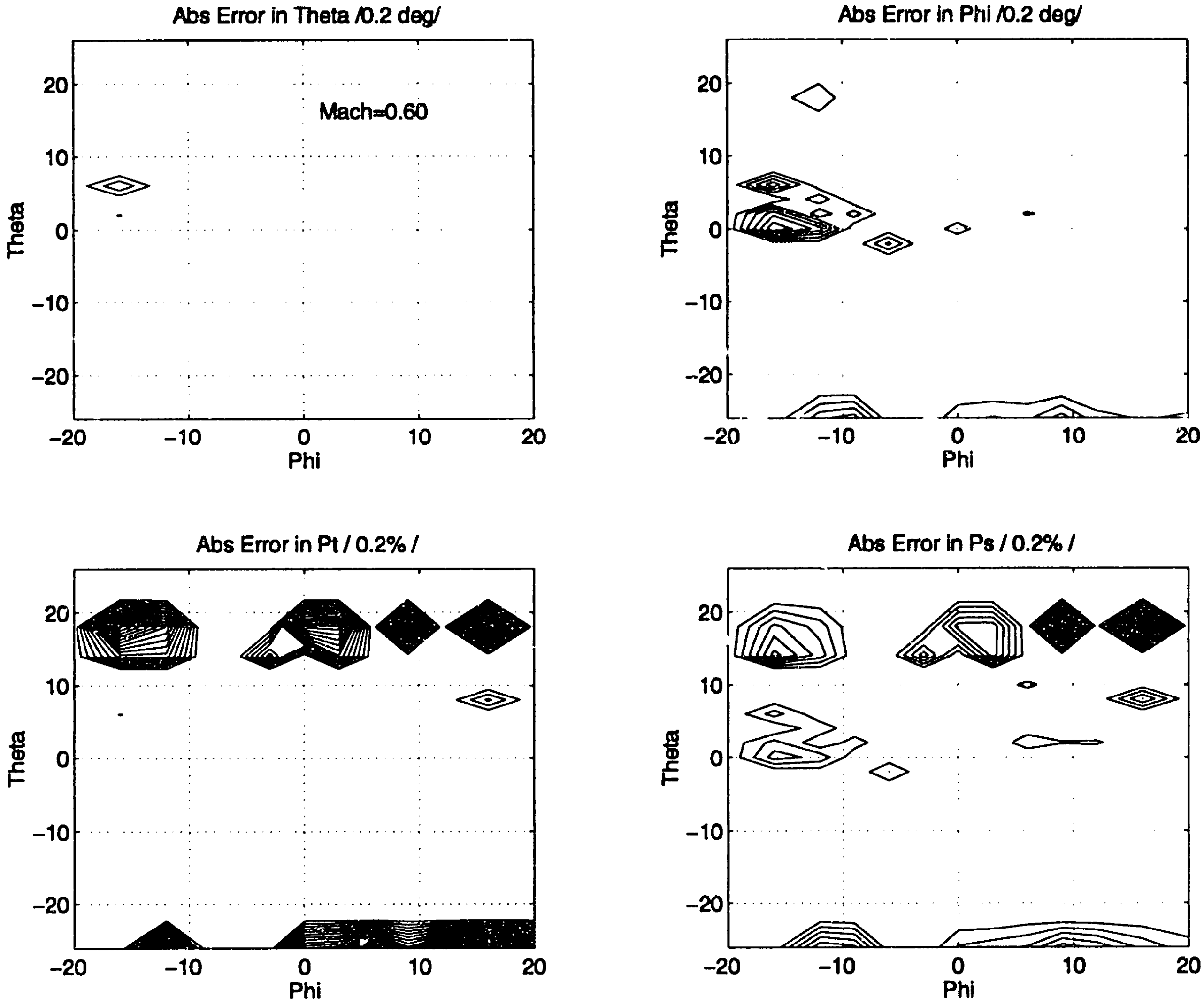

Figure C.15 Errors in predicted θ, ϕ, Pt and Ps as function of actual θ and ϕ for M=0.60

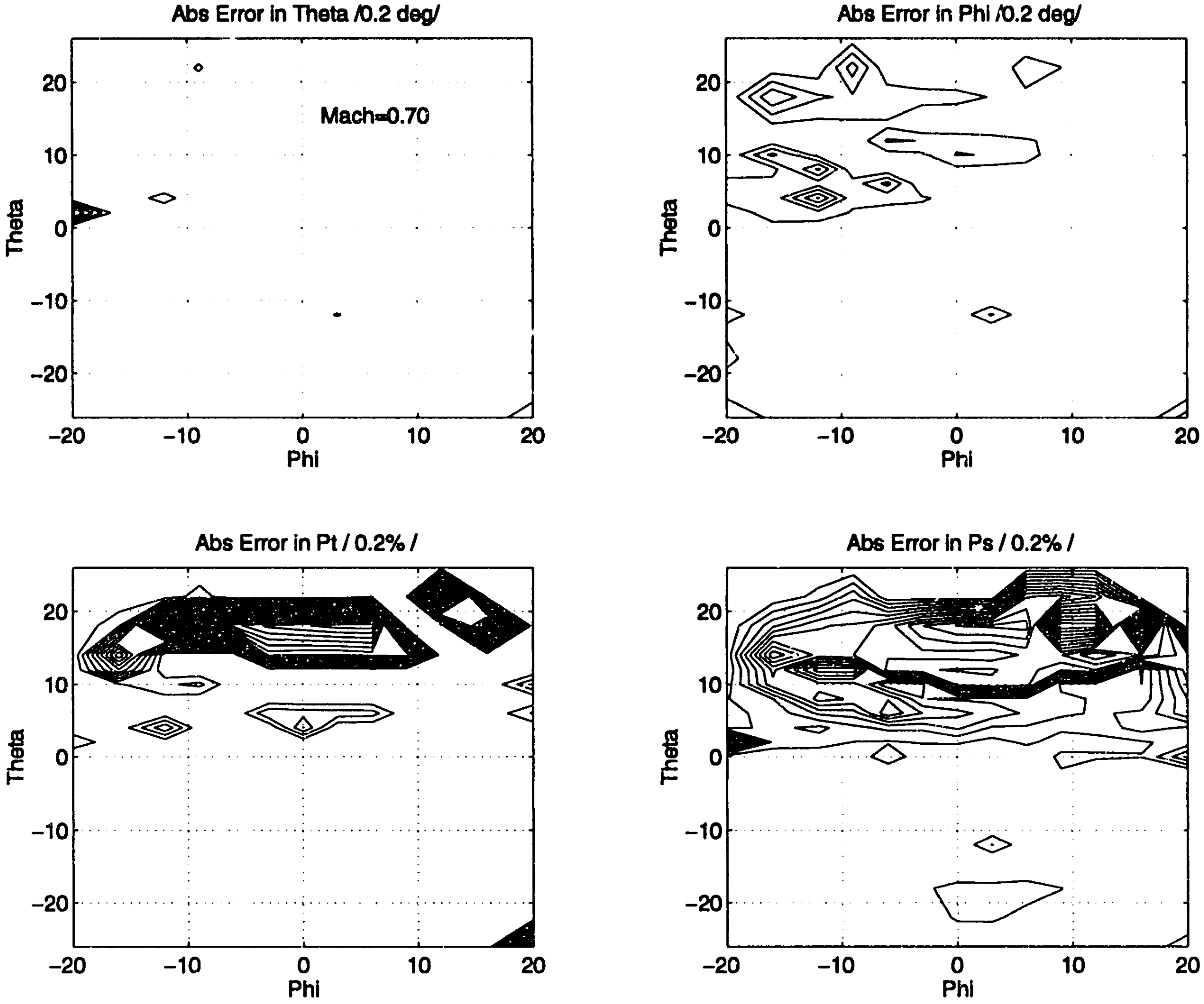

Figure C.16 Errors in predicted θ, ϕ, Pt and Ps as function of actual θ and ϕ for M=0.70

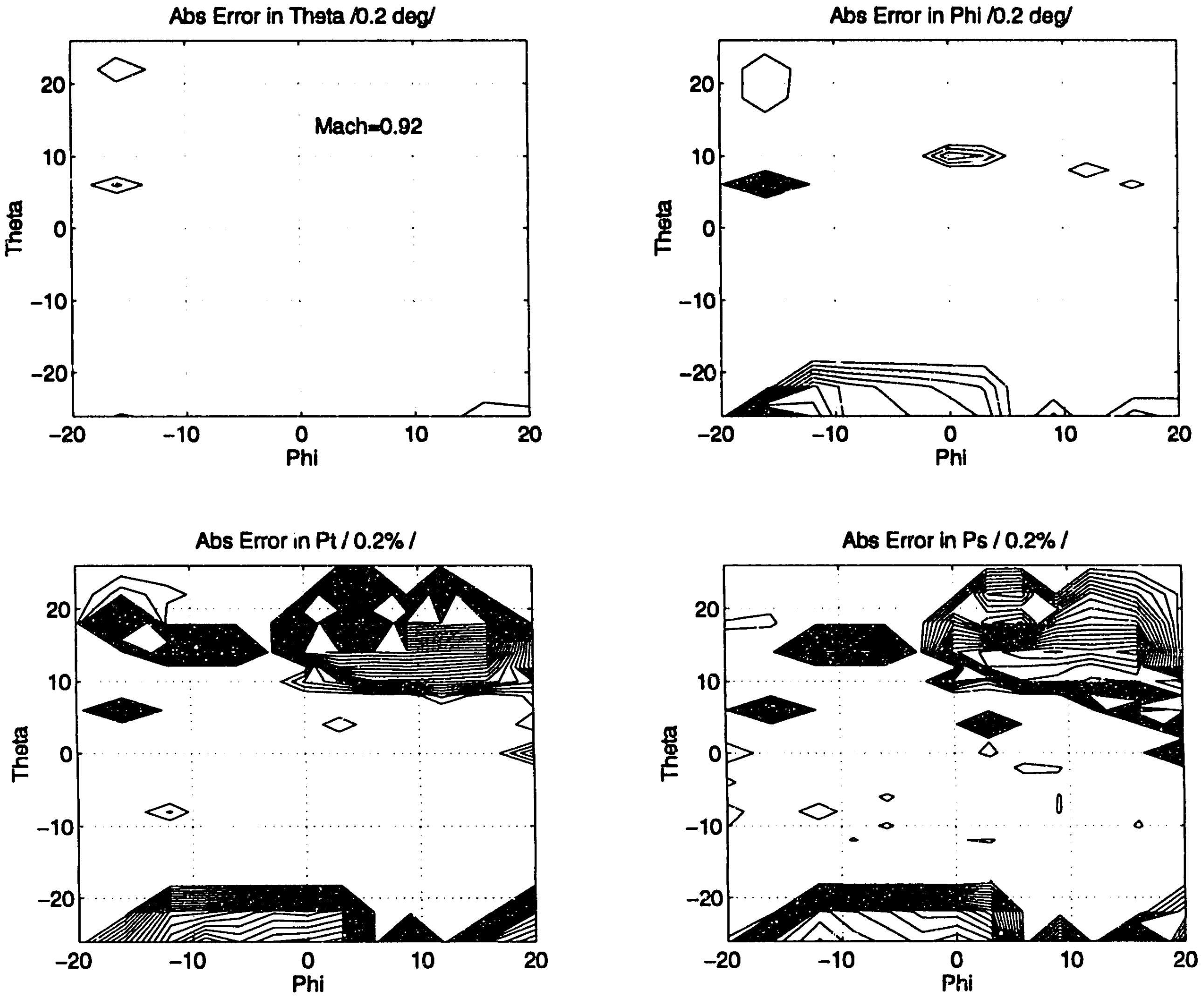

Figure C.17 Errors in predicted θ, φ, Pt and Ps as function of actual θ and φ for M=0.92

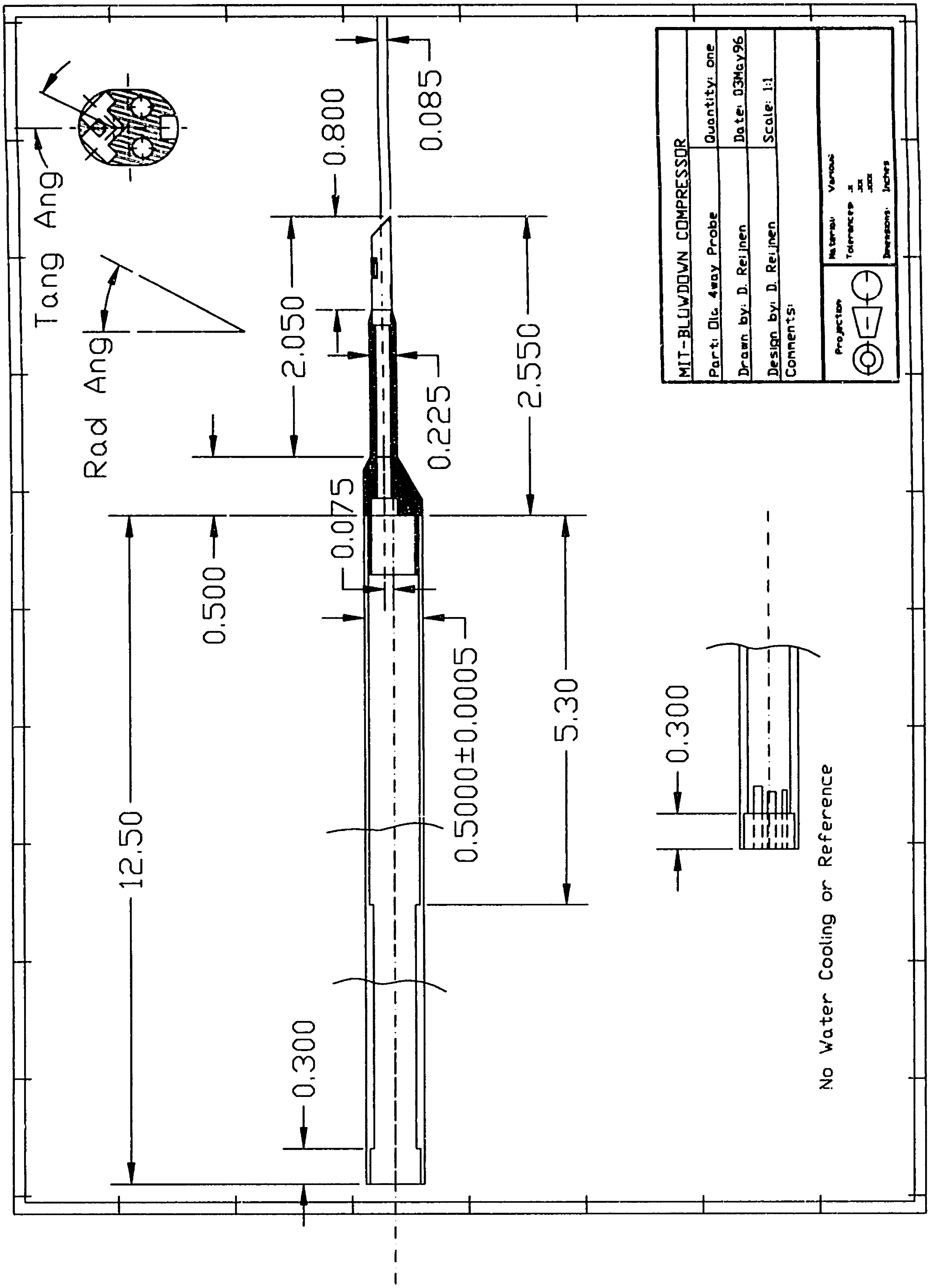

Figure C.18 Global Dimensions of 4Way Probe

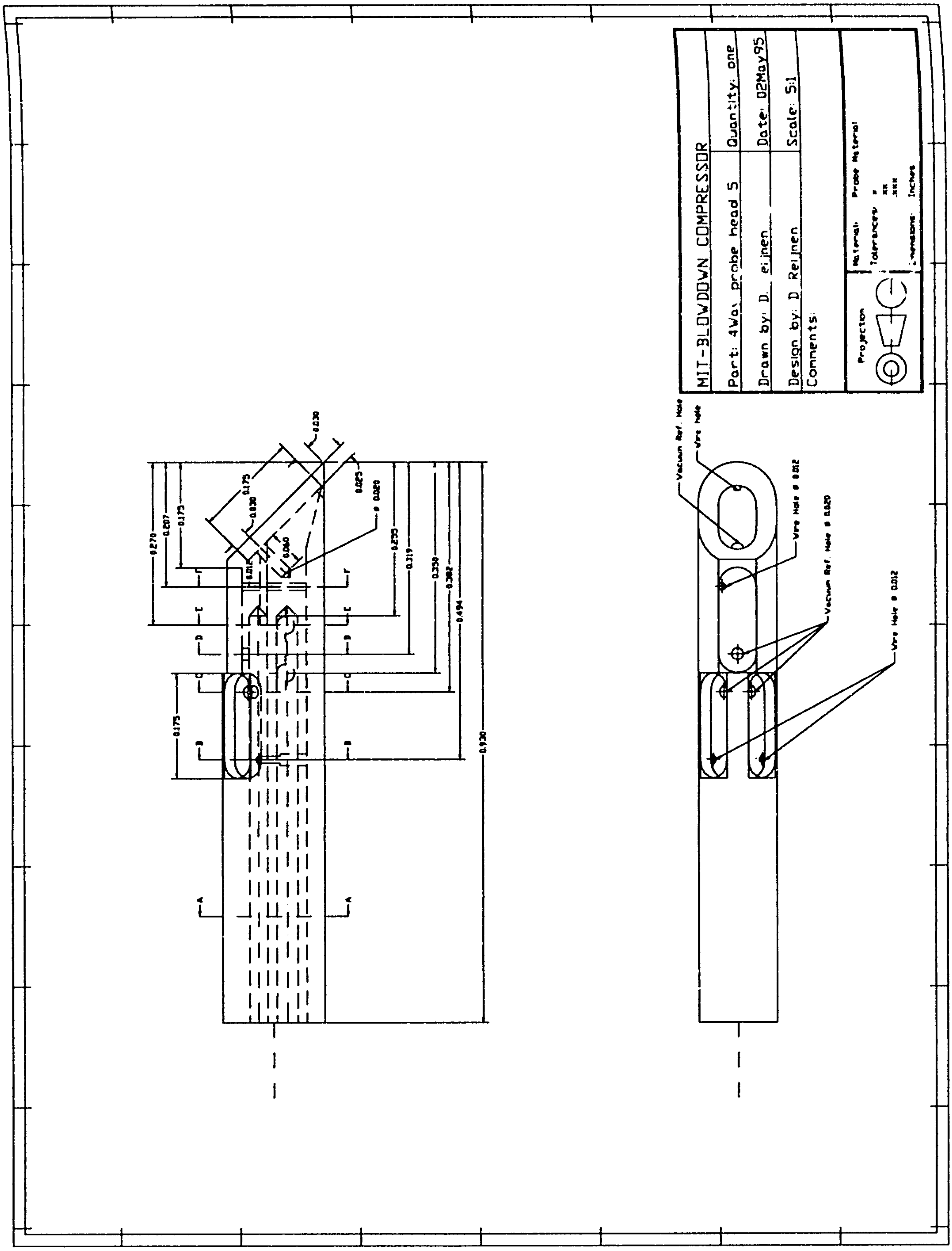

Figure C.19 Definition of Cross Section Planes of 4Way Probe Head

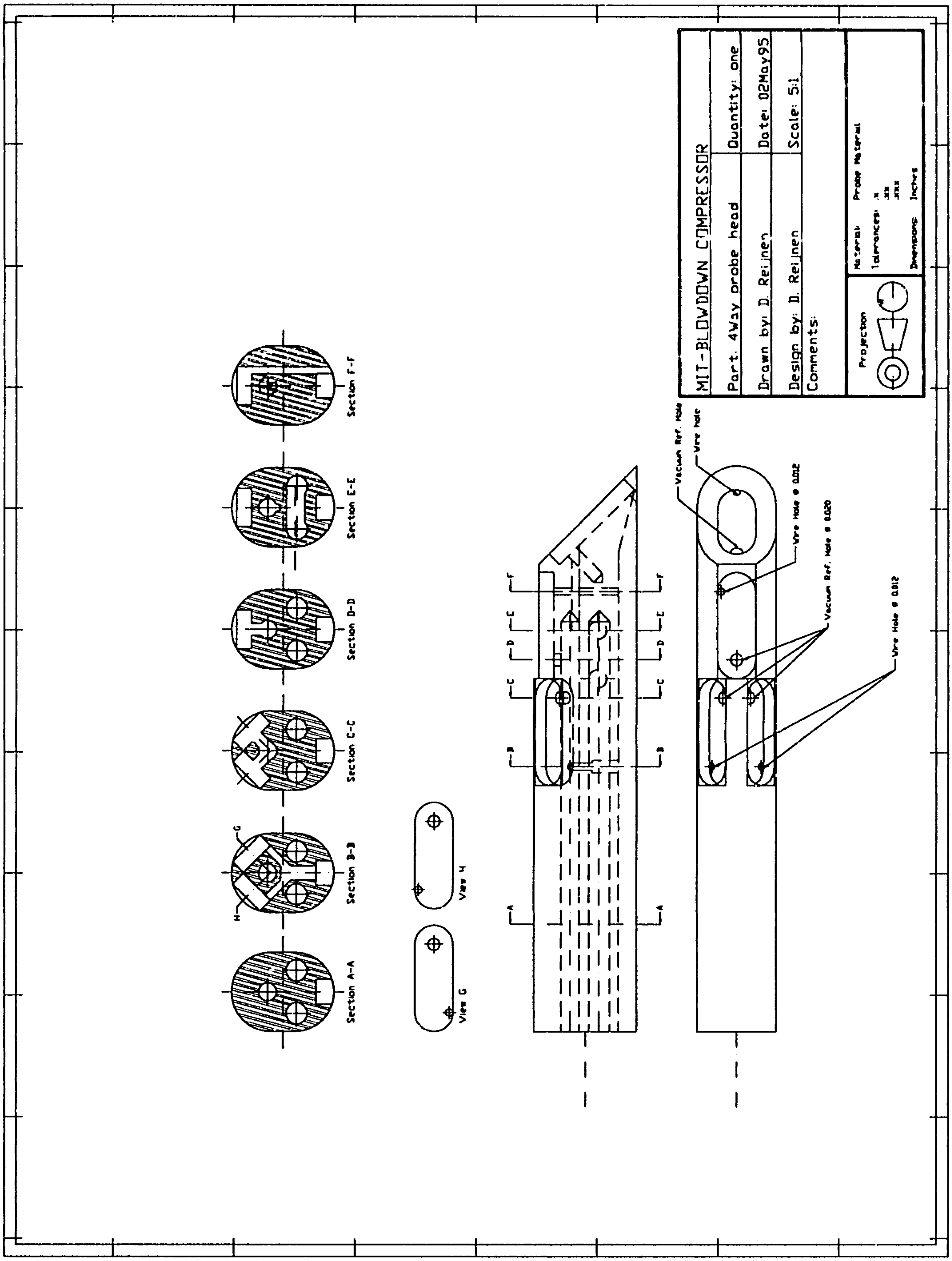

Figure C.20 Cross Sections of Head of 4Way Probe

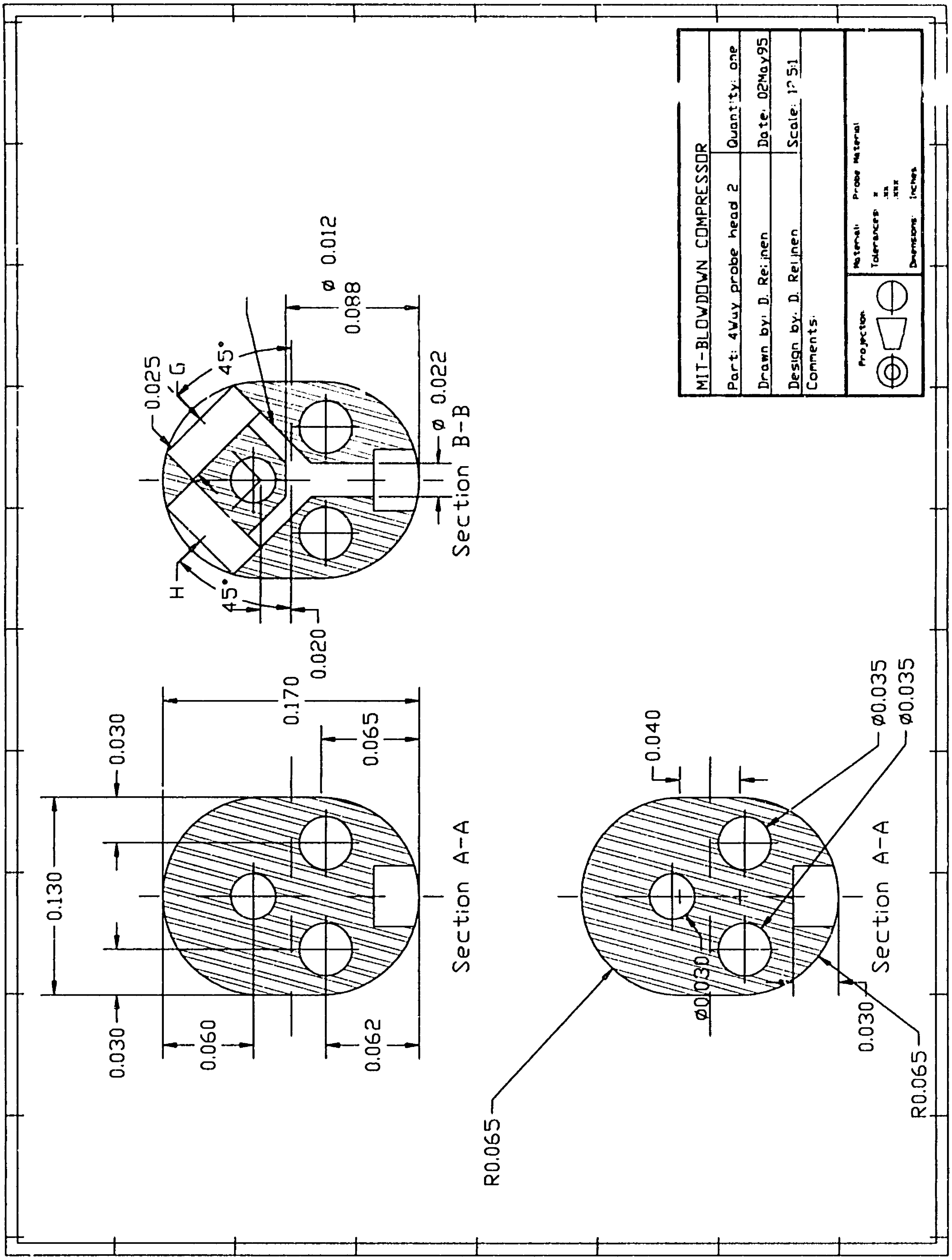

Figure C.21 Detailed Cross Sections of Head of 4Way Probe

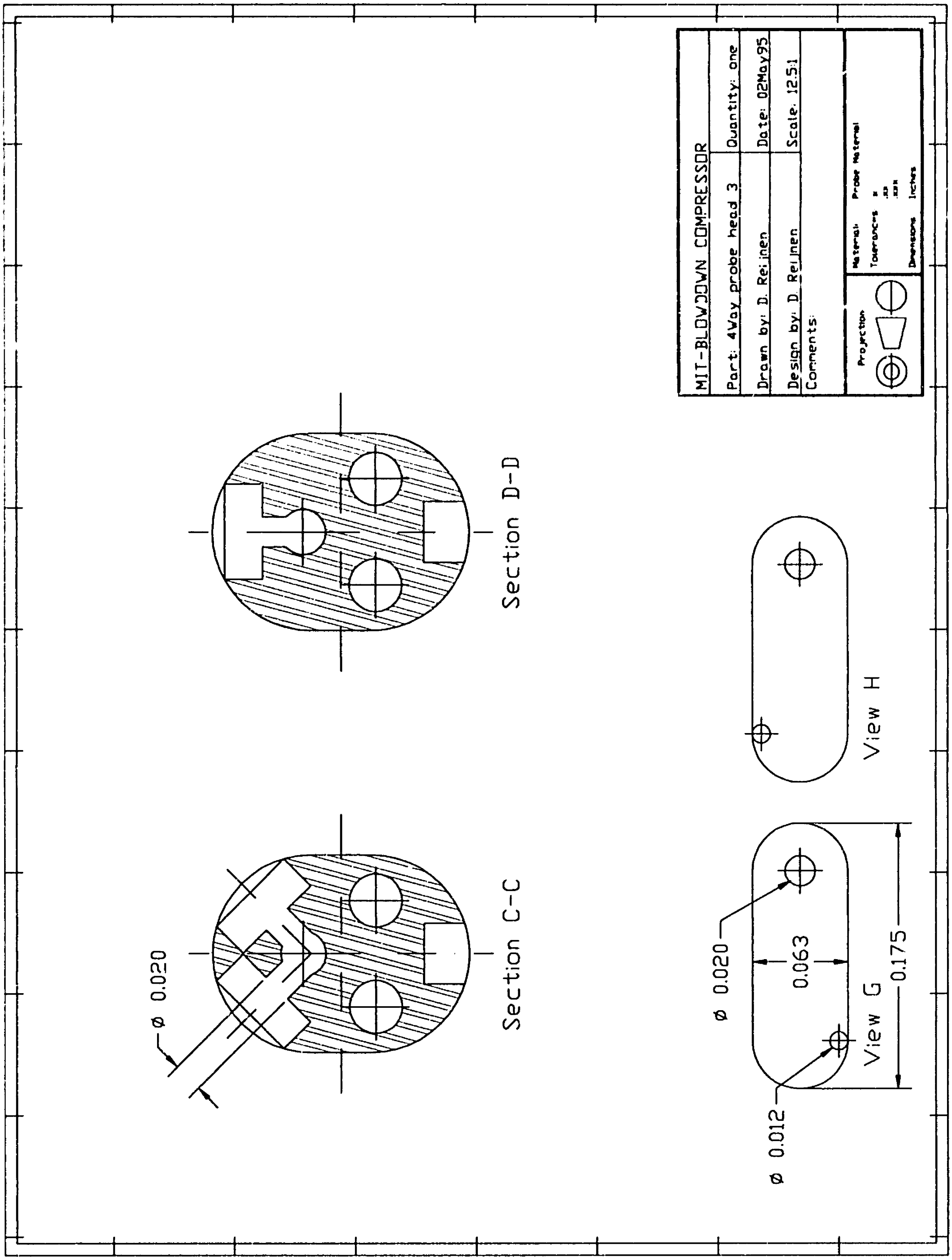

Figure C.22 Detailed Cross Sections of Head of 4Way Probe

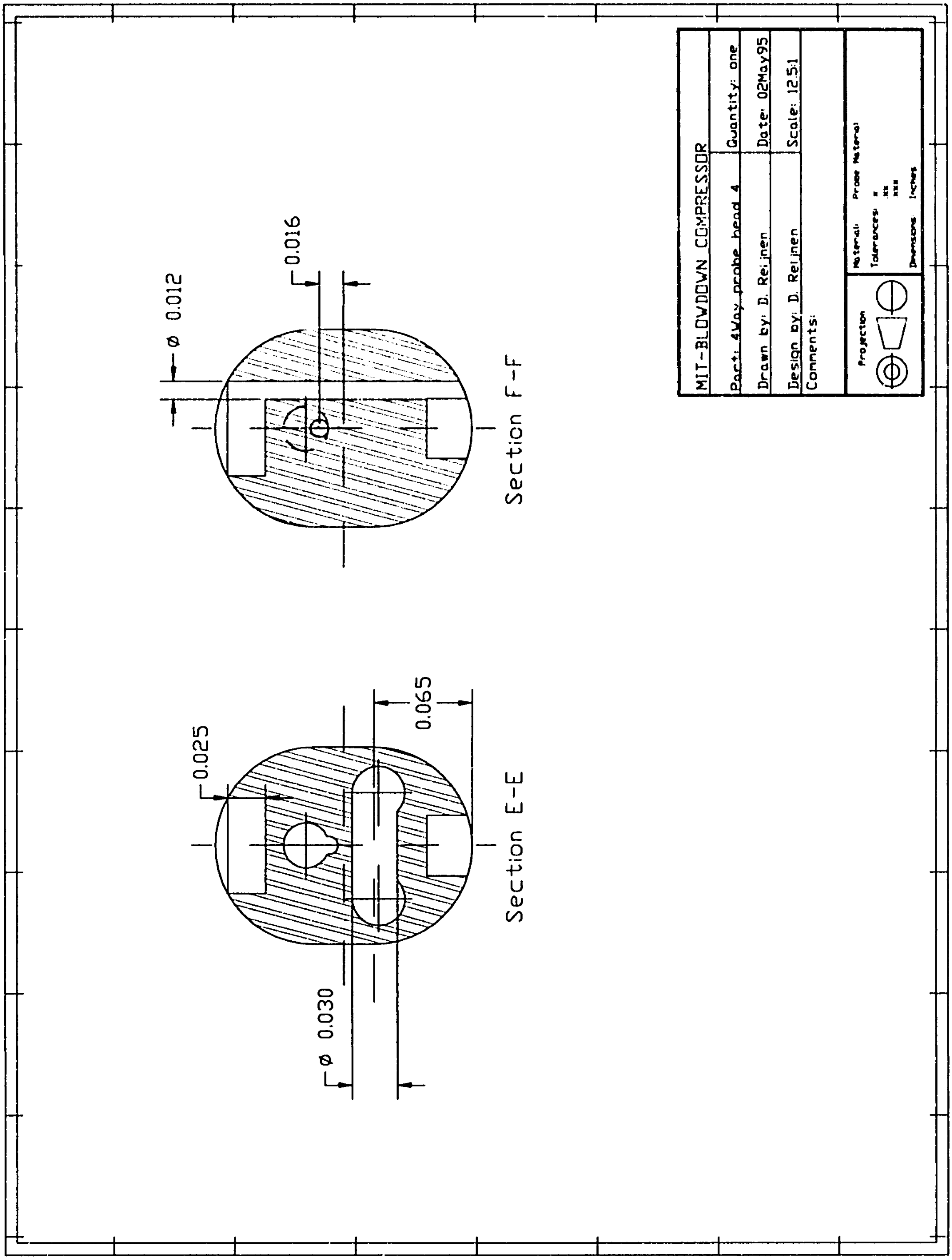

Figure C.23 Detailed Cross Sections of Head of 4Way Probe

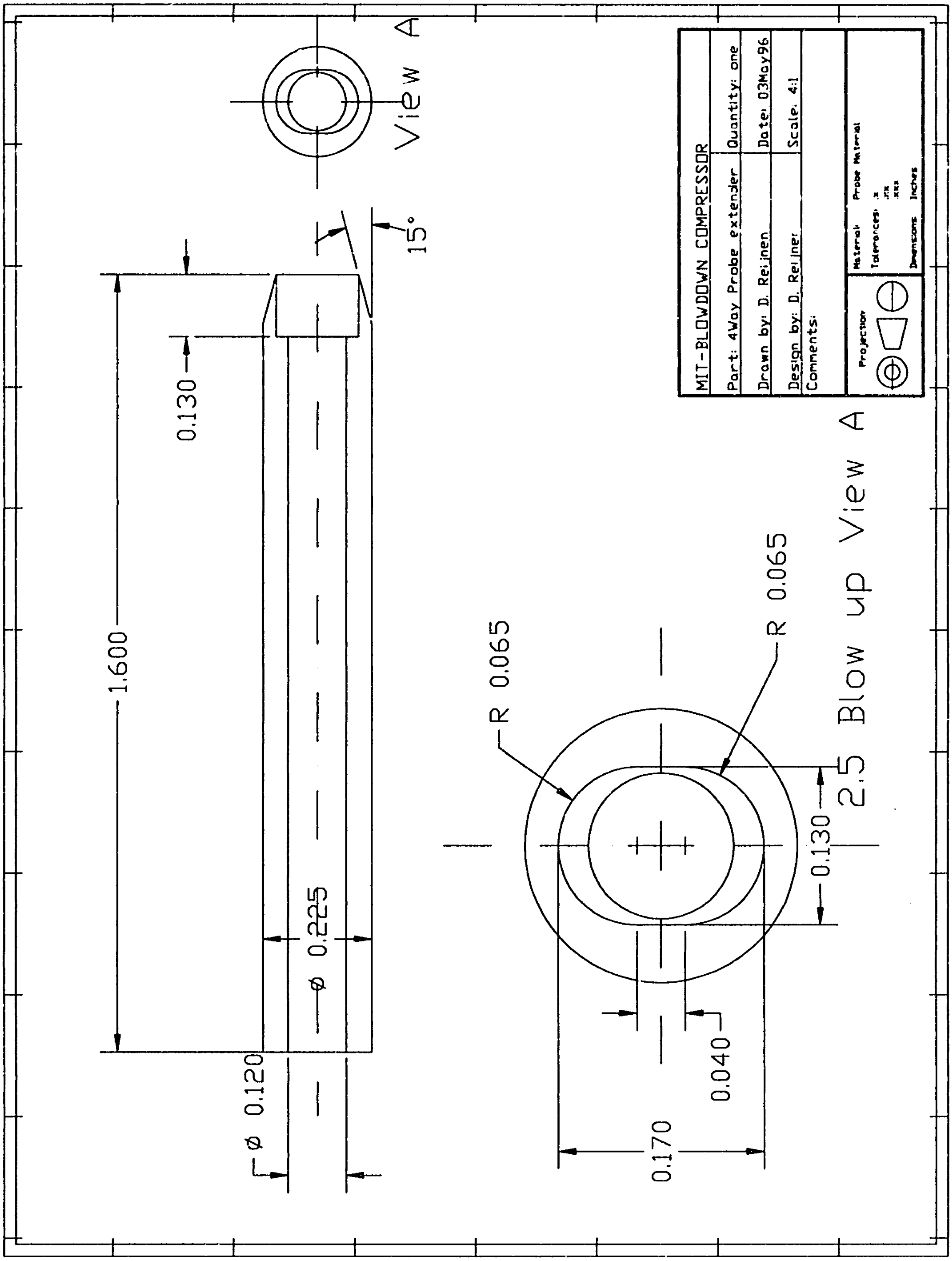

Figure C.24 4Way Probe Extender

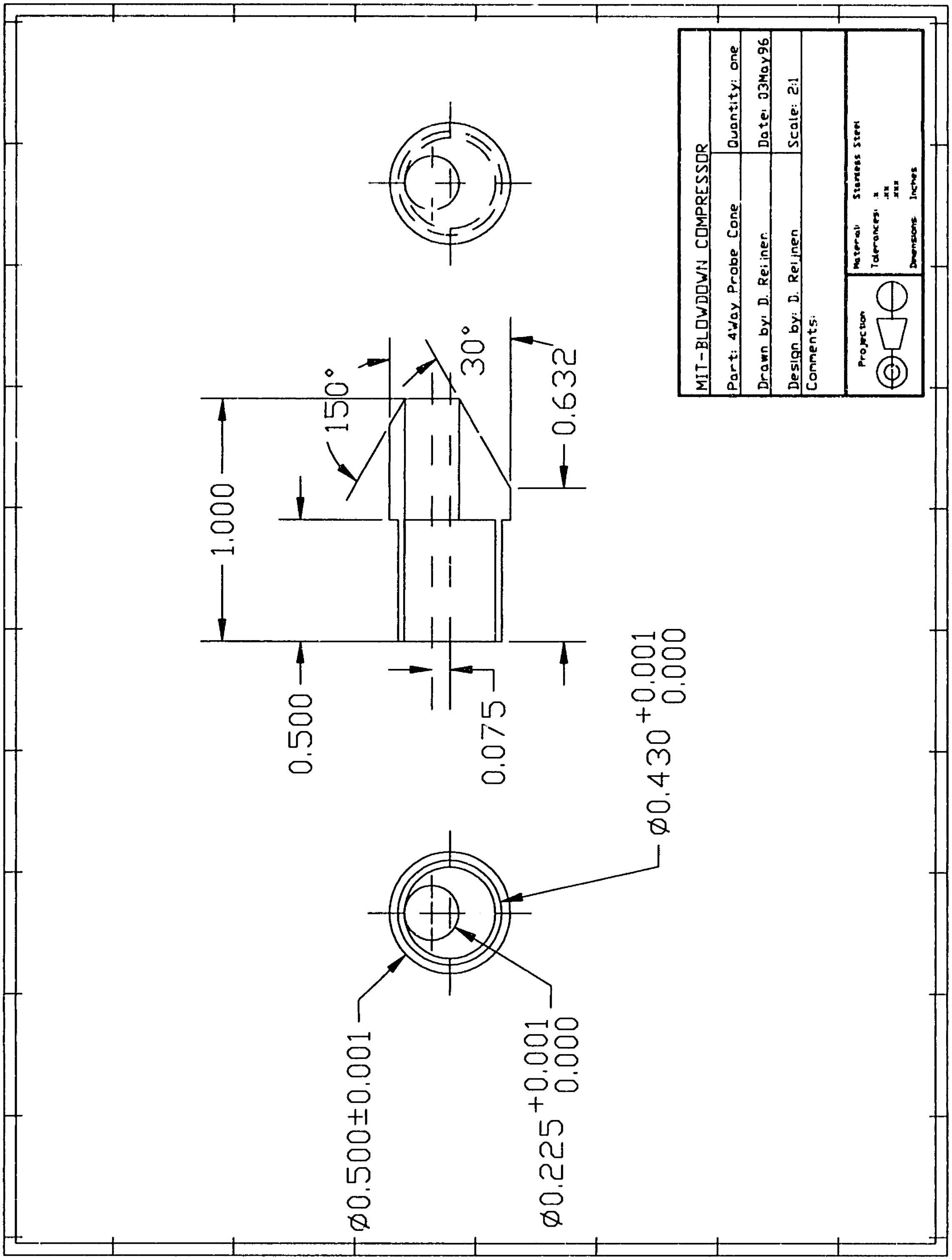

Figure C.25 4Way Probe Cone

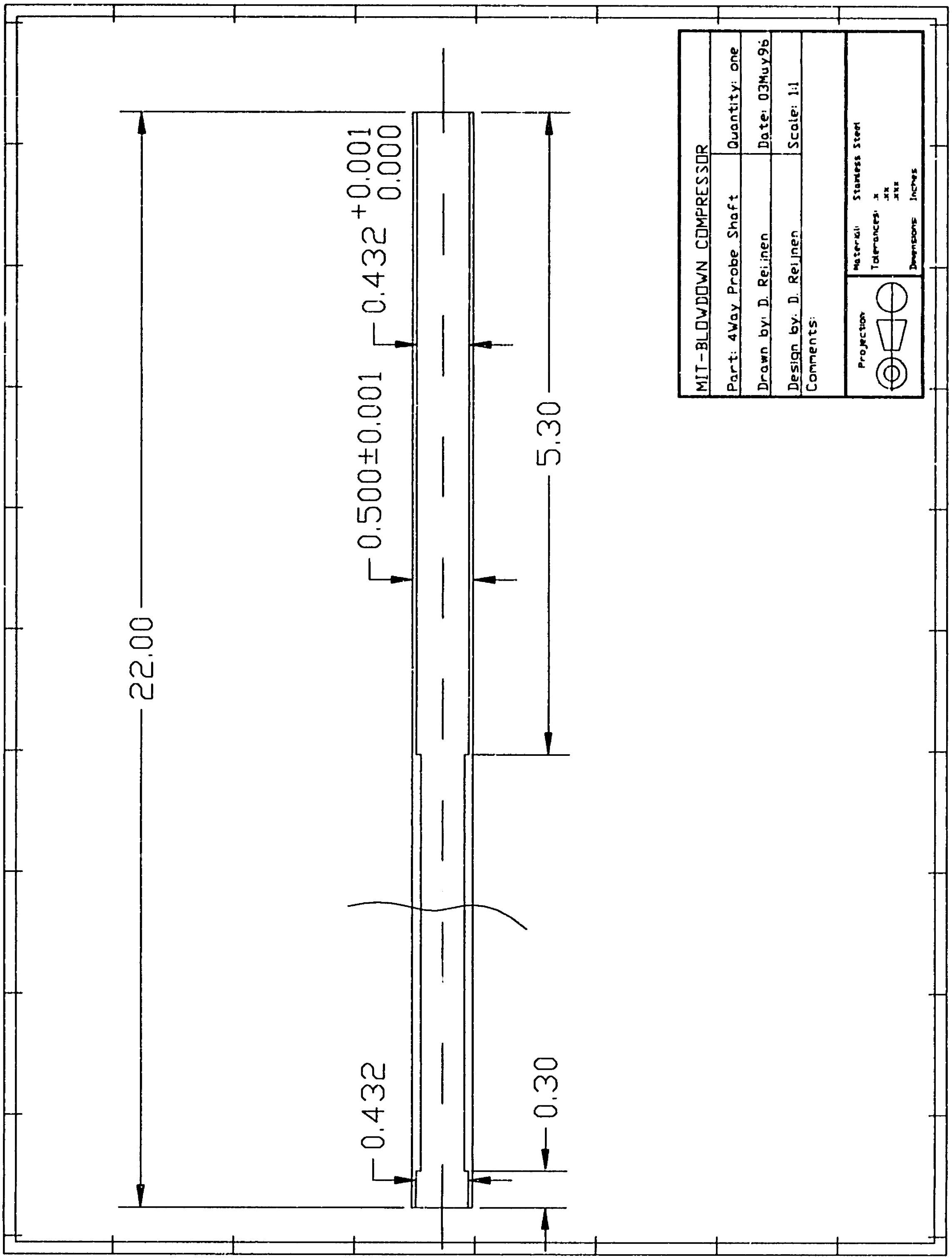

Figure C.26 4Way Probe Shaft

Appendix D Streamline Curvature Code

Due to the problems encountered running this code the author will elaborate a little bit on using this code for the good of future users. In general the code is very user friendly but it does have some rough edges.

D.1 General Comments

First the grid generator uses a constant grid step in axial direction. This forces the user to choose a step which best matches his geometry. For example if most axial dimensions are fractions of 1/4 Inch a (non dimensional) grid step which is the equivalent of 1/4 Inch in m-r units is an appropriate step. However the maximum number of grid points in axial direction is 128 so a very small step is not possible. In addition the rotor, stator or any other geometry change must start at a grid point.

Second, the grid generator supplied for the code only allows the user to specify the casing height, hub radius at domain inlet, rotor inlet & outlet, stator inlet & outlet, and domain outlet. This results in 5 separate ramps. However, because the grid generator is not directly coupled to the main code, the user can change the grid and the axial grid point were the rotor and stator start, resp. end. This done by changing their node positions in the xxxxdata.dat file. These positions do not have to coincide with a change in ramp angle at the hub! Also, the author made his grid by making two separate grids using the grid generator: the shape of the inlet for the first, and the shape of the rotor and stator for the second. These were easily combined to one grid in Matlab using a Matlab m-file written by the author called combgrid.m. This enables the user to make a more complex grid.

Third, the author modified the code to include three additional I/O options. Now, the user can save the grid he converged on, and can also save/load the state variables of the flow field he converged on. This is important, because it enabled the author to converge at significant higher mass flows and losses. Initially, the code would blow ,up on the first iteration because the initial condition was not set accurate enough. Now the user can start with a easy case. Save the grid and state found. Increase the losses or inlet Mach number slightly (1% loss or 0.005 Mach number), restart the code, load the grid and state from the previous case, increase the relaxation factor to somewhere between 0.99 and 0.5, and converge to these new boundary conditions.
It was found that a very high what the code calls a relaxation factor, 0.99 or 0.999, was the best weapon against blowing up. After the initial 10 iterations the relaxation factor can be adjusted to other desired values.

D.2 Grid Format

The grid is stored in the xxxdata.dat file in a very simple way. The first column contains the m positions of each consecutive streamline starting at the hub. For example for 13 streamlines and 20 stations, it will contain the 20 m positions for the first streamline, followed by the 20 m positions of the second etc. So a total of 20x13=260 entries.

The second column is similar and contains the r positions of each streamline.
The streamline curvature code also uses a xxxdata.dat file containing flow and grid information. This file explains itself. Do note that nothing withholds the user of setting a different rotor and stator position than used to produce the grid. This can be very useful for complicated geometries.

D.3 Larry Smilg Mises Interface

Another important detail is the fact that the interface with MISES requests a name. What is meant here is a name which has the following form: either r07 or s09. R denotes rotor and s denotes stator. The number mentioned denotes the streamline the code is going to write to disk. Numbering starts at the hub.

Appendix E MISES Modifications and Results

This appendix discusses the details of setting up the files necessary to run MISES. In addition the modifications made to MISES to allow it to model a 6 blades are presented. Finally the results of MISES calculations for the baseline rotor are included.

E.1 Application of Streamline curvature solution to MISES

To be able to operate, MISES needs to know the radial shift of the streamline, the radial contraction of the streamline and the Mach number at the inlet boundary and the non dimensional pressure ratio over the cascade.

The resulting grid of the streamline curvature method was used to generate the streamline radius and height files which MISES needs for its quasi 3D calculations. The streamlines were interpolated to planes corresponding to an inlet radius at the rotor of resp. R/Rt= 0.7, 0.8, 0.9, 1.0. In contrast to the work done by Larry Smilg and Willy Ziminsky, the whole streamline path from far upstream to far downstream was used by MISES. Smilg and Ziminsky only used the path inside the rotor or stator and added a constant radius and stream tube thickness in front and aft of the blade row. The improved approach does complicate the process of setting the boundary conditions in MISES. Now the relative inlet Mach number is not set at the same radius thus different. The inlet Mach number used in the new approach is simply obtained from the streamline curvature code at a position equivalent to the inlet plane of the MISES grid. The inlet plane of MISES was chosen to be approximately 1.2 axial chord upstream in order to keep the number of cells in the inlet under control, resulting in a small and efficient grid. The outlet plane is positioned at about 0.80 axial chord behind the trailing edge. The total Mach number (not based on total temperature but combination of all components) in the absolute and relative frame (M_{tot} & M_{totrel}) were obtained from the streamline curvature code and interpolated to the 4 streamlines defined above.

These Mach numbers and the measured static exit/absolute total pressure ratio P_{s_exit}/P_{t_inlet} of the rotor at design condition are used for calculation of the input variables for MISES:

$$Rotrel = \frac{\Omega L_{ref}}{a_{01}} = \frac{(\Omega R_{tip}) L_{ref}/R_{tip}}{\sqrt{\gamma R T_{totrel}}} = M_{tip}\frac{L_{ref}}{R_{Tip}}\sqrt{\frac{1+\frac{(\gamma-1)}{2}M_{tot}^2}{1+\frac{(\gamma-1)}{2}M_{totrel}^2}}$$

$$\frac{P_2}{P_{01}} = \frac{P_{exit}}{Pt_{rel-inlet}} = \frac{Ps_{exit}}{Pt_{inlet}}\frac{Pt_{inlet}}{Pt_{rel-inlet}} = \frac{Ps_{exit}}{Pt_{inlet}}\left(\frac{1+\frac{(\gamma-1)}{2}M_{tot}^2}{1+\frac{(\gamma-1)}{2}M_{totrel}^2}\right)^{\gamma/(\gamma-1)}$$

The inlet Mach number which has to be specified in MISES will of course be $M_{tot\ rel\ inlet}$.

E.2 Six Blade Analysis

In order to qualitatively simulate the effect of 5 modified blades in a base rotor, MISES was modified to be able to accommodate multiple blade passages and individual blade boundary layer control. This was achieved by increasing the number of blades and streamlines MISES was able to handle:

mises/src/STATE.INC	NBL 2 -> 6, and JX 30 -> 60.
mises/src/update.f	IDIM 256 -> 1024
mises/panel/PANEL.INC	IEX 2->6.

However, having multiple passages did cause some problems. The properties of the flow required an offset grid which decreased the control the user has over the grid dramatically. In an offset grid the number of grid points on a streamline in the inlet or outlet is set by the grid point density in the passage itself. This is usually not a problem but it is in this case as will become clear. When the number of blade passages is doubled the number of grid points increases by quite more than a factor of two because besides of the doubling of the number of streamlines which doubles the number of grid points, the domain also becomes longer. The inlet and outlet of the domain are extended perpendicular to the flow direction. But the grid must also be able to allow pressure disturbances to travel over the periodic grid boundary in the next (identical) domain. Thus the minimum amount of grid necessary is set by drawing a line perpendicular to the flow at the leading edge of the leading blade (point A in figure E.1) and extend this line until it intersects with the last streamline of the domain (point B). The distance between this point and the point were this last streamline hits the leading edge of its blade (BC) has to be added in front of the leading edge of the first (leading) blade to allow pressure disturbances to propagate to the next domain. To allow for disturbances which originate just upstream of the first blade to propagate one additional block of grid cells (ED) is added. When the stagger angle is high this effect is very pronounced and the length of the grid increases very rapidly.

Because of this size problem the maximum number of passages which could be modeled with a fair grid density on the blade and in the passages, was limited to 6. Six blade passages resulted in slightly over 200 MB of RAM required and a 12 minutes per iteration run time. This was just within the limits of the available equipment in the laboratory.

Results of this analysis are presented in the Discussion of Experimental Results chapter.

E.3 Convergence problems of MISES

During the use of MISES some severe problems were encountered. The compressor rotor operates very highly loaded resulting in extensive viscous layers. This complicates the task of converging to a solution dramatically because we have transonic flow in a channel with moving walls. A small change in the boundary layer has relatively great effect on the shape of the separation region thus having a great effect on the boundaries of the channel in the Euler solver. Because of this no regular solution could be obtained for the tip case where these effects are the strongest. In addition one has to keep in mind that MISES assumes quasi 3D flow. When large areas of separation occur this induces strong radial transport towards the tip. So it is important to use these solutions only as a first guideline to facilitate the interpretation of the experimental data.

One should also note that MISES is a steady state solver. If large scale unsteady behavior is expected like shock oscillation or unsteady separation MISES is unlikely to converge reliably, if at all.

E.4 Results for Baseline Rotor

Mach contours and boundary layer properties for the streamlines of interest to this investigation are shown in figure E.3-E.18. The displacement and momentum thickness are expressed as a fraction of the chord length.

The solution shown for the flow at the tip was obtained by running MISES with the boundary layer coupling engaged until the position of the shock was constant and the solvers go into a hysteris cycle which prevents convergence. At this point the changes per iteration in the flow field are already very small and the boundary layer is now already very similar to the boundary layer which would be obtained in a regular convergence. The next step was to freeze the boundary layer and converge the case. Run a couple of iteration with the coupling included, freeze it again and reconverge. This was repeated several times to try to obtain the best solution.

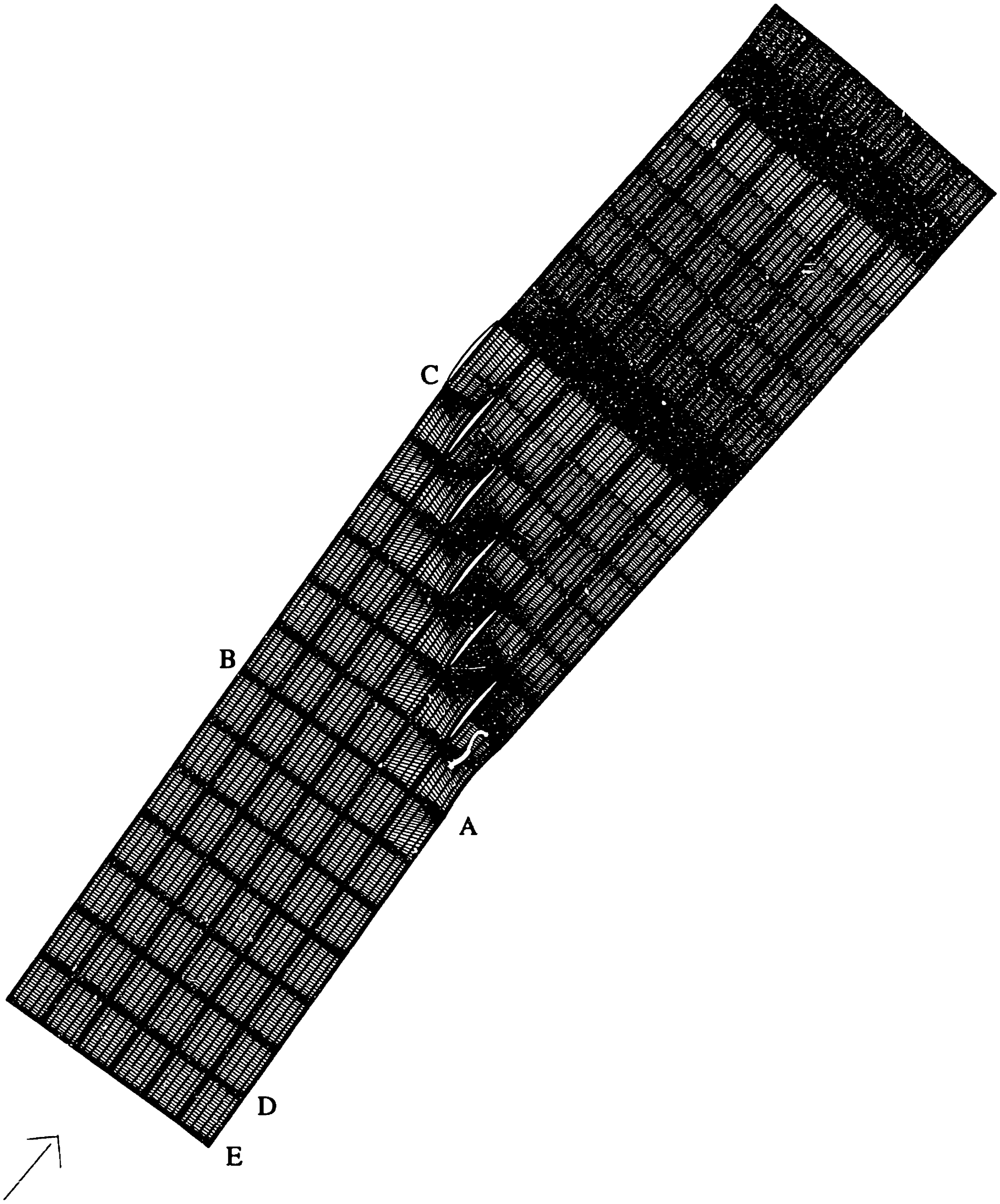

Figure E.1 Grid for 6 blade MISES analysis

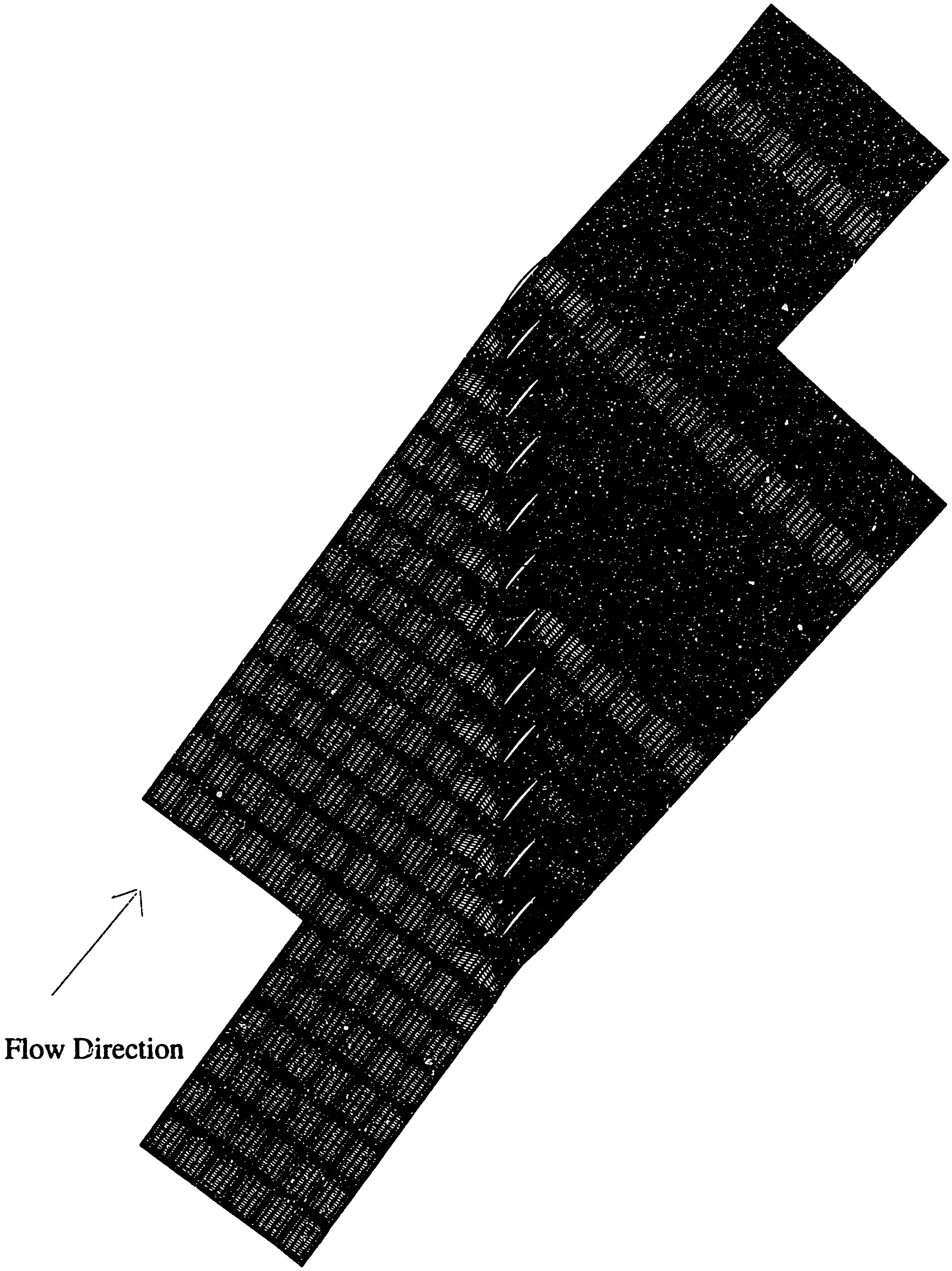

Figure E.2 Grid for 6 blade MISES analysis showing two computational domains

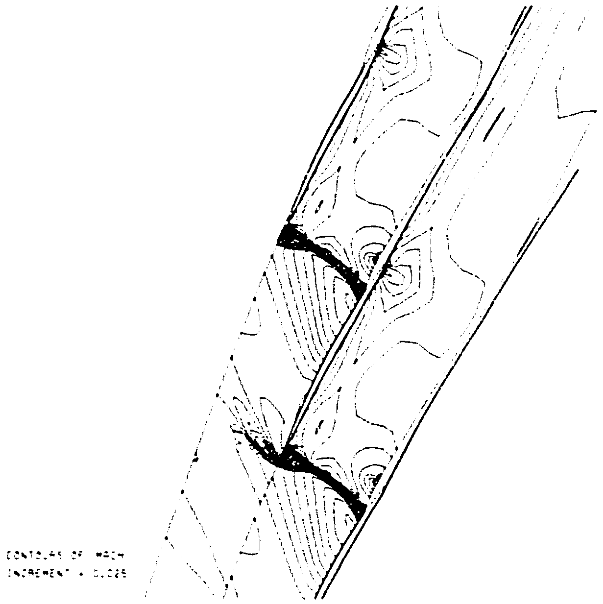

Figure E.3 Mach contours at R/R_t=1.0

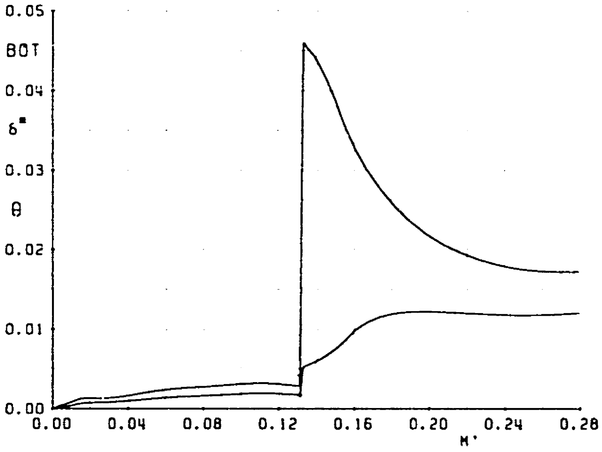

Figure E.4 Pressure surface displacement and momentum thickness at R/R_t=1.0 as fraction of the streamwise chord

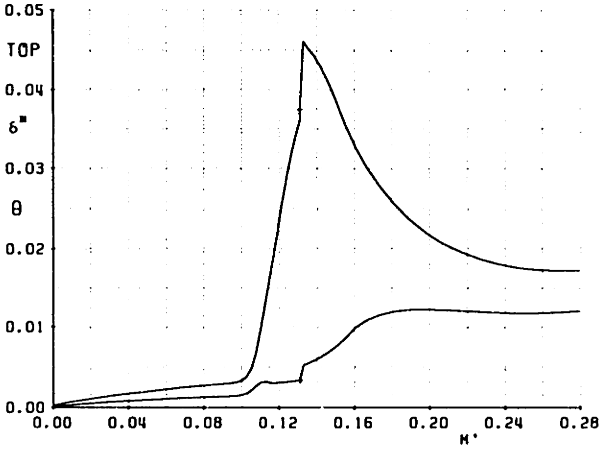

Figure E.5 Suction surface displacement and momentum thickness at R/R_t=1.0 as fraction of the streamwise chord

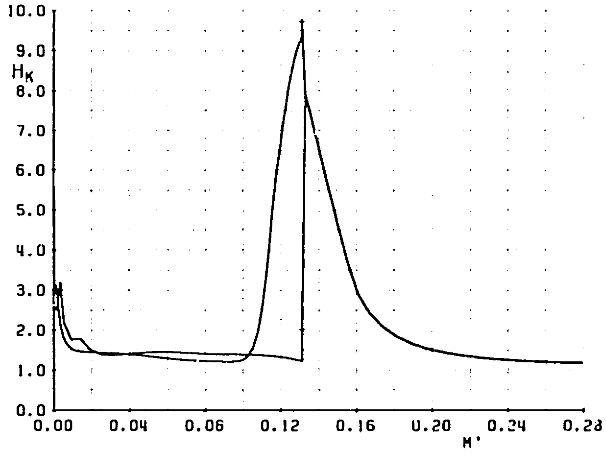

Figure E.6 Shape factor at R/R_t=1.0

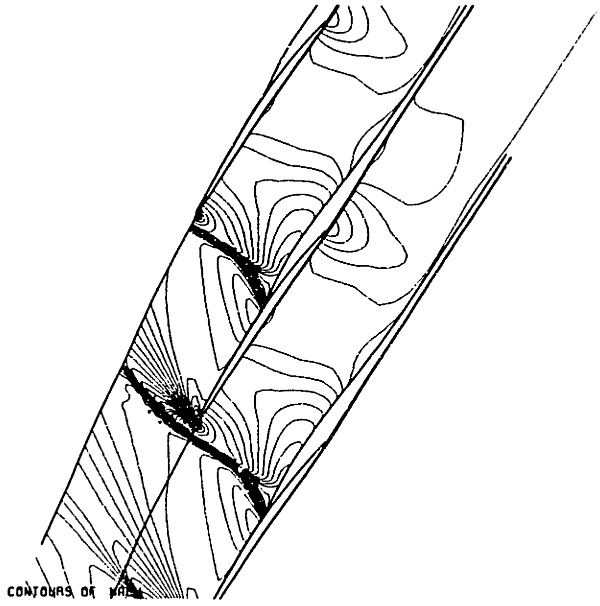

Figure E.7 Mach contours at R/R$_t$=0.9

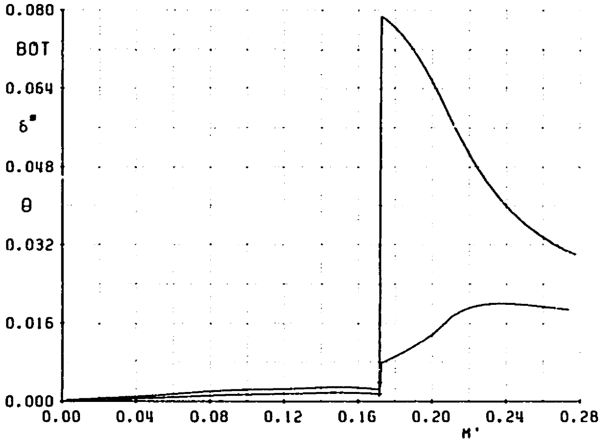

Figure E.8 Pressure surface displacement and momentum thickness at R/R$_t$=0.9
as fraction of the streamwise chord

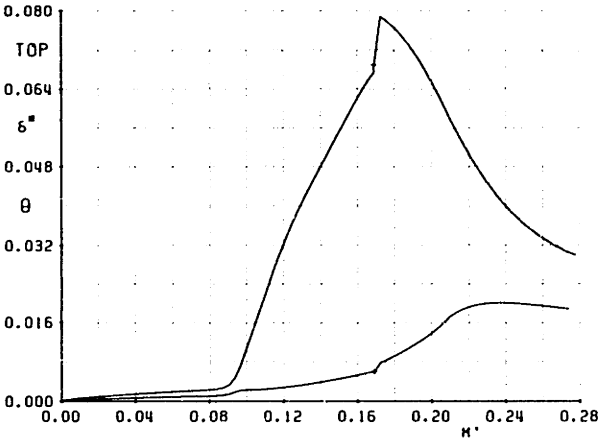

Figure E.9 Suction surface displacement and momentum thickness at R/R_t=0.9 as fraction of the streamwise chord

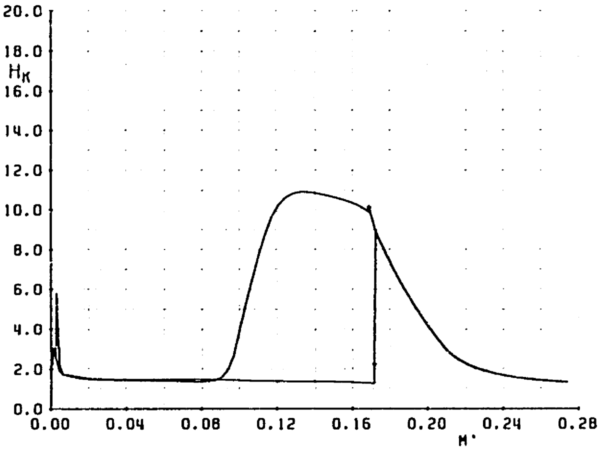

Figure E.10 Shape factor at R/R_t=0.9

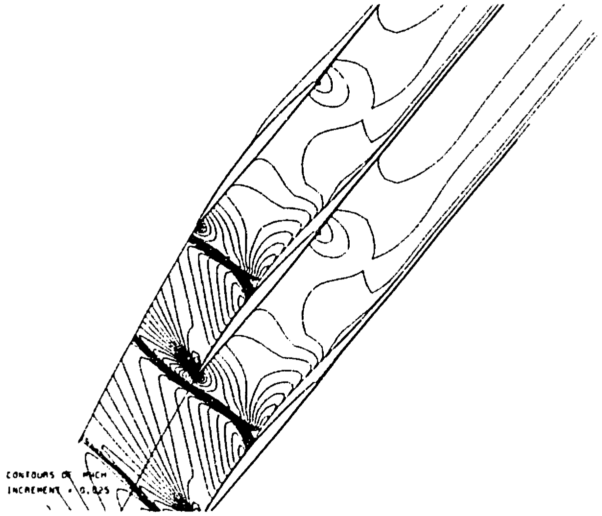

Figure E.11 Mach contours at R/R_t=0.8

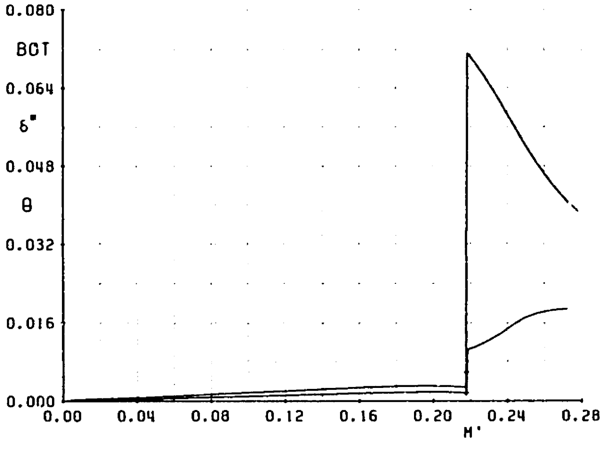

Figure E.12 Pressure surface displacement and momentum thickness at R/R_t=0.8 as fraction of the streamwise chord

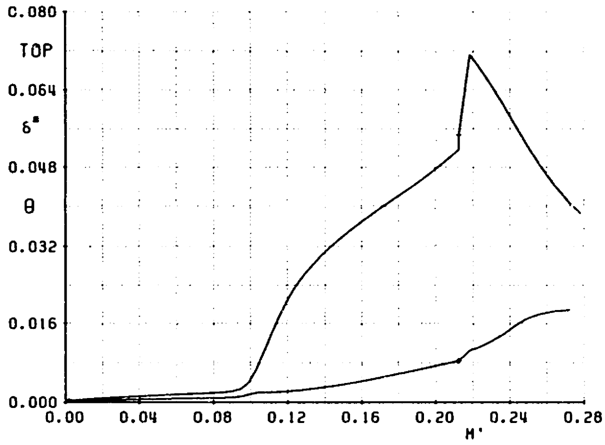

Figure E.13 Suction surface displacement and momentum thickness at R/R_t=0.8 as fraction of the streamwise chord

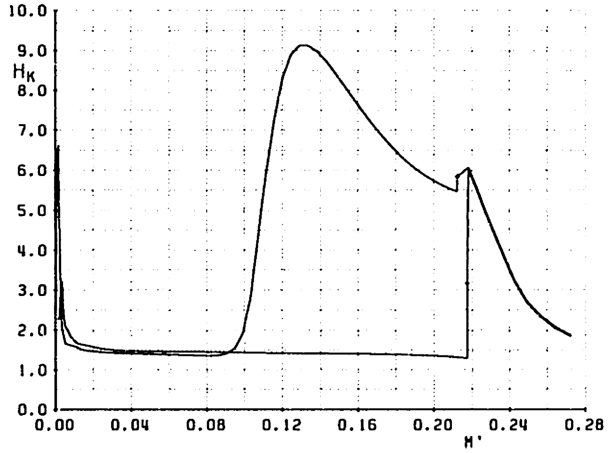

Figure E.14 Shape factor at R/R_t=0.8

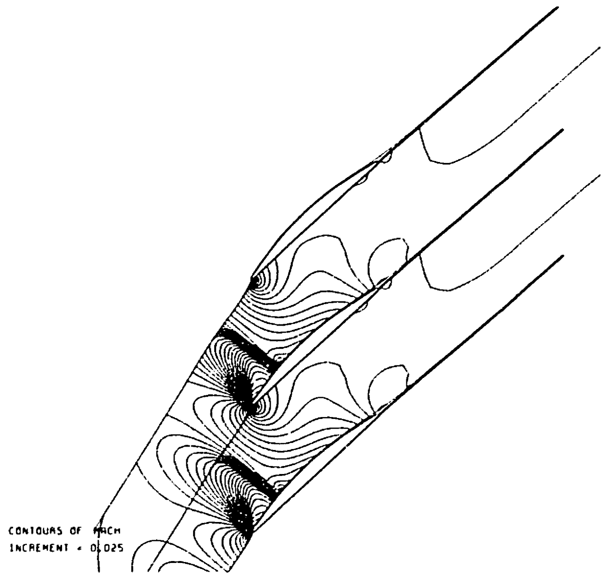

Figure E.15 Mach contours at R/R_t=0.7

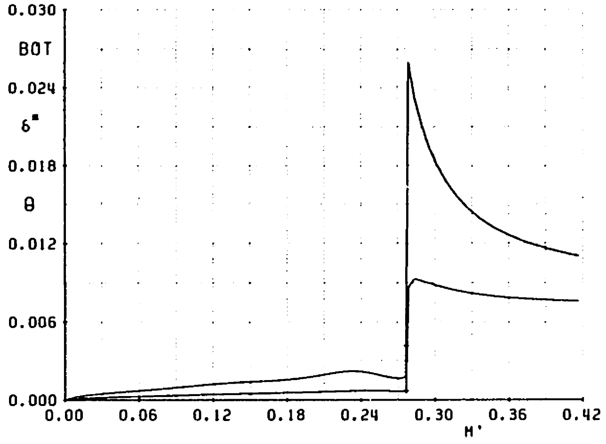

Figure E.16 Pressure surface displacement and momentum thickness at R/R_t=0.7
as fraction of the streamwise chord

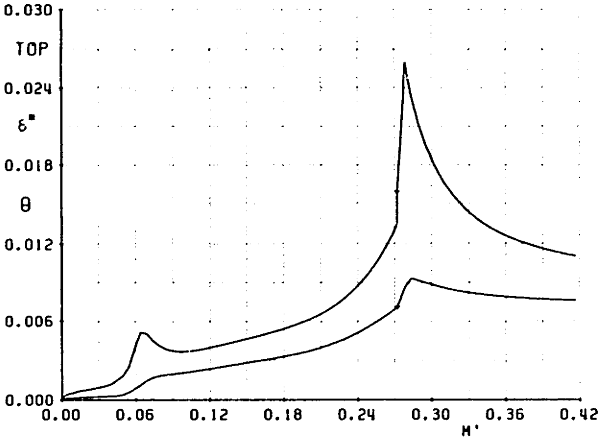

Figure E.17 Suction surface displacement and momentum thickness at R/R_t=0.7 as fraction of the streamwise chord

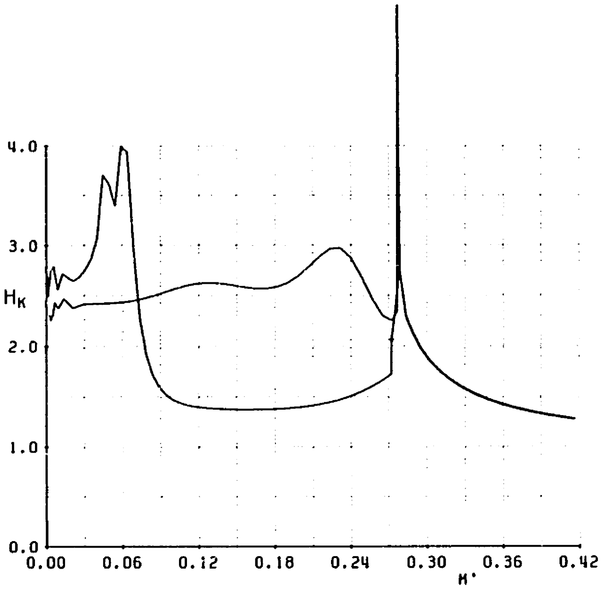

Figure E.18 Shape factor at R/R_t=0.7

References:

1.1 Kerrebrock, J.L., "Flow in Axial Compressors", AIAA Paper 80-0124, Dryden Lectureship in research, Pasadena, CA.

1.2 Kotidis, P.A., and Epstein, A.H., "Unsteady Radial Transport in a Transonic Compressor Stage", J. Turbo machinery, Vol. 113, April 1991, pp. 207-218.

2.1 Stalker, E.A., “Axial Blower”, U.S. Patent 23,108, May 3, 1949.

2.2 Stalker, E.A., “Compressors”, US Patent 2,749,025./2.749,027 June 5 ,1956.

2.3 Stalker, E.A., “Compressors”, US Patent 2,830,754. April 15, 1958.

2.4 Erwin, J.R., “Continuous Boundary Layer Control in Compressor”, US Patent 2,720,356, Oct. 11 1955.

2.5 Conrad , O., et al., “Guide Blades of Axial Compressors”, Daimler-Benz, US Patent 3,694,102, Sept 26 1972.

2.6 Meauze, G.D., et al., “Supersonic Compressor”, ONERA, US Patent 3,993,414, Nov. 23 1976.

2.7 Loughery, R.J., Horn, R.A. and Tramm, P.C., "Single Stage Experimental Evaluation of Boundary Layer Blowing and Bleed Techniques for High Lift Stator Blades", NASA CR-54573, March 1971.

2.8 Syber, J. and Koncsek, J.L., "Bleed System Design Technology for Supersonic Inlets", AIAA Paper 72-1138, Nov. 1972.

2.9 Hamed, A. and Shang, J.S., "Survey of Validation Data Base for Shockwave Boundary Layer Interaction in Supersonic Inlets", J. Propulsion, Vol. 7, No.4, July-Aug. 1991, pp. 617-25.

2.10 Strike, W.T. and Rippy, J., "Influence of Suction on the Interaction of an Oblique Shock with a Turbulent Boundary Layer at Mach 3", Arnold Engineering Development Center TN-61-129, Oct. 1961.

2.11 Hingst, W.R. and Tanji, F.T., "Experimental Investigation of Two-Dimensional Shock Boundary Layer Interaction with Bleed", AIAA Paper 83-0135 also NASA TM-83057, 1983

2.12 Squire, L.C. and Smith, M.G., "Interaction of a Shock Wave with a Turbulent Boundary Layer Disturbed by Injection", Royal Aeronautical Society, May 1980, pp. 85-110.

2.13 Wong, W.J., "Application of Boundary Layer Blowing to Suppress Strong Shock Induced Separation in Supersonic Inlets", AIAA Paper 77-147, Jan. 1977

2.14 Morris, M.J., Sajben, M. and Kroutil, J.C., "Experimental Investigation of Normal-Shock/Turbulent Boundary Layer Interactions with and without Mass Removal", AIAA Journal, Vol. 30, No. 2, Feb. 1992.

2.15 Wong, W.J., "The Application of Boundary Layer Suction to Suppress Strong Shock Induced Separation in Supersonic Inlets", AIAA Paper 74-1063, Oct. 1974.

2.16 Hall, G.R., "A Criterion for Prediction of Airframe Integration Effects on Inlet Stability with Application to Advanced Fighter Aircraft", Technical paper presented at Agard Symposium on Airframe/Propulsion interaction, Rome, Italy 3-6 Sept. 1974, AGARD CP150.

2.17 Rimlinger, M.J., Shih, T.P., and Chyu, W.J., "Three Dimensional Shock Wave Boundary Layer Interactions with Bleed through a Circular Hole", AIAA Paper 92-3084.

2.18 Hamed, A. and Lehnig, T.," The Effect of Bleed configuration on Shock Boundary Layer Interactions", AIAA Paper 91-2014.

4.1 Kerrebrock, J. L., The MIT Blowdown Compressor Facility, MIT Gas Turbine Report 108, Sept 1975.

4.2 Dennis, J., An experimental study of blade tip clearance suction applied to a high speed compressor, Master's thesis, Department of Aeronautics and Astronautics, Massachusetts Institute of Technology, 1993.

4.3 Ziminsky, W.S., Design of a high pressure ratio transonic compressor stage with active boundary layer control. Master's thesis, Department of Aeronautics and Astronautics, Massachusetts Institute of Technology, 1996.

4.4 Epstein, A.H., Quantitative density visualization in a transonic compressor rotor. MIT-GTL report No 124, September 1975.

4.5 Epstein, A.H., "Quantitative Density Visualization in a Transonic Compressor Rotor", Journal of Eng. for Power, Vol. 99, July 1977, pp. 460-475.

5.1 Thompkins, W.T. Jr., "An Experimental and Computational Study of the flow in a Transonic Compressor Rotor", MIT-GTL Report No. 129, 1976.

6.1 M. Drela, H. Youngren. A user guide to MISES 2.3, December 1995, Massachusetts Institute of Technology, Computational Aerospace Sciences Laboratory

6.2 L.Smilg. Design of a high pressure ratio fan stage to take advantage of boundary layer suction. Master's thesis, Department of Aeronautics and Astronautics, Massachusetts Institute of Technology, 1994.

6.3 W.S. Ziminsky. Design of a high pressure ratio transonic compressor stage with active boundary layer control. Master's thesis, Department of Aeronautics and Astronautics, Massachusetts Institute of Technology, 1996.

6.4 A. Merchant. Design and analysis of supercritical airfoils with boundary layer suction. Master's thesis, Department of Aeronautics and Astronautics, Massachusetts Institute of Technology, 1996.

6.5 R.M. Hearsey. A revised computer program for axial compressor design. Aerospace Research Laboratory Report ARL-TR-75-0001, Wright Patterson AFB, Dayton, Ohio, January 1975

C.1 Gertz, Jeffrey B., "Unsteady Design-Point Flow Phenomena in Transonic Compressors", p.10-18, GTL Report No. 188, 1986.

C.2 Figueriedo, W.A., "Spherical Pressure Probe for Retrieving Free Stream Pressure and Directional Data", 1977.;

C.3 Analog Digital Technology, "AD-830 user's manual", acquired Jan. 1993.